MODELING, ANALYSIS AND SIMULATION OF A DC GRID SINGLE ENDED PRIMARY INDUCTANCE CONVERTER FOR DC LOAD

By

Samuel Taiwo AJAYI, B.Eng. (ABU) 2007

MSC/ENG/05614/08-09

A THESIS SUBMITTED TO THE SCHOOL OF POSTGRADUATE STUDIES,

AHMADU BELLO UNIVERSITY, ZARIA

IN PARTIAL FULFILLMENT OF THE REQUIREMENTS FOR THE AWARD OF A MASTER OF SCIENCE (M.Sc.) DEGREE IN ELECTRICAL ENGINEERING

DEPARTMENT OF ELECTRICAL AND COMPUTER ENGINEERING, FACULTY OF ENGINEERING, AHMADU BELLO UNIVERSITY, ZARIA

NIGERIA

DECEMBER, 2014

DECLARATION

I declare that the work in this Thesis entitled MODELING, ANALYSIS AND SIMULATION OF A DC GRID SINGLE ENDED PRIMARY INDUCTANCE CONVERTER FOR DC LOAD has been carried out by me in the Department of Electrical and Computer Engineering. The information derived from the literature has been duly acknowledged in the text and a list of references provided. No part of this thesis was previously presented for another degree or diploma at this or any other Institution.

Samuel T. AJAYI

_____ _____

Signature Date

CERTIFICATION

This thesis entitled MODELING, ANALYSIS AND SIMULATION OF A DC GRID SINGLE ENDED PRIMARY INDUCTACE CONVERTER FOR DC LOAD by Samuel Taiwo AJAYI meets the regulations governing the award of the degree of Masters of Science (M.Sc.) Electrical Engineering of the Ahmadu Bello University, and is approved for its contribution to knowledge and literary presentation

Dr. J. Y. Oricha		
(Chairman Supervisory Committee)	Signature	Date
Prof J. O. Ojo		
(Member Supervisory Committee)	Signature	Date
Dr. M. B. Muazu		
(Head of Department)	Signature	Date
Prof. A. Z Hassan		
(Dean, School of Postgraduate Studies)	Signature	Date

DEDICATION

This work is dedicated to the Almighty God the giver of life and the finisher of our faith. This thesis is also dedicated to my parents: Elder and Deaconess Ajayi Ibitolu for their love and support.

ACKNOWLEDGEMENT

I thank the Almighty God who through His son Jesus Christ kept me and lifted me up from the impossible depth to which I had fallen and who progressively over this years is making a place for me.

I would like to say thank you to several people whose contributions, suggestions made this work to see the light of the day. There would be those who made obvious and tangible contributions to its success and those who in no less measure simply prayed in their hearts hoped and desired ones success, may God bless you.

I will like to thank Dr. J.Y Oricha my major supervisor for everything for his advice, encouragement for me becoming a good researcher. You thought me to do my work without fear. I will like to thank Prof. J.O Ojo my minor supervisor for his contribution from the beginning of the work. May God bless you for all the concern shown, advices given and support you rendered to me.

I will like to thank my parents: Mr. and Mrs. Zacchaeus Ajayi Ibitolu, my siblings, my Uncles in persons of Mr. and Mrs. Joseph Oladimeji Ibitolu and Mr. and Mrs Gbenga Ibitolu for your prayers. I would also thank Dr O. Ajayi of the Department of Chemcal Engineering for his fatherly advice, Bro Dan (Home Cell leader) for the support through prayers. I am grateful to you all that I don't have to meet any minimum standards to get your love and support.

I thank the Head of Department, Department of Electrical and Computer Engineering Dr. M.B. Muazu, for his leadership and for showing concern in the course of my research work. I will also like to thank Prof B.G Bajoga for his fatherly role and concern for all Msc and PhD students. I am also grateful to Dr. S.M. Sani, for his contributions to my success, A big thank you to Dr. B. Jimoh, Dr. D.D Dajab and Dr. Usman for all the advice they gave me in the course of my studies. Engr. Josiah for his encouragement to finish this work timely. Dr Sikiru Tajudeen Humble for his support in ensuring I finish this work timely. Thanks to Dr. O. Akinsami and Dr. S. Garba (the Departmental Post Graduate Coordinators) for their untiring efforts to seeing to the completion of our studies. Engr. Gbenga for being there for me with research papers to help my work and indeed all staff of the department of Electrical and Computer Engineering both

academic and non-academic, you have all contributed in no small measure in molding and making me the man that I am.

I will like to thank my wife Habibatu Emike Taiwo for her encouragement, prayers and support, you have been a wonder wife all along ensuring I never go hungry at the point of writing this thesis. I will like to thank my colleagues and friends for their support. The MSc. Electrical Engineering (Power Systems Option) class of 2008/2009: Uche, Mattews, Alhaji Sani of PHCN Mando, Engr Abiodun, Engr Zubeiru, Engr Mattew, Kolo Yetu. I am grateful to God to have met and known every one of you. To my very friend Emmanuel Handan Hyet there is no way to quantify the help you rendered to me during the course of my studies, God bless you all.

TABLE OF CONTENTS

Title Page

Declaration……....i

Certification……ii

Dedication……...iii

Acknowledgement.……iv

Table of Contents……....vi

List of Tables.……ix

List of Figures...……..x

List of Appendices……....xiii

Abbreviations and Symbols……..xiv

Abstract……xvi

CHAPTER ONE: INTRODUCTION……..1

1.1 Overview……...1

1.2 Statement of Problem. ……3

1.3 Aim and Objectives of the Study. ……..3

1.4 Significance of the Study……4

1.5 Thesis Outline. ……. ……...4

CHAPTER TWO: LITERATURE REIVIEW.....6

2.1 Introduction……..6

2.2 Review of Fundamental Concepts…….....6

2.2.1 Definition of Power Converter……6

2.2.2 Terminologies used to describe converter operations……..…..10

2.2.3 SEPIC basic concept…….....15

2.2.4 Bi-directional Converter basic concept……..…21

2.2.5 Permanent Magnet dc motor…….....24

2.3 Review of Similar Works……...26

2.4 Conclusion……..30

CHAPTER THREE: MATERIALS AND METHODS…….…….....31

3.1 Introduction……....31

3.2 Solar Insolation Data for Zaria ……..31

3.3 MATLAB/Simulink ……..32

3.4 Methodology ……...…...34

3.5 Model derivation and Design Considerations…….35

3.5.1 Model Derivation of a Complete System……..36

3.5.2 Steady State Equations……..41

3.5.3 Design Considerations……..…47

3.6 Simulation Equations……59

3.7 Conclusion……..60

CHAPTER FOUR: RESULTS AND ANALYSIS ……..…….61

4.1 Introduction……61

4.2 Steady State Analysis…….61

4.2.1 Harmonic Balance Technique Applied to SEPIC System……....61

4.2.2 Steady State Calculations…….……63

4.3 Results…….68

4.4 Conclusion …….…....83

CHAPTER FIVE: CONCLUSION AND RECOMMENDATIONS. ……....84

5.1Summary.……...…….....…..84

5.2Conclusion.……..…….....84

5.3 Limitation of the Study. ……85

5.4 Recommendations for Further Work …...……..85

LIST OF TABLES

Table 2.1 Truth table for switching function ……..….9

Table 2.2 Comparison of SEPIC with Bi-directional converter ……...24

Table 3.1 Frequency table for Solar insolation in Zaria from NASA……32

Table 3.2 Frequency Table for Solar Insolation in Zaria from ABUDECE weather workstation.32

Table 3.3 System Parameters…….57

LIST OF FIGURES

Figure 1.1 System Configuration…….2

Figure 2.1 Schematic block diagram of Power Converter……...7

Figure 2.2 Elementary dc to dc Converter (SEPIC)……....8

Figure 2.3(a) SEPIC Mode I circuit topology…….…….…9

Figure 2.3(b) SEPIC Mode II circuit topology……..…..9

Figure 2.3(c) SEPIC Mode IIII circuit topology…….…...10

Figure 2.4 Idealized waveform of dc to dc Converter …….…11

Figure 2.5(a) Reference Signal at a particular duty ratio of D=0.8……...12

Figure 2.5(b) Triangular Signal waveform……....12

Figure 2.5(c) Switching Function Signal……...12

Figure 2.6 Switching Function Signal of a typical Converter……..…13

Figure 2.7 SEPIC…….....16

Figure 2.8 Mode I Circuit Configuration……..…….16

Figure 2.9 Mode II Circuit Configuration……..…..…..17

Figure 2.10 Mode III Circuit Configuration…….....18

Figure 2.11 Bi-directional Converter…….....22

Figure 2.12 Mode I of Bi-directional Converter……....22

Figure 2.13 Mode II of Bi-directional Converter …….…22

Figure 2.14 Permanent Magnet dc motor……..25

Figure 3.1 MATLAB M-File Editor Interface……...33

Figure 3.2 Simulink Interface for Simulation……34

Figure 3.3 Detailed Configuration of the Studied System ……35

Figure 3.4 Schematic of SEPIC…….……....37

Figure 3.5 Bi-directional Boost Converter…….....38

Figure 3.6 Battery Structure……...39

Figure 3.7 Grid Topology…….....…40

Figure 3.8 Permanent Magnet dc Motor……....41

Figure 3.9 Algorithm for finding Steady State of the System……...46

Figure 3.10 Schematic of SEPIC…….…..…51

Figure 3.11 Schematic of Bi-directional Converter……...…55

Figure 4.1 Algorithm for finding Steady State and Ripple quantities of the SEPIC System …….…...67

Figure 4.2 Power versus Voltage Curve of the Solar panel……...68

Figure 4.3 Current versus Voltage Curve of the Solar panel ……....69

Figure 4.4 Voltage at Maximum power versus Solar Insolations……..70

Figure 4.5 Current at Maximum power versus Solar Insolations ……70

Figure 4.6 Output Current of the SEPIC versus duty ratio……....71

Figure 4.7 Motor Speed versus duty ratio with Load torque as a parameter (S = 245 W/m^2)…72

Figure 4.8 Motor Speed versus duty ratio with Load torque as a parameter (S = 850 W/m^2)…73

Figure 4.9 Battery Current, Bi-directional Output Current, Armature current versus duty ratio..74

Figure 4.10 Battery Current versus duty ratio of Bi-directional Converter……...75

Figure 4.11 Torque versus Speed…….……..76

Figure 4.12 SEPIC Output Voltage …….…….....77

Figure 4.13 Steady State average quantities for state variables…….....78

Figure 4.14 Steady State average quantities for state variables (devices current and voltage)….79

Figure 4.15 Steady State average ripple quantities (State Variables)……....80

Figure 4.16 Steady State ripple quantities (devices current and voltage)……..……81

Figure 4.17 SEPIC Output Voltage versus time……....…82

Figure 4.18 Motor Speed versus time……82

Figure 4.19 Grid Current versus time……83

LIST OF APPENDICES

APPENDIX A: SEPIC Side……..……..…90

APPENDIX B: Maximum Power point Determination…….……96

APPENDIX C: Bi-directional dc-dc Converter Model……...…..98

APPENDIX D: Harmonic Balance Technique Analysis…….....101

APPENDIX E: System Parameters…….....108

APPENDIX F: Program Listing…….……..…110

APPENDIX G: Simulink Model for Simulation Studies…….……125

APPENDIX H: NASA Hourly Solar Insolation Data in Zaria…….…...126

ABBREVIATIONS AND SYMBOLS

ABUDECE	Ahmadu Bello University Department of Electrical and Computer Engineering
dc	Direct Current
ac	Alternating Current
IEEE	Institute of Electrical and Electronic Engineers
NASA	National Aeronautics and Space Administration
PV	Photo voltaic
KVL	Kirchhoff's Voltage Law
KCL	Kirchhoff's Current Law
S1, S2, S3, S4	Switching functions
CCM	Continuous Current Mode
DCM	Discontinuous Current Mode
PM	Permanent Magnet
MATLAB	Matrix Laboratory
MPP	Maximum Power Point
W (.)	Lambert Function
V_b	Battery Voltage
DG	Distributed Generation
SC	Super Capacitor
FC	Fuel Cell

PPPT	Parallel Power Processing Topology
SEPIC	Single Ended Primary Inductance Converter
$p = \frac{d}{dt}$	Operator

ABSTRACT

This research studied a circuit topology of a solar based Single Ended Primary Inductance Converter (SEPIC) system and a battery furnishing a permanent magnet dc motor with current via a dc grid. The complete model equations of the entire system were derived. Harmonic balance technique was used to determine the converter steady state and ripple quantities. Analyses investigating the relationship of the converter state variables as a function of its duty ratio were developed. Results show that operating the converter between 0 – 0.4 duty ratio give best system performances. On the other hand, results show that operating the converter above this range limits the converter optimal performance. The consequence of operating the system with duty ratios above 0.4 is that the ripples in the voltage and current waveforms increase. More so, results also show that for a steady state current of 12 A, for the permanent magnet dc motor in a period of low solar insolation, operating a Bi-directional converter at specific values of duty ratio causes the battery to discharge much faster compare to operating at duty ratio of 0.78. Two solar insolation data for Zaria (Lat 11.067^0N Long 7.7^0E) was obtained from National Aeronautics and Space Administration (NASA) for a period of January to December 2013 and another ground level captured from Electrical & Computer Engineering Department using the data acquisition module (model TQ 140876-002) from August 17 to September 24, 2014. These insolation data from both stations were used to validate the efficiency of the proposed design. The targeted load demand of approximately $2441.43W$ was achieved. This represents 97.66 % of the load demand designed for in this research. The designed solar energy system contributed 70% of the power to the load, while the battery supplied 30% of the load demand power. An effective hybrid storage system based on solar and battery was achieved, which met the designed objective of this research.

CHAPTER ONE

INTRODUCTION

1.1 Overview

Solar fed systems can be used as an alternative source of power in meeting the electricity requirement of some rural dwellers not connected to the national grid in Nigeria. Their application area is limited to low power level such as street lighting, battery charging, irrigation, etcetera. The application area nevertheless is further limited to difficulty in terrain, mountainous hills, topography of these rural areas just to mention but few. A suggestion for meeting the electricity requirement of these rural dwellers and the need for high power application area is to use a solar fed SEPIC system viz a viz a storage energy system **(Thouthong, 2011; Veerachary, 2012)**. The purpose of the SEPIC is twofold: (i) To buck or boost varying output voltage from the solar module to a voltage suitable for meeting the requirement of the dc grid. (ii) Furnish the dc load with power via a dc grid linking the output of the converter and the dc load. However, the approach in (ii) requires a battery in mitigating the load power demand for short fall in solar insolation. To determine the performance of a dc grid SEPIC based solar electricity for dc load equipped with a battery, the method of harmonic balance technique is used in the analysis of the SEPIC state variables (**Sangho *et al,* 2006**). The method is different from that of averaging technique in that it basic application in addition to solving for average values of the SEPIC variables can further be use to:

(i) Predict ripples

(ii) design filter

(iii) predict ripple dynamics

The harmonic balance technique consequent to the fact that it is assumed the converter variables is decomposed into average and fundamental ripple component. This allows for studying the steady state current from the output of the SEPIC. Furthermore, the current

supplied to the load are greatly influenced by the current supplied from the battery when the solar insolation is low. It is shown that the current drawn by the load is the sum total of the current from the SEPIC system and the battery current. For this reason the accompanying procedure is to study the general influence of the converter duty ratio on the load current. However, in considering the dc to dc power converter for this study as a practical example, under certain conditions of duty ratio variations, the current contribution of the solar and battery can only be met to some values of duty ratio. The harmonic balance technique permit the study of the ripple and steady state quantities of the SEPIC duty ratio variations between [0,1]. Figure 1.1 shows a block diagram of a solar fed SEPIC based system feeding a load via a dc grid equipped with a storage system. This thesis is focused on modeling and simulation of a dc grid SEPIC based electricity for a dc load, for a range of duty ratio variation of the SEPIC. Equations are presented in proper modes for each sub-system. In arriving at the system model based on different differential equations describing the modes of operation of the system, it is possible to achieve sufficient understanding of the system and to develop insight into the general influence of the various parameters on the behavior of the system.

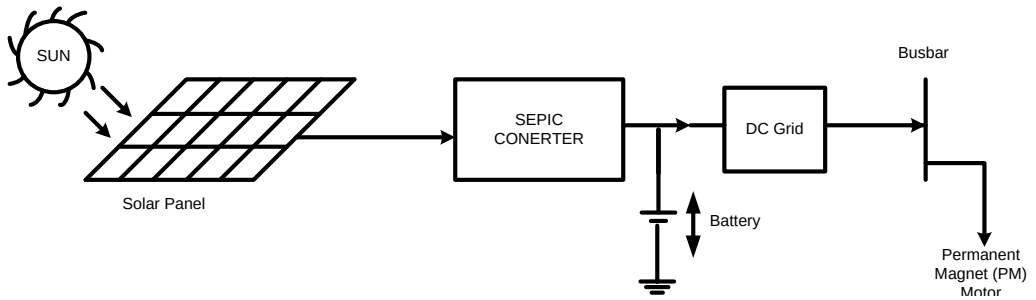


Figure 1.1 System Configuration

1.2 Statement of Problem

The published works have shown techniques in supplying electricity to dc distribution system using varied kind of converter as a link to supply electricity to load. There have been efforts to (i) enhance the power handling capacity of the dc link of a dc distribution system using a variant converters. (ii) enhance the power capabilities of constituent converters through the implementation of various control algorithms (iii) utilize alternative energy sources (mostly solar) to supply current to a dc load in a dc distribution network. However, using a solar based SEPIC system together with a battery system to supply dc load with current via a dc grid system for a range of converter duty ratio variations has not been addressed. In the light of this, there is need for a circuit topology that ensures real time collaboration between the solar PV cells and the battery energy storage system to furnish a dc load with power. This solar fed SEPIC system should be in addition to a storage system (battery) be able to meet part of the load current should there be low solar insolation. It is based on this that the research work is undertaken.

1.3 Aim and Objectives of the Study

The aim of this work is to study the overall system behaviour of a solar fed converter system feeding a dc load i.e permanent magnet (PM) dc motor and battery energy system.

The objectives are as follows:

(i) Development of the mathematical model that describes the dynamic and steady state performance of system.

(ii) Implementation of the principle of harmonic balance technique in finding the steady and ripple quantities of the SEPIC.

(iii) Determination of the terminal characteristics of the converter under steady state for continuous current mode (CCM) of the converter.

(iv) Determination of the systems parameters and dynamic analysis via simulation using MATLAB.

1.4 Significance of the Study

The current effort is focused on using a SEPIC based solar system and a battery to service a permanent magnet dc motor with power via a dc grid system. The work has been able to show the following:

(i) The contribution of the current delivered to the dc motor for some specific range of duty ratios of the Bi-Directional converter in a case of low solar insolation.

(ii) The steady state average quantities and steady state ripple quantities of the converter variables for a range of duty ratio variations.

1.5 Thesis Outline

The remaining part of this thesis is organized as follows:

Chapter Two presents a detailed literature review for the research. The review is divided into two viz. review of fundamental concepts and review of similar works. The necessity of the present work is highlighted within the context of reviewed works. Chapter Three presents the materials used and method adopted. Data and software tools have been used for the work. A detailed circuit configuration is given and the mode switching operations briefly discussed. Also, certain design considerations necessary for the determination of the parameters of the system are presented. Chapter Four shows the result of the steady state analysis and the Harmonic balance technique study carried out on SEPIC system. Various plots of different

analysis carried out are presented and discussed. A simulation study of certain aspects of the system is also included. Chapter Five reports the important conclusions of the thesis work. Recommendations are also made for future work. At the end of the thesis, cited references and appendices are provided.

CHAPTER TWO

LITERATURE REVIEW

2.1 Introduction

This chapter set forth the necessary background knowledge of the study system. It presents a review of pertinent concepts and a review of previous works done similar to the study area. A description of the various sub-systems of the study, their principle of operation, the constraints of circuit configuration and some methods of control, has been provided. Finally, a critical and systematic review of different articles similar to the study is provided.

2.2 Review of Fundamental Concepts

This section presents some basics definitions and concepts. It also outlines the underlying concepts relevant to the understanding of the study system.

2.2.1 Definition of Power Converter

A dc to dc power converter is a device for converting power at one voltage profile to power at another voltage profile. Systems that are formed out of the power converters can be used for power motor drives, automotive ignitions, washing machines, space power supply just to mention but few. The application can also be extended to hybrid electric vehicle, battery charger, laser power supply **(Ned, 2003)**. This is achieved by using a transistor switched successively many times within a switching period of T in seconds. where $T = \frac{1}{f}$ and f is the switching frequency in Hz. The converter device should have the following characteristics: A transistor with fast switching capabilities, the transistor should be capable of operating as a switch, the converter system should have low switching loss and the efficiency should be high, the system should have small weight and small volume. The

conversion process of the power converter can be classified based on the following **(Ned, 2003)**:

(i) dc to dc converter- The process involves varying the voltage magnitude

(ii) dc to ac – The process involves varying the voltage magnitude and that of the frequency

(iii) ac to ac – the process involves varying of the phase angle

The power converter system can be buck, boost, and buck-boost variant. If the input voltage magnitude is greater than the output voltage magnitude, the converter system is a buck converter system. If the input voltage magnitude is less than the output voltage magnitude, the converter system is a boost converter. If the input voltage magnitude can either be raised or lowered with respect to the output voltage magnitude, the converter system is a buck-boost. Figure 2.1 shows a block diagram of a power electronic converter system.

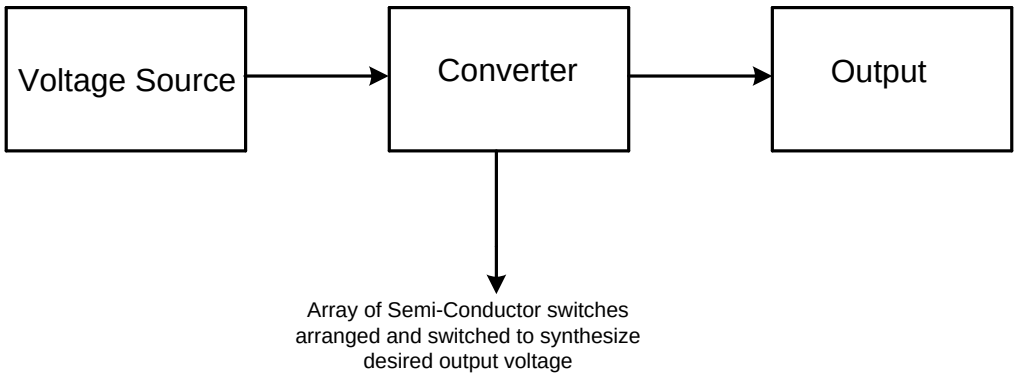


Figure 2.1 Schematic block diagram of power converter

In order to have a basic understanding of elementary dc to dc converter, take for example a typical buck-boost converter referred in Figure 2.2. S_1 and S_2 are switches whose status referred are defined within the interval [0 1]. In the mode I of the circuit configuration of Figure 2.2, new circuit topology is derived as shown in Figure 2.3 (a). Where switch S_1 is on

and S_2 is off. S_1 is assigned numeric value of one (1) when on and S_2 is assigned numeric value of zero (0) when off. Also, in the mode II of the same Figure 2.2, new circuit topology is also formed when S_1 is off and S_2 off., see Figure 2.3(b). In a situation where the two switches are on, it is define by a new circuit topology of Figure 2.3 (c). Table 2.1 denotes the truth table for the switching function depicting status of switch S_1 and switch S_2. CCM in the remark column of table 2.1 denote continuous current mode. DCM denote discontinuous current mode.

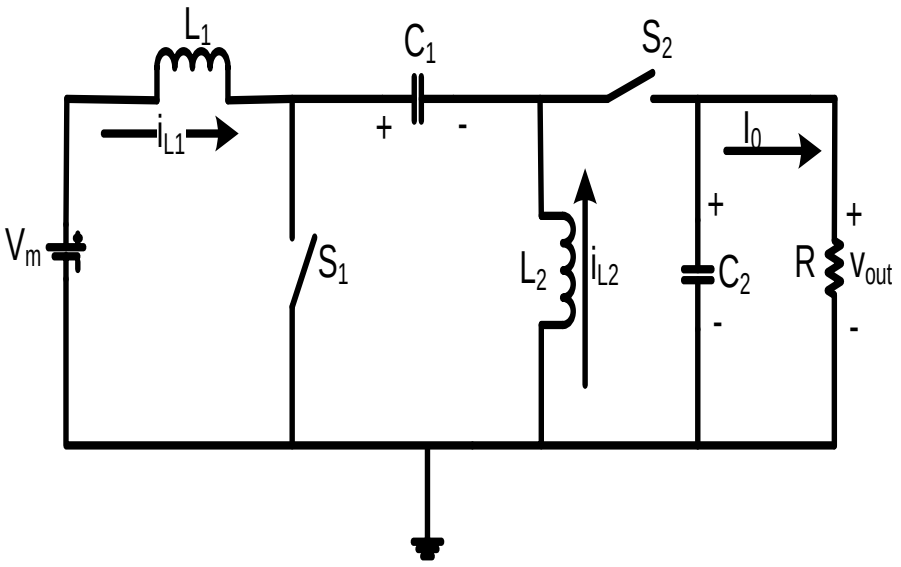


Figure 2.2 Elementary dc to dc Converter (SEPIC)

Table 2.1 Truth table for switching function

S_1	S_2	Remark
0	0	NULL STATE
0	1	CCM
1	0	CCM
1	1	DCM

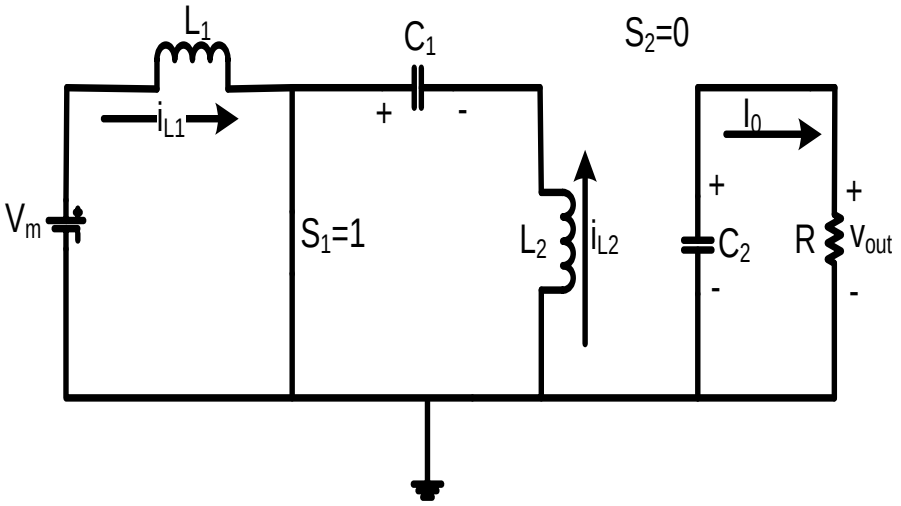


Figure 2.3 (a) SEPIC Mode I, circuit topology

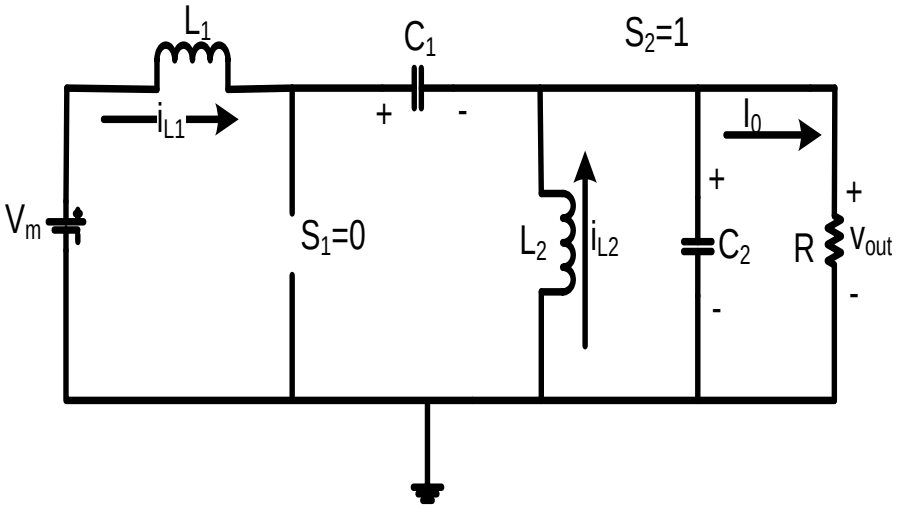


Figure 2.3 (b) SEPIC Mode II, circuit topology

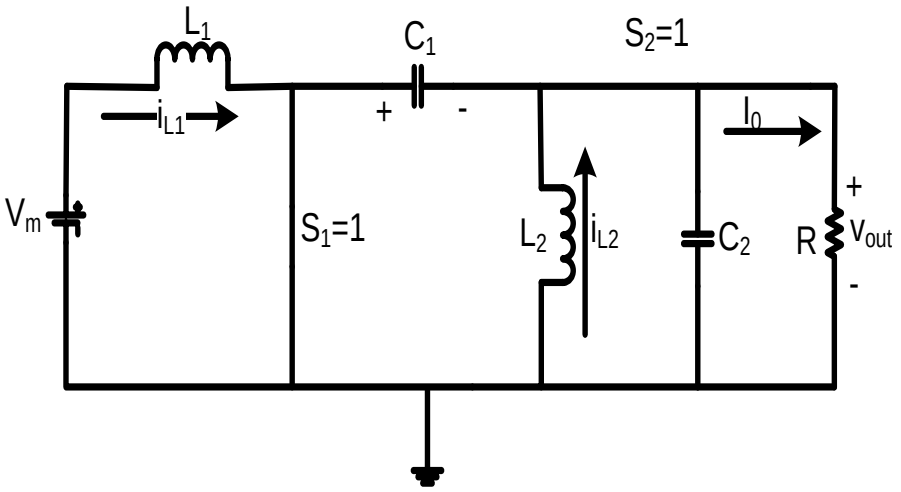


Figure 2.3 (c) SEPIC Mode III, circuit topology

2.2.2 Terminologies Used to Describe Converter Operation

There are two operating regimes of the dc to dc converter operations described in Figure 2.2 namely: (i) Continuous current mode (CCM) (ii) Discontinuous current mode (DCM)

CCM

In this mode of operation the converter inductor current never falls to zero. This mode of operation can be visualized by the idealized waveform of Figure 2.4(b).

DCM

In this mode of operating regimes the inductor current always fall to zero just before the end or at the end of the operating period. This mode of operation can be visualized by the idealized waveform of Figure 2.4(c).

Duty Cycle (D)

This refers to the length of time the converter switch is on taken the average for a full period T of the converter operations. If the switching period is T from the idealized waveform of

Figure 2.4. Mode I for the converter of Figure 2.3 only lasts for a period of $t_1 = DT$, and mode II last for a period $t_2 = (1-D)T$, such that $t_1 + t_2 = T$ for all values of t. Owing to the fact that the pulses of Figure 2.4 (a) are switched at a very high frequency, un-wanted harmonic ripples are generated in the voltage and current waveform of the power converter, which are smoothen out using an L-C filter which is seen at the output section of the converter.

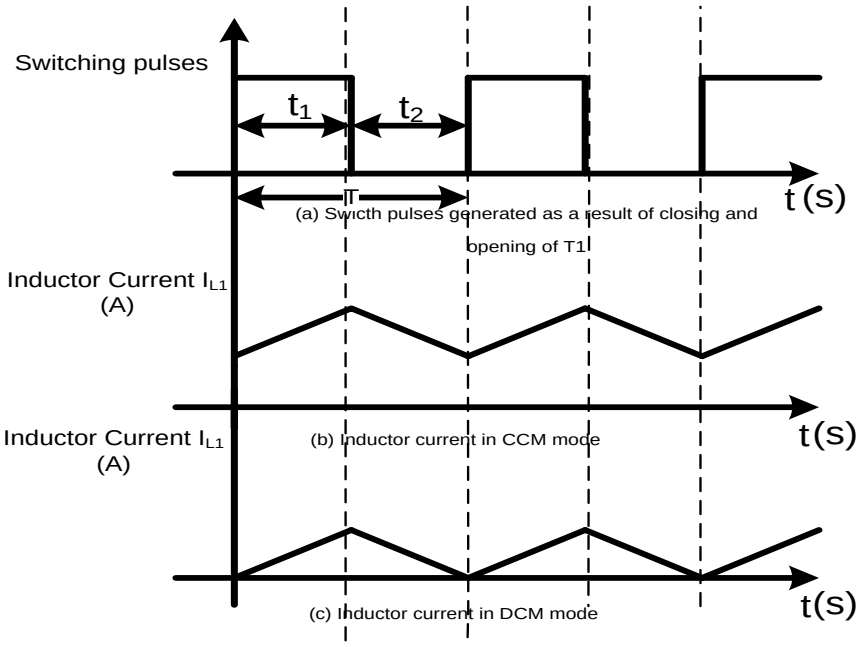


Figure 2.4 Idealized Wave form of dc to dc Converter

Switching Function Generation

A dc to dc power converters normally interface voltage sources with loads. The desired output of the converters can be synthesized for any application depending on the needs of such application: be it voltage magnitude, frequency or phase angle variations. In the case of dc to dc converter in this study for instance, the voltage magnitude is what is varied. This output is obtained by the switching ON and OFF the switches in the converter of Figure 2.2

in some form of repetitive pattern shown in Figure 2.4(a). So, a train of pulses of amplitude one (1) is applied to the switching device. This train of pulses is referred to as the switching function. When the switching function is 1, the switch is turned ON and when it is zero, it is turned OFF. The desired output characteristics of the converter (voltage magnitude, output voltage ripple quantity) are obtained by the pattern of these repetitive groups of pulses. This is obtained by manipulating or comparing a triangular signal in Figure 2.5(b) with a constant reference signal in Figure 2.5 (a) to give the switching signals in Figure 2.5 (c). Figure 2.5 shows an example of a switching function waveform for switching S_1 and S_2 of the SEPIC circuit topology. Figure 2.6 shows a simple switching function signal enlarged version.

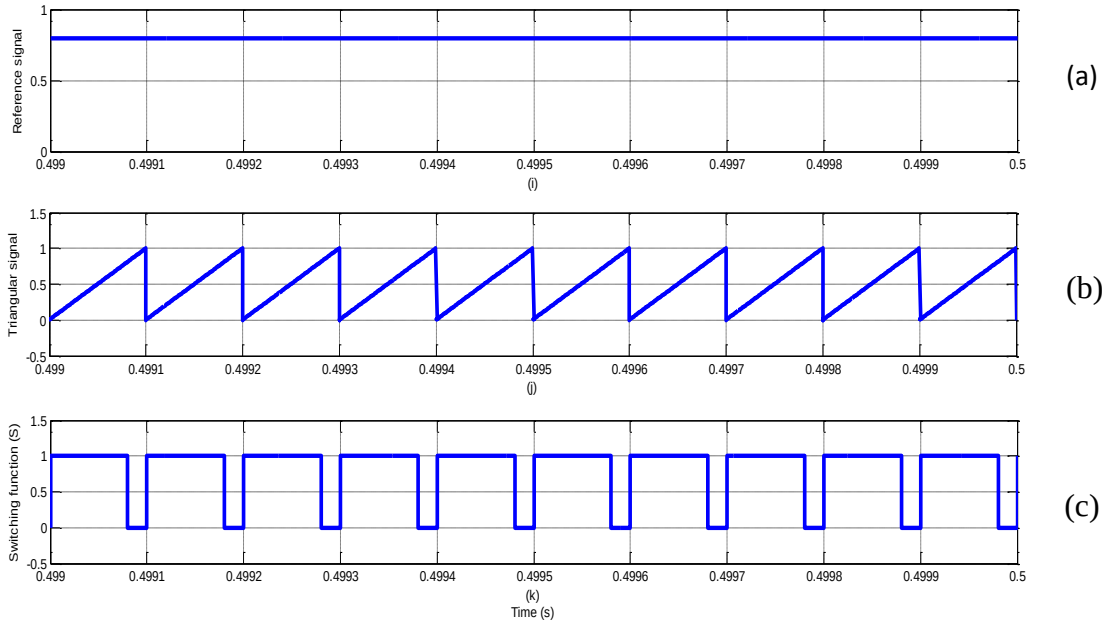


Figure 2.5 (a) Reference Signal at D=0.8, (b) Triangular Signal, (c) Switching Function Signal

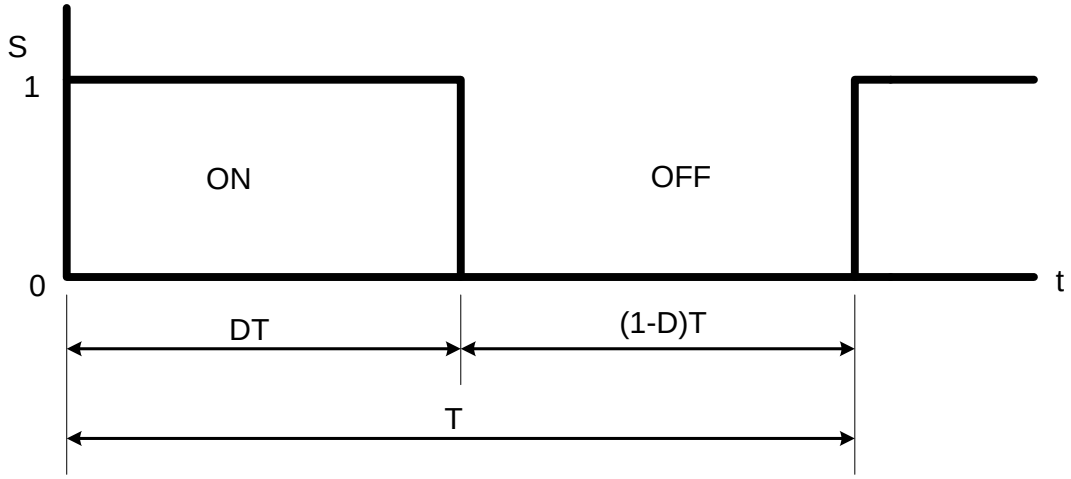


Figure 2.6 Switching Function of the Converter

Fourier Series Analysis Of The Switching Function

The switching function when applied to modes of the converters discussed in section 2.2.3 presents some difficulties in getting analytical close-form solutions. In solving this problem Fourier analysis is applied to get rid of these discontinuities **(Ned, 2003)**. The two modes of operation of the converter discussed for one switching cycle are as given in Figure 2.6. The expression for the average (dc) components of the switching function can be found for this analysis. The function so derived is used for the derivation of the dynamic equation for the average and ripple quantities using harmonic balance Technique which will be discussed in Chapter four. It is remarked that this technique adopted is an effective method for studying the steady state of the system comprising the average and ripple quantities of the SEPIC system.

The switching function can be discretize to emulate the function as describe below:

$S = 1$ For $t \in (0, DT)$ and $S = 0$ for $t \in (DT, T)$. This periodic sequence of switching function as describe by Figure 2.6, can be represented by a trigonometric series represented in the form given by equation (2.1). **(Edwin, 2006).**

$$f(t) = a_0 + \sum_{n=1}^{\infty} D_n \sin(n\omega_s t + \varnothing_n) \qquad (2.1)$$

Where:

$$\left.\begin{aligned} a_0 &= \frac{1}{T}\int_0^T f(t)\,dt \\ a_n &= \frac{2}{T}\int_0^T f(t)\cos(n\omega_s t)\,dt \\ b_n &= \frac{2}{T}\int_0^T f(t)\sin(n\omega_s t)\,dt \\ D_n &= \sqrt{a_n^2 + b_n^2} \\ \varnothing_n &= \tan^{-1}\left(\frac{a_n}{b_n}\right) \end{aligned}\right\} \qquad (2.2)$$

T is the period, represented as $f_s = \frac{1}{T}$ where f_s denote the switching frequency. ω_s is the radian frequency define by $\omega_s = 2\pi f_s = \frac{2\pi}{T}$

For $n = 1$

The average value and the ripple quantities can be quickly found. For our case,

$$f(t) = \begin{cases} 1 & 0 \le t \le DT \\ 0 & DT \le t \le T \end{cases} \qquad (2.3)$$

$$
\left.
\begin{aligned}
a_0 &= \frac{1}{T}\left(DT-0\right)=D \\
a_0 &= d_{10}=D \\
a_1 &= \frac{2}{T}\int_0^{DT} f\left(t\right)\cos\left(n\omega_s t\right)dt \\
a_1 &= \frac{1}{\pi}\sin\left(2\pi D\right) \\
b_1 &= \frac{2}{T}\int_0^{DT} f\left(t\right)\sin\left(n\omega_s t\right)dt \\
b_1 &= \frac{1}{\pi}\left[1-\cos\left(2\pi D\right)\right] \\
d_{11} &= \frac{1}{\pi}\sqrt{\left(\sin\left(2\pi D\right)\right)^2+\left(1-\cos\left(2\pi D\right)\right)^2}=\frac{1}{\pi}\sqrt{2\left(1-\cos\left(2\pi D\right)\right)}
\end{aligned}
\right\} \qquad (2.4)
$$

2.2.3 SEPIC Basic Concept

A good way to begin the study of the SEPIC is to take a closer look at the circuit topology in Figure 2.7. By successively opening and closing the power transistor switch T_1 for necessary length of times, the output voltage is controlled. There are three modes of operation of this converter. Let S_1 and S_2 denote the switching function of transistor T_1 and diode D_2. In Figure 2.7, the transistor is the active switch and the diode is the passive switch. During the first switching interval, the inductor current i_{L1} and i_{L2} increases. During the next switching interval, the inductor current i_{L1} and i_{L2} falls. The resulting waveform is shown in the idealized waveform as shown in Figure 2.4. In power electronics, dc-dc converters are to a great extent efficient based on the following:

(1) The desired output voltage levels are synthesized by repetitive switching of an active switch linking the given source voltage side with the output side.

(2) Pulses resulting from the action are filtered using filter element L and C.

(3) Switching can be realized using transistors and this elements show non-linear properties.

A set of differential equation describes the system for each mode of operations. Consider the SEPIC shown in Figure 2.7.

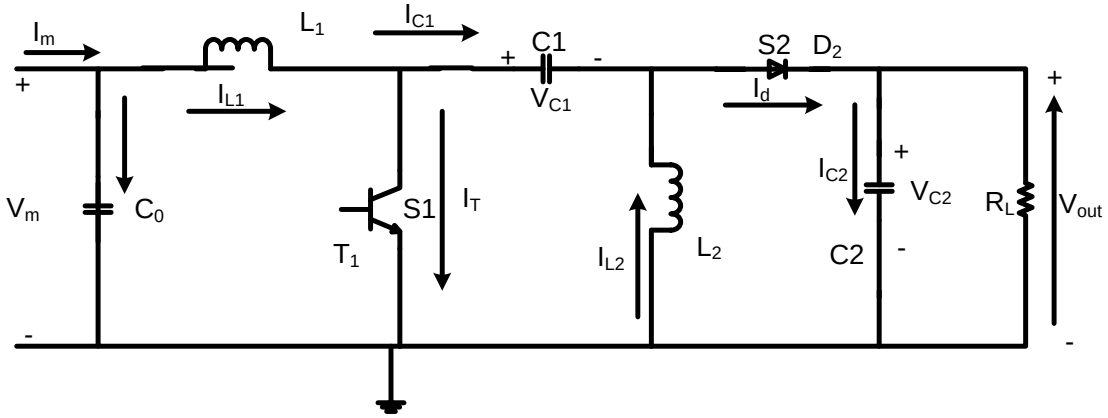


Figure 2.7 SEPIC

For Mode I,

S_1 is on and S_2 is off, the circuit reduces to what is obtained in Figure 2.8, the KVL and KCL equations are; note, $p = \frac{d}{dt}$; throughout this work

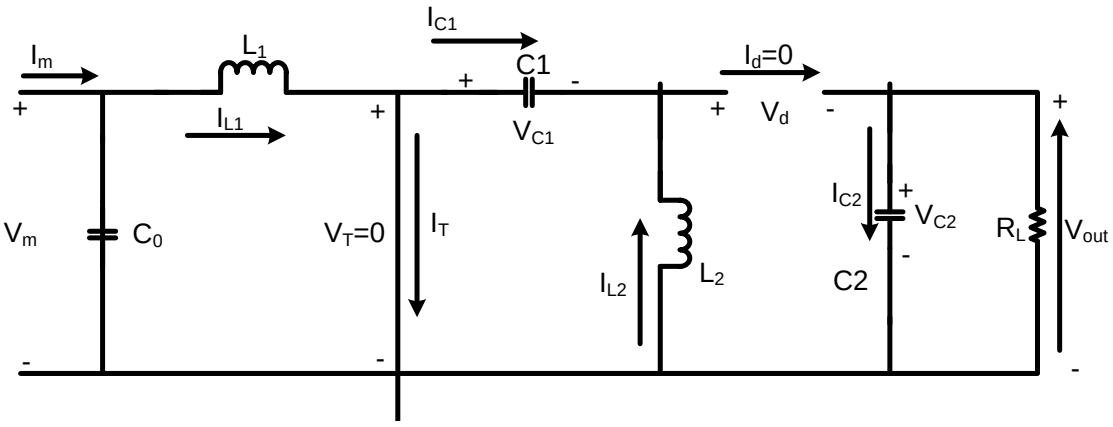


Figure 2.8 Mode I Circuit Configuration

$$\left.\begin{aligned} C_0 pv_m &= i_m - i_{L1} \\ L_1 pi_{L1} &= v_m \\ L_2 pi_{L2} &= v_{C1} \\ C_1 pv_{C1} &= -i_{L2} \\ C_2 pv_{C2} &= -\left(\frac{1}{R_L}\right) v_{out} \\ v_{C2} &= v_{out} \end{aligned}\right\} \qquad (2.5)$$

Devices current and voltages for this mode are:

$$\left.\begin{aligned} i_T &= i_{L1} + i_{L2} \\ v_T &= 0 \\ i_d &= 0 \\ v_d &= -v_{C2} - v_{C1} \end{aligned}\right\} \qquad (2.6)$$

For Mode II,

S_1 is off and S_2 is on, the circuit reduces to what is obtained in Figure 2.9.

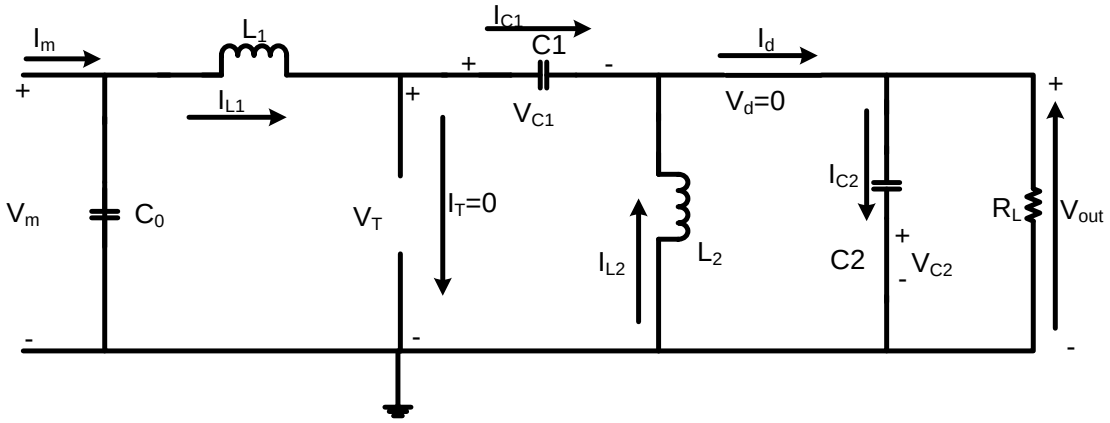


Figure 2.9 Mode II Circuit Configuration

The KVL and KCL equations are;

$$\left.\begin{aligned} L_1 pi_{L1} &= v_m - v_{C1} - v_{C2} \\ L_2 pi_{L2} &= -v_{C2} \\ C_1 pv_{C1} &= i_{L1} \\ C_2 pv_{C2} &= \left(i_{L1} + i_{L2}\right) - \left(\frac{1}{R_L}\right) v_{out} \\ v_{C2} &= v_{out} \end{aligned}\right\} \qquad (2.7)$$

Devices current and voltages for this mode are:

$$\left.\begin{aligned} i_T &= 0 \\ v_T &= v_{C2} + v_{C1} \\ i_d &= i_{L1} + i_{L2} \\ v_d &= 0 \end{aligned}\right\} \qquad (2.8)$$

For Mode III, Discontinuous current mode (DCM)

S_1 and S_2 is on, the circuit reduce to what is obtained in Figure 2.10.

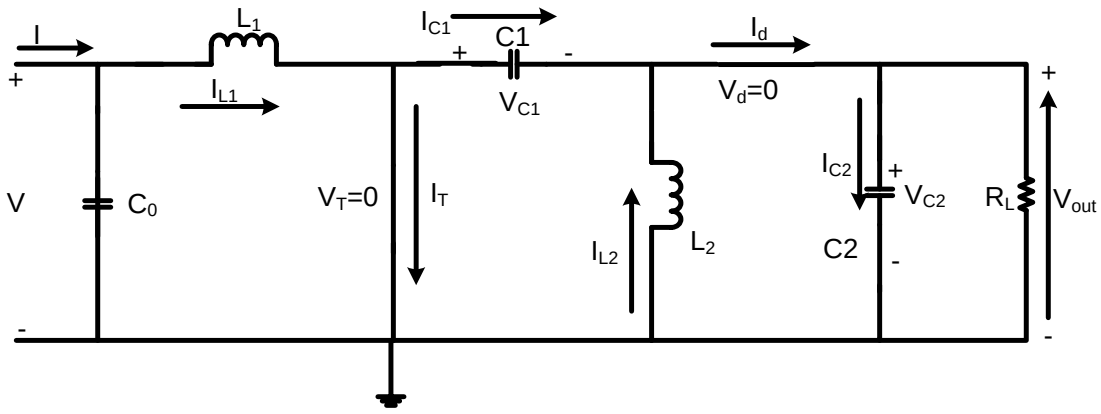


Figure 2.10 Mode III Circuit Configuration

The KVL and KCL equations are;

$$\left.\begin{aligned} L_1 p i_{L1} &= v_m \\ L_2 p i_{L2} &= -v_{C2} \\ C_1 p v_{C1} &= i_d - i_{L2} \\ C_2 p v_{C2} &= -\left(\frac{1}{R_L}\right) v_{out} \\ v_{C2} &= -v_{out} \end{aligned}\right\} \qquad (2.9)$$

Devices current and voltages for this mode are:

$$\left.\begin{aligned} i_T &= i_{L1} + i_{L2} - i_d \\ v_T &= 0 \\ i_d &= i_{C1} + i_{L2} \\ v_d &= 0 \end{aligned}\right\} \qquad (2.10)$$

Averaging The Three Modes Of Operations

Applying switching function to the state equations:

$$S_1 + S_2 + S_3 = 1, \qquad (2.11)$$

Where S_1 and S_2 switching function for continuous current mode (CCM). S_3 is the switching function for discontinuous current mode (DCM) of the converter operation.

Multiply equations (2.5)-(2.6) by S_1, equations (2.7)-(2.8) by S_2 and equations (2.9)-(2.10) S_3 and rewriting the equation in compact form yields:

$$\left.\begin{aligned} L_1 p i_{L1} &= v_m - S_2\left[v_{C2} + v_{C1}\right] \\ L_2 p i_{L2} &= S_1 v_{C1} - \left[S_2 + S_3\right] \times v_{C2} \\ C_1 p v_{C1} &= -i_{L2} S_1 + S_2 i_{L1} - S_3 i_{L2} + S_3 i_d \\ C_2 p v_{C2} &= S_2\left(i_{L1} + i_{L2}\right) - \left(\frac{1}{R_L}\right) v_{out} \\ v_{C2} &= v_{out} \end{aligned}\right\} \qquad (2.12)$$

Devices current and voltages are;

$$\left.\begin{aligned} i_T &= (S_1 + S_3)(i_{L1} + i_{L2}) - S_3 i_d \\ v_T &= S_2\left[-v_{C2} + v_{C1}\right] \\ i_d &= S_2 i_{L1} + i_{L2}(S_2 + S_3) + S_3 i_{C1} \\ v_d &= S_1\left[-v_{C2} - v_{C1}\right] \end{aligned}\right\} \tag{2.13}$$

For CCM mode $S_3 = 0$. So only S_1 and S_2 is considered for the modes. Equation (2.5)-(2.13) reduces to equation (2.14)- (2.15) But for DCM mode all the three switching variable function S_1, S_2, S_3 are all considered. The dynamic equations are:

$$\left.\begin{aligned} pi_{L1} &= \frac{1}{L_1}\left(v_m - (1 - S_1)\left[v_{C2} + v_{C1}\right]\right) \\ pi_{L2} &= \frac{1}{L_2}\left(S_1 v_{C1} - (1 - S_1) v_{C2}\right) \\ pv_{C1} &= \frac{1}{C_1}\left(-i_{L2} S_1 + (1 - S_1) i_{L1}\right) \\ pv_{C2} &= \frac{1}{C_2}\left((1 - S_1)(i_{L1} + i_{L2}) - \left(\frac{1}{R_L}\right) v_{out}\right) \\ v_{C2} &= v_{out} \end{aligned}\right\} \tag{2.14}$$

Devices current and voltage switching function are;

$$\left.\begin{aligned} i_T &= (S_1)(i_{L1} + i_{L2}) \\ v_T &= (1 - S_1)\left[-v_{C2} + v_{C1}\right] \\ i_d &= (1 - S_1) i_{L1} + i_{L2}(1 - S_1) \\ v_d &= S_1\left[-v_{C2} - v_{C1}\right] \end{aligned}\right\} \tag{2.15}$$

Equations (2.14) and (2.15) could be used for simulation to study the dynamic behavior of the SEPIC.

2.2.4 Bi-directional Converter Basic Concept

A good way to begin the study of the Bi-directional converter is to take a closer look at the schematic circuit in Figure 2.11. Let S_3 and S_4 denote the switching function of transistor T_3 and T_4. There are two operating regimes of the converter namely: Charging and discharging regimes. During the charging regime, transistor T_3 is on and T_4 is off. The battery is charged via the diode across T_3. Inductor L_4 and C_b serves as a filter to remove unwanted ripples present in the charging current during charging. During the discharging regime; there are two mode of operation of this converter shown in Figure 2.12 and Figure 2.13. During the first switching interval, T_3 is off and T_4 is on. The new circuit topology for this mode is as shown in Figure 2.12. During the next switching interval, T_3 is on and T_4 is off. The new circuit topology is as shown in Figure 2.13. A set of differential equation which describes the system for each mode of operations is derived and given by equation (2.16) and (2.17).

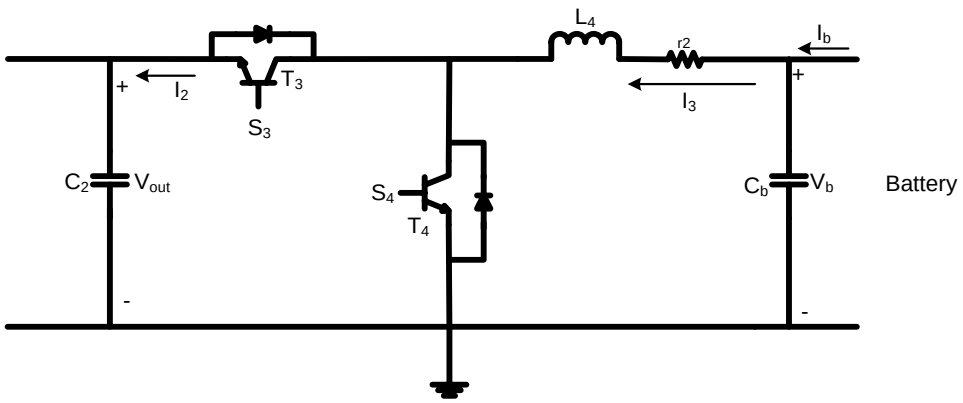


Figure 2.11 Bi-Directional Converter

In mode I,

S_4 is on and S_3 is off, the circuit of Figure 2.11 reduces to what is obtained in Figure 2.12, the KVL and KCL equations are; note, $p = \frac{d}{dt}$; throughout this work

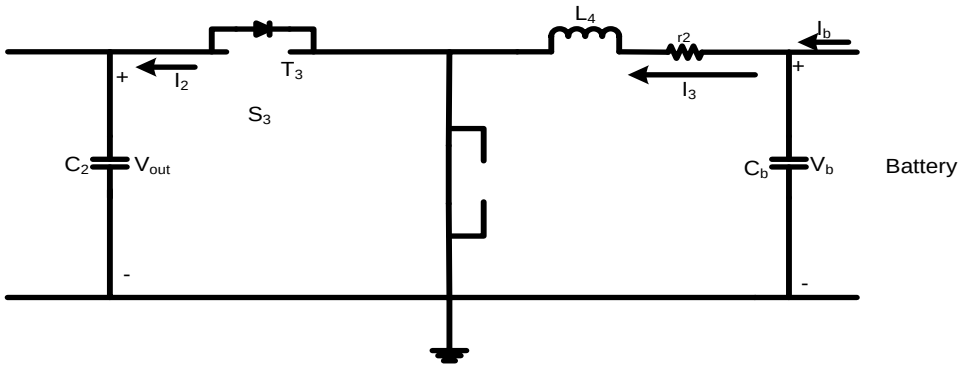


Figure 2.12 Mode I of Bi-Directional Converter

$$\left.\begin{aligned} C_b p v_b &= i_b - i_3 \\ L_4 p i_3 &= v_b - i_3 r_2 \\ i_2 &= 0 \end{aligned}\right\} \qquad (2.16)$$

In Mode II,

S_4 is off and S_3 is on, the circuit of Figure 2.11 reduces to what is obtained in Figure 2.13.

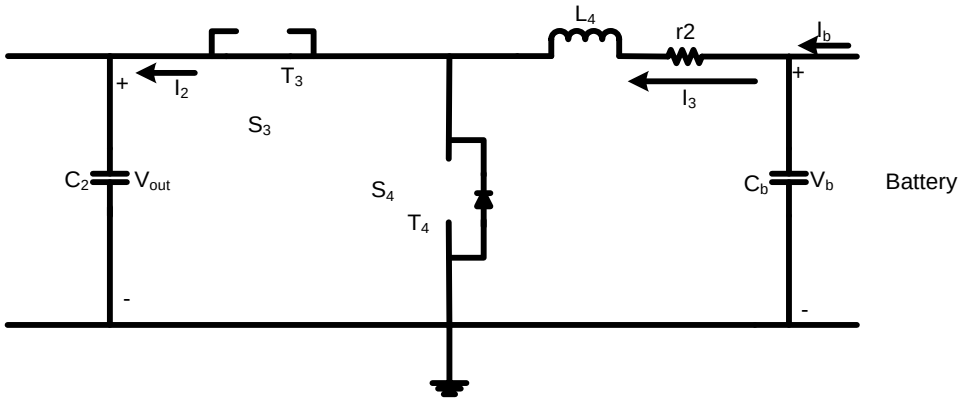


Figure 2.13 Mode II of Bi-Directional Converter

The KVL and KCL equations are;

$$\left.\begin{aligned} C_b p v_b &= i_b - i_3 \\ L_4 p i_3 &= v_b - v_{out} - i_3 r_2 \\ i_2 &= i_3 \end{aligned}\right\} \tag{2.17}$$

Averaging The Two Modes Of Operations

Applying switching function to the state equations based on constraint equation:

$$S_3 + S_4 = 1, \tag{2.18}$$

Multiply equation (2.16) by S_4, equation (2.17) by S_3 and rewriting the equation in compact form yield.

$$\left.\begin{aligned} C_b p v_b &= i_b - i_3 \\ L_4 p i_3 &= v_b - (1 - S_4) v_{out} - i_3 r_2 \\ i_2 &= (1 - S_4) i_3 \end{aligned}\right\} \tag{2.19}$$

Equation (2.19) could be used for simulation to study the dynamic behavior of the Bi-directional converter.

To understand the distinct difference between the SEPIC and Bi-directional converter refer to Table 2.2.

Table 2.2 Comparison of SEPIC with Bi-Directional Converter

SEPIC	Bi-directional Converter
i) Power transfer is from input to output only through the converter	i) Power transfer is from input to output or vice-versa
ii) The topology constitute one transistor and one diode	ii) The topology constitute two transistor one of which operate in one mode together with the other anti-parallel diode to furnish power to the load
iii) Can operate in CCM and DCM mode	iii) `Can only operate in CCM mode and not DCM,

For SEPIC and Bi-directional converter system to operate in CCM the following conditions must be met:

i) Inductor current never goes to zero. Otherwise CCM is not guaranteed
ii) Ripple current should be small as possible such that $i(t) = I$ at steady state
iii) The switching frequency of the devices should be far much greater than the corner frequency of the storage devices in the circuit.

The major functions of the SEPIC interfaced to a PV are three fold:

i) Step-up the variable PV output voltage to upper voltage of the dc bus
ii) Regulate the varying dc output voltage of the panel
iii) Implementation of the maximum power point of the solar panel.

The energy storage function is two-fold:

i) Mitigation of the variability and intermittency of PV power generating system by ensuring the load is fed with current from the battery if solar not available.
ii) Load leveling that is, meeting the electricity of the load in a period of low insolation with electricity stored in battery during period of low electricity demand.

The Bi-directional converter function is in two-fold:

i) Allowing power to flow in both forward and backward direction

ii) Control of the power flow between the dc bus and battery by adjusting the converter duty ratio.

2.2.5 Permanent Magnet dc Motor

Figure 2.14 shows a circuit representation of a permanent magnet dc motor. When compared to other dc motor of its kind take for example series dc motor, shunt dc motor, self excited dc motor, present some advantages. The advantages are due to the following characteristics:

(i) It can produce high torque at low speed

(ii) There is no need for external excitation as the permanent magnet in them supplies the required flux

(iii) It is very rugged, compact and can adapt to wide range of power sources.

(iv) The Torque-Speed characteristic of the motor is approximately linear.

Based on these aforementioned itemized characteristics, the dc motor is used in this work as a load and it torque speed characteristics are studied for some specific solar insolation and varied duty ratio variations.

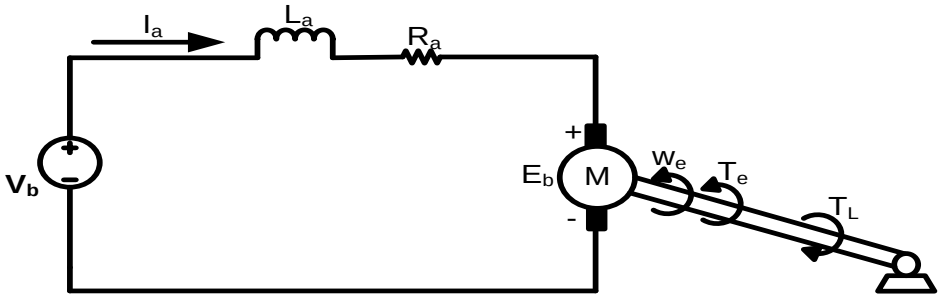


Figure 2.14 Permanent Magnet dc Motor

Applying KVL and KCL to Figure 2.14. The mathematical equation connecting the electrical and mechanical aspects of the dc motor is given by equation (2.20)

$$\left.\begin{aligned} L_a p i_a &= v_b - i_a R_a - k_m \omega_m \\ Jp\omega_m &= k_m i_a - T_L - B\omega_m \\ T_e &= k_m i_a \end{aligned}\right\} \qquad (2.20)$$

Where i_a the armature current of the motor, R_a Armature resistance of the motor, L_a armature inductance of the motor, T_L load torque, ω_m rotor speed , B damping coefficient, J moment of

inertial of the motor, k_m is the motor constant and T_e is the electromagnetic torque developed by the motor and V_b is the battery voltage applied to the motor.

2.3 Review of Similar Works

Han *et al* (1999) carried out a study on resonant fly back converter for dc distribution system to supply electricity to rural or remote area. The converter system using the fly back converter changed a high voltage to low voltage dc using thyristors with galvanic isolation of the input and output circuit. The scheme employed resonant commutation to put the thyristors off successfully without any cause for expensive commutation circuit. However the system using the fly back circuit topology was not simple to construct and also was bulky, unattractive, switching losses are high due to input pulsating current of the fly back converter. Moreso, because of the hard switching nature of the thyristor adopted in the circuit, it was difficult to implement series operation of several units to increase sustain current.

Caisheng *et al* (2008) worked on a power management strategy of an ac linked hybrid of PV/wind/Fuel Cell (FC) energy storage system on a standalone network topology. The PV and the wind been the primary energy source were coupled to an ac link to meet load requirements with the FC as an auxiliary power supply to meet load requirement when the system falls short of its primary energy supply. However the link between the energy sources was not dc, so the bulk power seen by the load was less due to inter-stage conversion process involved.

Chen *et al* (2009) carried out studies on a transformer-less dc-dc converter to obtain high step-up voltage gain at the expense of low current. The steady-state analysis of the voltage gain of the derived model equation and boundary operating conditions validated the theoretical analyses of a 40 watt prototype. The design in its form had simple structural topology and was easy to implement. However, it could not be relied upon to drive a dc motor owing to the low current delivered by the converter.

Yuan *et al* (2010) investigated a predictive model of voltage control for three-phase grid connected PV converter based on energy balance modeling in one control period and concluded that to maintain energy balance coupled with a fast dynamic response at steady state, the dc-link capacitor should be switched in as fast as possible within the period of

overshoot to ensure an excellent fast dynamic response of the system. However, the system did not include an energy storage system.

Liaw *et al* (2011) worked on the combination of a switch reluctance generator, a boost dc-dc converter, a battery energy storage system and a single phase three wire inverter for generating ac voltage at 220/110 V at 60Hz. The bi-directional converter and energy storage system inclusive in the design was able to improve the dc grid power supporting tendencies to meet load requirements in step should there be fault in the main power source, The system so designed was a success. However the circuit topology of the proposed system did not include a solar system, the battery energy storage system has to rely on an auxiliary fly back switch mode rectifier charging system to charge the battery from an external source.

Thounthong (2011) investigated renewable hybrid power plant that is fed by a PV source with super-capacitor (SC) storage device suitable for distributed generation (DG). In the work, the PV system used is the main generator. The SC functioned as an auxiliary source for supplying transient and steady state power deficit of the PV module. It was reported that for high power application four parallel boost converters and four parallel bi-directional converters were implemented in addition to PV system and storage device. With the fact that adding energy storage system to the distributed power system improved power quality and efficiency. However, the SC had a higher self discharge rate compared to other known energy storage elements like FC or battery in supplying the steady state deficit in power of the PV to the load.

Veerachary (2012) studied two-loop controlled buck-SEPIC for input source power management where the observations were that to reduce the burden on primary energy source to meet common load demand, dc sources have to be connected in parallel with additional power sources such as a battery or a super capacitor in parallel to the load. **(Chen *et al* 2012)** attempted a similar but different circuit topology of integrating a buck and a buck-boost with power drawn from low and high voltage sources to service common dc load. However the system was not equipped with energy storage system.

Wandhare *et al* (2012) proposed a novel control scheme to minimize and accommodate the disturbance on the PV fed distributed generation (DG) systems. The complimentary energy storage system in the proposed circuit topology was to mitigate the fluctuations or disturbances in PV system using an ultra- capacitor to absorb effect of intermittent solar insolation. The system was harmonized such that sudden fall in PV power, accord other

sources (e.g hydro, steam turbine e.t.c) connected to the system to take over. The ultra-capacitor integrated with the system has the ability to charge/discharge very rapidly in order to meet power requirement of the load as quickly. However, the switching arrangement of the ultra-capacitor requires sophisticated electronic control which is add to cost of the entire design.

Badawy *et al* (2014) worked on an idealogy of the parallel power processing topology (PPPT) to process the majority of the power from PV system to the load through direct energy part without exposure to converter losses. The proposed method was workable, however, failed in meeting most part of the load demand due to the exclusion of a dc to dc converter for processing the power to load.

Mahmud *et al* (2014) worked on controlling the current injected to a three phase grid connected PV system, the performance of the system under standard and charging atmospheric condition were studied alongside the performance under a single and three phase short circuit fault. The controller performance studied was also checked to observe the robustness of the system. The system was able to meet some of the system specification largely; however no provision was made for a battery to meet load demand when there is deficit in power to load.

Mapurunga *et al* (2014) investigated a proposed new converter system for water pumping and treatment system. The converter system was designed to drive a three phase induction machine directly from a PV source via a modified boost converter and three phase inverter system. The system performance using the modify converter was achieved, however the system has no back-up energy storage system to support the load in a situation of low solar output.

By and large with respect to PV cell there has been several methods for determining the maximum power point of the PV panel either connected in series or parallel assembly, amongst this are linear oriented coordinated method, perturb and observe, incremental conductance as proposed by **Yao *et al,* (2011).** In line with the methods adopted by these authors, determining maximum power point (MPP) requires solving the non-linear I-V equation to find the point at which $\frac{dp}{dv} = 0$. A method proposed recently by **Roshan *et al,* (2012)** known as Lambert function involves manipulating the non linear power equation $p = i \times v$, into an exponential function that represents Lambert function representation. The

method calculates the voltages and current at MPP with less computational time compare to other known technique of Newton Raphson method **Canale *et al*, (2011)**. This research adopts the Lambert function method to calculate the voltage and current at MPP. The choice of the SEPIC is based on the observed electrical characteristics itemized as follows:

(i) Compare to fundamental dc-dc converters such as buck, boost and buck-boost, whose output voltage is fixed for a particular duty cycle. The output voltage of SEPIC varies over a wide range, which makes it a better candidate suitable for solar application whose output voltage is often fluctuated and affected by weather.

(ii) The transfer capacitor between the output and input assures galvanic isolation of the input and the output circuit ensuring that short-circuit on the output of the SEPIC does not affect the PV power supply panel side.

(iii) The output diode can be replaced with a transistor which can be switched in synchronal with the main switch just like a synchronous type of converter.

The SEPIC amongst its other variant converters such as CUK, ZETA in the same classes, has the following advantages:

(i) SEPIC transfer power to the output without polarity reversal unlike the CUK and ZETA converters which transfer power to the output with polarity reversal.

(ii) The driver switch for the main switch of the SEPIC can be built using a low side driver other than ZETA converter whose drive switch need a high side driver to pull power from input to the output.

(iii) The ripple current in SEPIC is less compare ZETA due to advantage of grounded switch at the input of the converter.

(iv) The input current is non-pulsating.

Due to these aforementioned advantages and observed electrical characteristics itemized above SEPIC is a better candidate as an interface between PV system and load. More so, it was reported by **Zhao *et al*, (2009**) the preference of SEPIC for battery charging systems due to the advantage of the blocking diode at the output of the converter.

2.4 Conclusion

In this chapter, the theoretical background and review of similar works of the study system has been presented. The principle of operation and relevant mathematical theories is presented. Also, a summary of reviewed works similar to the area of study is presented. The reviewed literatures have shown considerable efforts or progress made using a PV system, converter and a storage energy system to support load power. This research work set-forth to determine the performance studies of a permanent magnet (PM) dc motor on a dc grid network furnished with power from a solar fed SEPIC system equipped with a storage system. In carrying out the study a method of harmonic balance technique is used to analyze the SEPIC state variables with duty ratio variations. The technique is such that steady state, ripple quantities can be obtained in a single step. More so, the general influence of the current supplied by the SEPIC and the battery can be studied in meeting the load current demand.

CHAPTER THREE

MATERIALS AND METHODS

3.1 Introduction

This chapter provides a detailed description of the material used for the research and methodology adopted. Materials used are itemized as follows:

(i) National Aeronautics and Space Administration (NASA) solar insolation data for Zaria (Latitude 11.06^0N and Longitude 7.7^0E)

(ii) Solar insolation data for Zaria (Latitude 11.06^0N and Longitude 7.7^0E) obtained from power and machine Laboratory Department of Electrical and Computer Engineering ABU Zaria.

(ii) MATLAB/Simulink software.

3.2 Solar Insolation Data for Zaria

The insolation data used for this study was obtained from NASA spanning for a period of one (1) year. The data used is a monthly average taken at specific times of the day on a three hourly interval. The NASA data was used here due to the inability to obtain useful solar insolation data from Nigeria Metrological Agency (NIMET) at Nigeria College of Aviation Technology (NCAT) Zaria. In addition, solar insolation data were captured from the on ground weather work station set-up at the Department of Electrical and Computer Engineering (power and machine Lab). This data capture was based on second by second record from the data acquisition module set-up to interface to the solar module for a period from August 17 to September 24, 2014. However, comparison of the data obtained from NASA with surface measurement taken at the base line surface radiation network (BSRN) shows a root mean square error of 15.37 % (NASA, 2013). On the whole, the data obtained are thus adequate for the purpose of the study as an actual measurement might not give a significant excursion from what has been obtained. The obtained data were grouped according to Table 3.1 and Table 3.2 and the class mark used as representative of the group in the analysis. See data obtained included in Appendix H.

A frequency table was constructed from the above data as follows:

Table 3.1 Frequency Table for Solar Insolation in Zaria obtained from NASA

Solar insolation W/m^2	Frequency	Class Mark W/m^2
-95-140	24	
150-340	0	245
350-540	15	445
550-740	12	645
750-940	9	845
950-1140	0	1045

Table 3.2 Frequency Table for Solar Insolation in Zaria obtained from the Weather Hawk IP (ABUDECE) (10.255.7.251).

Solar insolation W/m^2	Frequency	Class Mark W/m^2
10-230	190	120
240-460	203	350
470-690	142	580
700-920	198	695
930-1150	63	1040

3.3 MATLAB/Simulink

Power electronics converters modules are usually light weight and are used to transfer power in the form of dc-dc, dc-ac, ac-ac, ac-dc to the load depending on the application (Ned, 2003). The circuit topology of power electronics systems change with changes in mode. During this modal operating regimes new circuit topology are defined from the original studied circuit when it has not be subjected to switching action. Hence, closed form solutions of the state of power electronic systems as a function of time are usually not possible. Computer simulations have made it possible to model such systems and observe their responses to certain

conditions. There are two basic types of tools for simulation (Ned, 2003), Circuit Oriented Simulators and Equation Solvers.

MATLAB does function as an equation solver. MATLAB is extensible and highly integrated. MATLAB can be used for computation, programming, as well as visualization and simulation. Simulink is the companion tool of MATLAB used for simulation. Take for example in MATLAB, a system can be represented by its model equations (be it differential equations or/and algebraic) in its different mode of operation and a solution obtained. MATLAB provides the capability of obtaining solution in various visual forms. MATLAB/Simulink version 9 m-file editor and the accompanying Simulink has been used in the present work because it provides all the capability needed for the work. Figure. 3.1 shows the MATLAB editor interface for version 9 while Figure. 3.2 shows a Simulink model for simulation using the embedded MATLAB function.

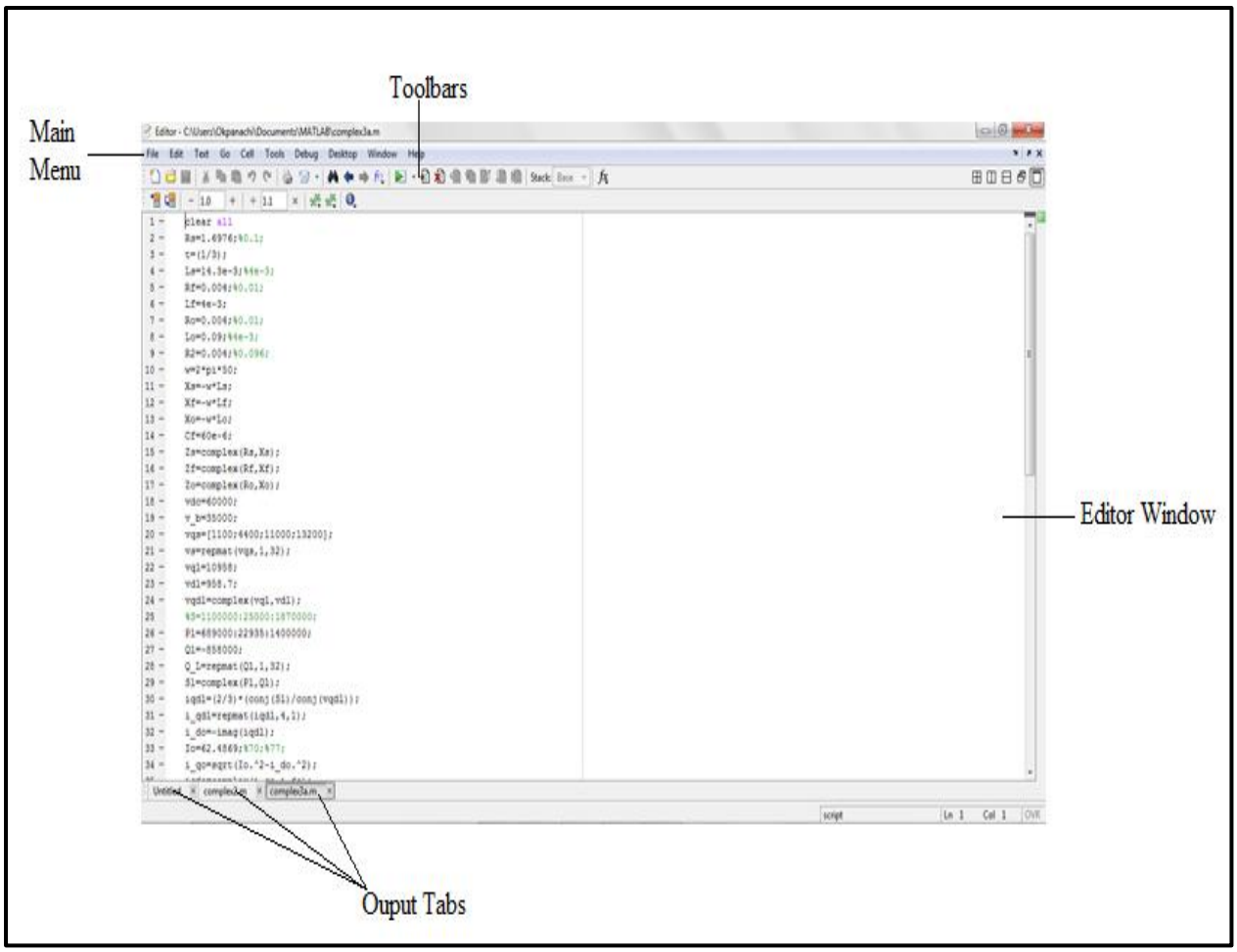


Figure. 3.1: MATLAB M- File Editor Interface (Version 9)

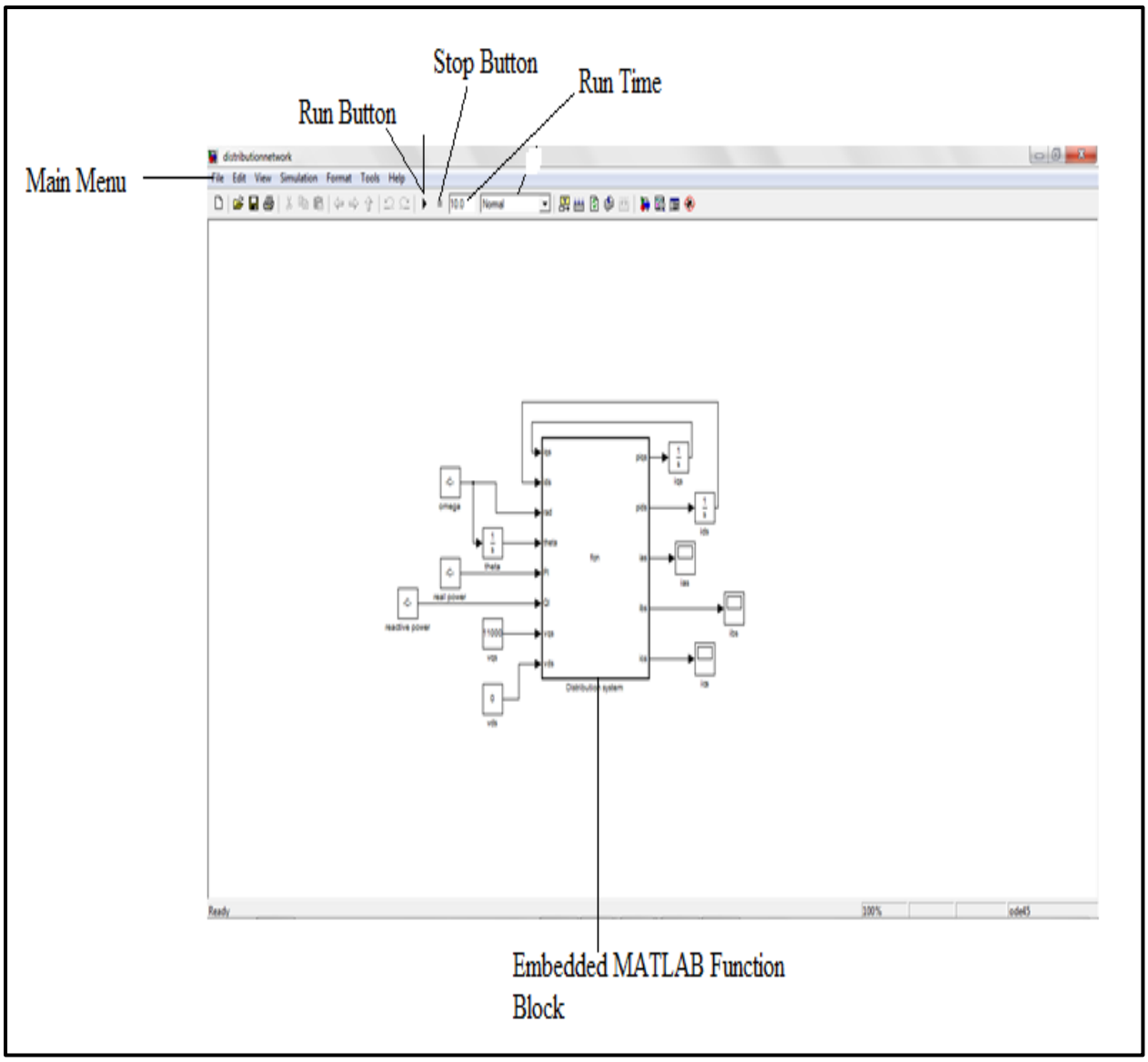


Figure. 3.2: Simulink Interface for Simulation

3.4 Methodology

The following steps have been followed for the research:

I. Modelling of the PV system
II. Modelling of the SEPIC system
III. Modelling of loads (Permanent magnet (PM) d.c motor and battery)
IV. Simulation of the SEPIC
V. Steady state analysis of the system
VI. Simulation of the coupled system
VII. Validation of the system performance using the solar radiation data for Zaria

3.5 Model Derivations and Design Considerations

This section entails the complete derivation of the entire system under study. Firstly, the model equations are derived sub-component by sub-component in order to aid understanding of the design considerations. Next, steady state equations are then obtained from the complete system dynamic equations by setting the differential quantities (i.e $px = \frac{d}{dt} = 0$, where x is constant) equal to zero. The converter switching function which was described in Section 2.2.2 has been used for the two converters in the system, to obtain the converter model equations. Figure 3.3 shows the complete schematic of the studied system. It has been divided into sub-circuit namely: $P-V$ module side, SEPIC side, grid side, battery side, bi-directional converter side, permanent magnet dc motor side for ease of understanding.

For the studied system, two cases of insolation levels were considered to study the system mode of operations.

i. low solar insolation (S = 245 W/m^2)

ii. High solar insolation insolation (S = 850 W/m^2)

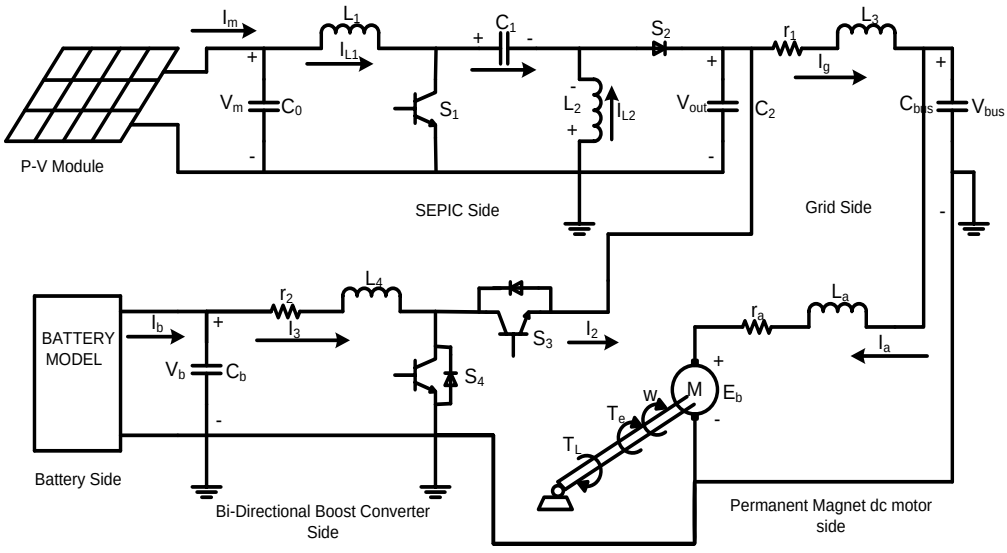


Figure 3.3 Detailed Configuration of the Studied System

3.5.1 Model Derivations of the Complete System

From Figure 3.3, the model derivations of the sub-systems of the entire system are as shown in this section. Please note that throughout this text $p = \frac{d}{dt}$

P-V Model

The complete model for the P-V module is given by **(Karimi *et al*, 2011; Yazdani *et al*, 2009)**

$$i = n_p i_{ph} - n_p i_{rs}\left[\exp\left(\frac{qv}{k\theta A n_s}\right) - 1\right] \tag{3.1}$$

$$i_{ph} = \left[i_{src} + k_\theta\left(\theta - \theta_r\right)\right]\frac{S}{100} \tag{3.2}$$

where i is the output current, i_{ph} photo –current dependent on radiations and temperature, i_{src} short circuit current of one photo-voltaic cell unique to every cell, i_{rs} reverse saturation current unique to every cell, v output voltage across $P-V$ module, n_p the number of series strings connected in parallel, n_s the number of series connected cells, k_θ temperature coefficient unique to every cell, θ cell temperature, θ_r reference temperature, S the solar irradiation level, A ideality constant, q the electronic charge(1.602×10^{-19}), k the Boltzman constant (1.38×10^{-23}). Note the power of the PV module is obtained as

$$P_S = iv \tag{3.3}$$

where P_S is the power obtained from the solar. The maximum power can be obtained by differentiating equation (3.3) thus, $\frac{dP_S}{dv} = 0$, this enables the voltages and current at maximum power point to be found analytically.

SEPIC Model

Figure 3.4 shows the SEPIC topology, C_0 is the input capacitor interfacing the solar and the SEPIC, C_1 is the transfer capacitor providing a path for the transfer of power from the SEPIC input to the SEPIC output, C_2 is the output capacitance, L_2 is the output inductance, L_1 is the input inductance, i_{L1} input current through inductor L_1, i_{L2} current through inductor L_2, v_{C1} voltage across C_1, v_{out} voltage across capacitor C_2 of the SEPIC respectively. i_g grid current, i_2 bi-directional converter current delivered to the grid.

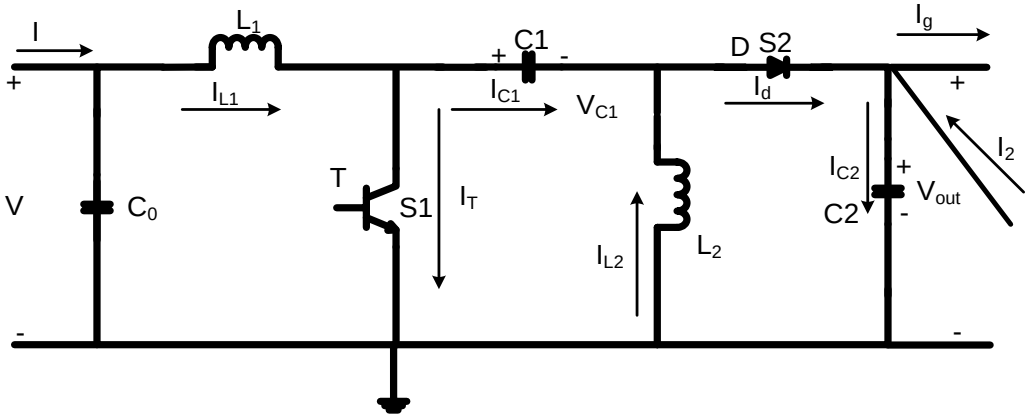


Figure 3.4 Schematic of SEPIC

From Figure 3.4 Let S_1 denote the switching function of transistor T, and S_2 denote the switching function of the diode D. Applying KVLand KCL to the circuit topology, the compact equation of the SEPIC model in the two modes of the operating regimes for continuous current mode (CCM) viz. applying averaging technique is as shown in equation (3.4) under the constrain equation, $S_1 + S_2 = 1$ for CCM operations.

Recall: $p = \dfrac{d}{dt}$

$$\left.\begin{aligned} C_0 pv &= i - i_{L1} \\ L_1 pi_{L1} &= v - (1-S_1)(v_{C1} + v_{out}) \\ L_2 pi_{L2} &= S_1 v_{C1} - (1-S_1) v_{out} \\ C_1 pv_{C1} &= (1-S_1) i_{L1} - S_1 i_{L2} \\ C_2 pv_{out} &= i_{L1}(1-S_1) + i_{L2}(1-S_1) + i_2 - i_g \end{aligned}\right\} \qquad (3.4a)$$

Devices Voltage and Current

$$\left.\begin{aligned} i_T &= (S_1)(i_{L1}+i_{L2}) \\ v_T &= (1-S_1)[-v_{out}+v_{C1}] \\ i_d &= (1-S_1)i_{L1}+i_{L2}(1-S_1) \\ v_d &= S_1[-v_{out}-v_{C1}] \end{aligned}\right\} \qquad (3.4b)$$

Bi-Directional Converter Model

Figure 3.5 shows the Bi-directional converter circuit topology. C_b is the dc link capacitor serving as an inter-phase between battery and bi-directional converter, v_b is the battery voltage, i_3 is the current through inductor L_4, r_2 is the parasitic resistance, S_4 and S_3 are switching function of bi-directional converter, i_b is the current from the battery delivered to the bi-directional converter, v_{out} output from SEPIC interfaced to grid and bi-directional converter, L_4 is the inductance of the bi-directional converter coil.

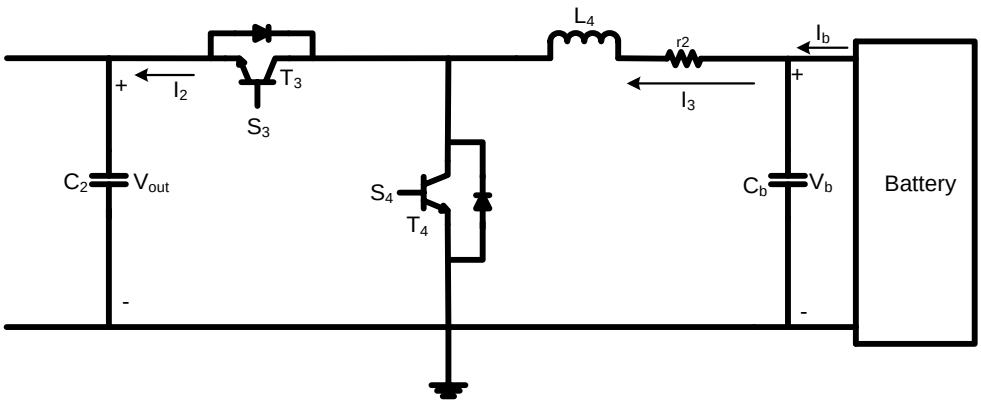


Figure 3.5 Bidirectional boost converter

From Figure 3.5 Let S_3 denote the switching function of transistor T_3, and S_4 denote the switching function of the diode T_4. Applying KVL, KCL and averaging technique to Figure 3.5. The compact model equation of the bi-directional converter for continuous current mode of the two operating regimes based on switching constraint $S_3 + S_4 = 1$ is shown by:

$$\left.\begin{aligned} i_2 &= (1-S_4)\,i_3 \\ C_b p v_b &= i_b - i_3 \\ L_4 p i_3 &= v_b - (1-S_4)\,v_{out} - i_3 r_2 \end{aligned}\right\} \qquad (3.5)$$

Recall: $p = \dfrac{d}{dt}$

Battery Model

Figure 3.6 shows the Battery topology **(Karimi et al, 2011)**, Where R_{b3} is the internal resistance of the battery accounting for the bulk electrolyte, R_{b4} internal resistance for the battery plate, R_{b2} and C_{b2} together model the battery overvoltage or polarization , v_{Cb1} internal electromotive force of battery, v_b terminal voltage of the battery, R_{b1} and C_{b1} account for self discharge of battery at high voltage and leakages. The model equation for the battery side is given by

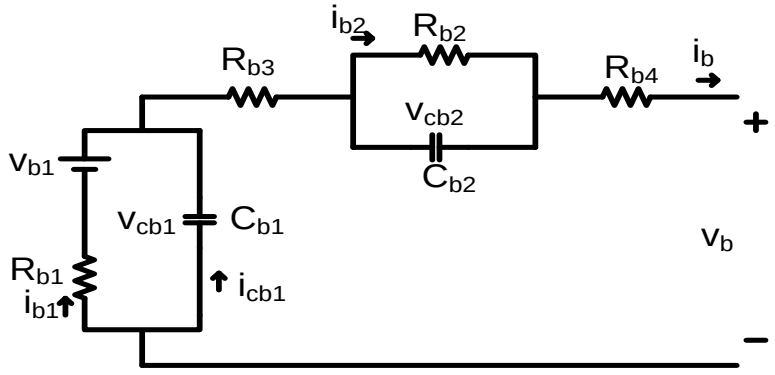


Figure 3.6 Battery Structure

$$\left.\begin{aligned} v_b &= -v_{Cb1} - v_{Cb2} - \left(R_{b3} + R_{b4}\right) i_b \\ R_{b1} C_{b1} p v_{Cb1} &= i_b R_{b1} - v_{b1} - v_{Cb1} \\ C_b R_{b2} p v_{Cb2} &= i_b R_{b2} - v_{cb2} \end{aligned}\right\} \tag{3.6}$$

DC-Grid Model

Figure 3.7 shows the grid topology, Where L_3 is the grid inductance of the line, r_1 the dc resistance of the grid line, i_g grid current, i_a armature current of the permanent magnet motor, v_{bus} voltage across the permanent magnet d.c motor, C_{bus} dc link capacitor as an interface between grid and permanent magnet motor.

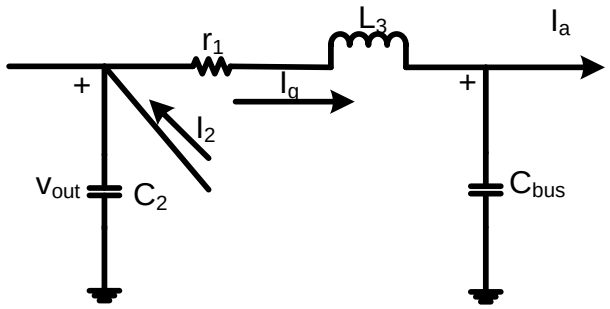


Figure 3.7 Grid Topology

From Figure 3.7, applying KVL, KCL to the model equation for the grid is given by:

$$\left.\begin{aligned} L_3 p i_g &= v_{out} - v_{bus} - i_g r_1 \\ C_{bus} p v_{bus} &= i_g - i_a \end{aligned}\right\} \tag{3.7}$$

Motor Model

Figure 3.8 shows the topology for a permanent magnet dc motor, Where i_a the armature current of the motor, R_a Armature resistance of the motor, L_a armature inductance of the motor, T_L load torque, ω_m rotor speed, B damping coefficient, J moment of inertial of the motor, k_m is the motor constant and T_e is the electromagnetic torque developed by the motor.

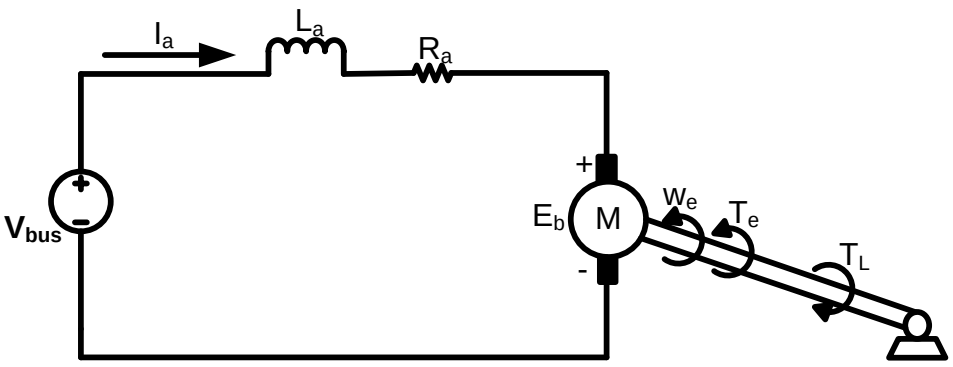


Figure 3.8 Permanent magnet dc motor

From Figure 3.8. Applying KVL, KCL. The model equation for the permanent magnet dc motor is given by:

$$\left.\begin{aligned} L_a p i_a &= v_{bus} - i_a R_a - k_m \omega_m \\ J p \omega_m &= k_m i_a - T_L - B\omega_m \\ T_e &= k_m i_a \end{aligned}\right\} \qquad (3.8)$$

3.5.2 Steady State Equations

At steady state, all the time varying quantities of equation (3.1) to (3.8) are set equal to zero. That is $px = \frac{d}{dt} = 0$, where x is a constant.

P-V Model

At maximum power point v and i are assumed to attain their steady state values, and these values are assumed as the optimum values at MPP and are substituted with v_m and i_m. At maximum power of the solar module $\frac{dp}{dv} = 0$ and the optimum values of the voltages is obtain using **(Roshan et al, 2012):**

$$v_m = \frac{W(ae^1) - 1}{b} \tag{3.9}$$

Where :

$W(.)$ is Lambert function,

$$\begin{cases} a = \left[i_{src} + k_\theta \left(\theta - \theta_r \right) \right] \dfrac{S}{100 i_{rs}} + 1 \\ b = \dfrac{q}{k \theta A n_s} \end{cases} \tag{3.10}$$

Equation (3.9) brings forth in a consise manner the equation for the determination of the maximum voltage analytically based on values of expression of a and b in equation (3.10)

SEPIC Model

At steady state $S_1 = D_1$, where D_1 is the duty ratio of the SEPIC. The relationship between input and output voltages of the SEPIC together with their respective current is given by equation (3.11). This value is the same as that obtained in **Mohan *et al* (2003):**

$$\left.\begin{aligned} \frac{v_m}{v_{out}} &= \frac{(1 - D_1)}{D_1} \\ \frac{i_m}{i_g - i_2} &= \frac{D_1}{1 - D_1} \end{aligned}\right\} \tag{3.11}$$

Bi-Directional Converter Model

At steady state $S_4 = D_4$, where D_4 is the duty ratio of the Bi-directional converter. The relationship between input and output voltages of the SEPIC together with their respective current is given by:

$$\left.\begin{aligned} i_b &= i_3 \\ i_2 &= (1-D_4)\, i_b \\ \frac{v_b - i_b r_2}{v_{out}} &= (1-D_4) \end{aligned}\right\} \tag{3.12}$$

Battery Model

At steady state equation (3.6) is further reduce to:

$$v_b = v_{b1} - i_b R_b \tag{3.13}$$

Where

$$R_b = (R_{b1} + R_{b2} + R_{b3} + R_{b4})$$

DC-Grid Model

At steady state equation (3.7) is further reduce to:

$$\left.\begin{aligned} i_a &= i_g \\ v_{out} &= v_{bus} + i_g r_1 \end{aligned}\right\} \tag{3.14}$$

Motor Model

At steady state equation (3.8) is further reduce to:

$$\left.\begin{aligned} v_{bus} &= i_a R_a - k_m \omega_m \\ T_e &= k_m i_a = T_L - B\omega_m \end{aligned}\right\} \tag{3.15}$$

Equation (3.15) contains key equations in the study of electromechanical conversion. It should noted that in both equations, current i_a and speed ω_m are present. A device based on

this equation (3.15) for its operation is termed a permanent magnet dc motor. It mode of operation is based on fixed excitations.

Putting up voltage equation of (3.11) through (3.13) in a single form we have a generalized equation connecting the battery current in terms of battery voltage, SEPIC duty ratio, Bi-directional converter duty ratio, voltage at maximum power and Bi-directional converter resistance:

$$\frac{v_m}{v_{out}} = \frac{(1-D_1)}{D_1} \tag{3.16}$$

$$\frac{v_b - i_b r_2}{v_{out}} = (1-D_4) \tag{3.17}$$

$$i_b = \frac{v_b(1-D_1) - v_m(1-D_4)D_1}{r_2(1-D_1)} \tag{3.18}$$

The current i_2 injected to the grid can be found from equation (3.12) to be

$$i_2 = (1-D_4)i_b \tag{3.19}$$

From equation (3.11), the current transfer ratio from the SEPIC input to the grid side is given by:

$$\frac{i_m}{i_g - i_2} = \frac{D_1}{1-D_1} \tag{3.20}$$

Putting (3.19) into (3.20), we have:

$$i_a = i_g = i_m \frac{(1-D_1)}{D_1} + i_2 \tag{3.21}$$

The electromagnetic torque developed by the motor is found to be:

$$T_e = k_m i_m \frac{(1-D_1)}{D_1} + k_m i_2 \tag{3.22}$$

From the load point and the grid side, the relationship of the torque speed can be derived using equation (3.14) and (3.15) by eliminating v_{bus} and i_a, equation (3.25) is obtained:

$$v_{bus} = v_{out} - i_a r_1 \tag{3.23}$$

$$\left.\begin{aligned} v_{bus} &= i_a R_a - k_m \omega_m \\ T_e &= k_m i_a = T_L - B\omega_m \end{aligned}\right\} \tag{3.24}$$

$$\frac{B\omega_m + T_L}{k_m} = \frac{v_{out} - k_m \omega_m}{R_a + r_1} \tag{3.25}$$

But $v_{out} = v_m \dfrac{D_1}{1 - D_1}$ from equation (3.11), substituting into (3.25) we have:

$$\omega = \frac{\dfrac{v_m k_m D_1}{1 - D_1} - T_L (R_a + r_1)}{B(R_a + r_1) + k_m{}^2} \tag{3.26}$$

Equations (3.18), (3.19) and (3.22) are coupled equations describing the steady state performance of the generalized system. The equations in addition to the means provide analytical technique of analysis. It has been used for computer simulation providing upon proper simplification at $px = \dfrac{d}{dt} = 0$. Where x is a constant.

A MATLAB code is developed (see Appendix F) to calculate and plot the steady state values using equation (3.9), (3.10), (3.18)-(3.19) , (3.21)-(3.22) and (3.26) respectively. The figures are shown in Figure (4.2) to Figure (4.12) respectively. Figure (3.9) shows the algorithm use to calculate and obtain the plot of Figure (4.2) to Figure (4.12).

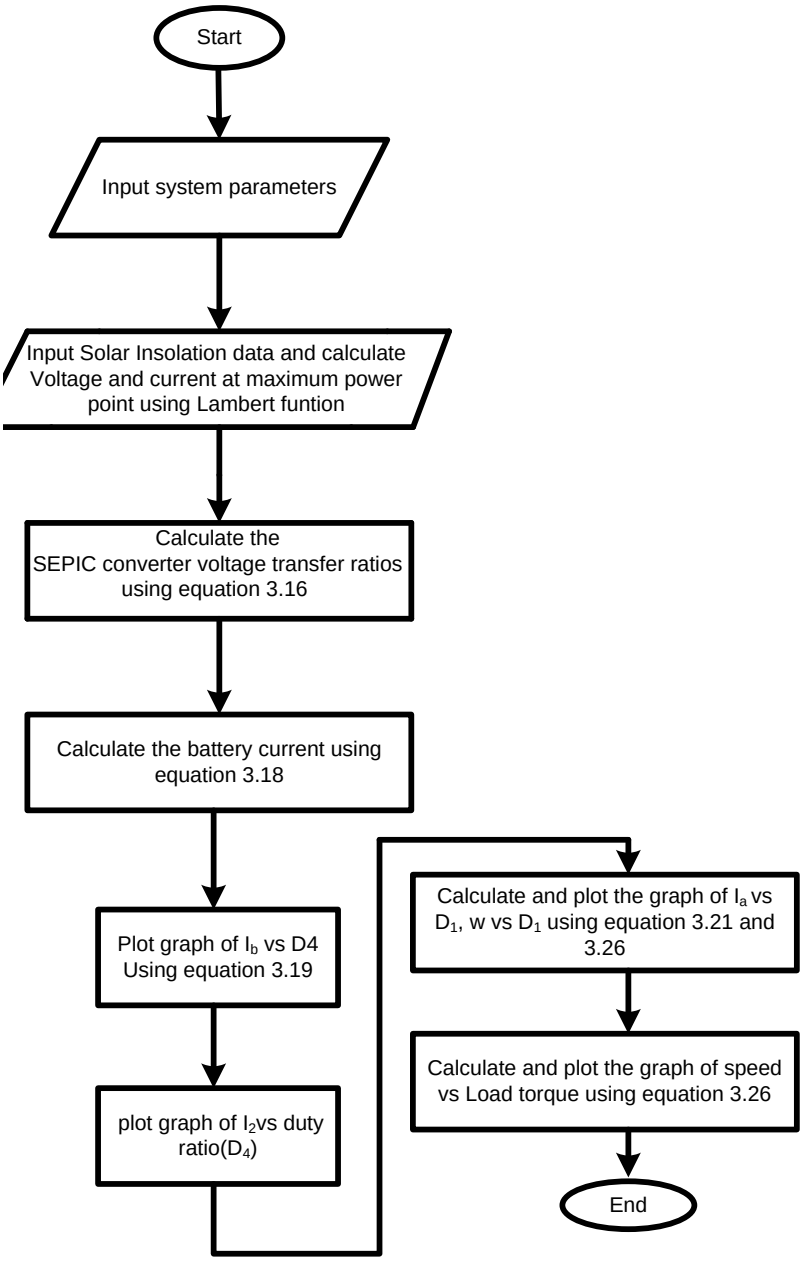


Fig. 3.9 Algorithm for Finding Steady State of the System

3.5.3 Design Considerations:

The studied system is designed for a load of approximately $2441.43W$. Knowledge of the solar hourly insolation data for Zaria (Latitude 11.067^0N, Longtitude 7.7^0E) were obtained from NASA for a period from January to December (year 2013). Moreso solar insolation data for Zaria (Latitude 11.067^0N, Longtitude 7.7^0E) was obtained on a seconds by seconds basis from the solarimeter mounted on the solar panel at the power and machine Laboratory ABUDECE between August 17 to September 24 the year 2014. In addition, a thorough evaluation and classification of the solar data into frequency distribution table was also carried out to compare the two solar data obtained. (see Table 3.1 and Table 3.2).

Distribution Network

The dc resistance of the cable conductor can be calculated based on IEC60287-1 Clause 2.1

$$r_1 = \frac{\rho l}{a}(\Omega) \tag{3.27}$$

The route length for this study is chosen to be $5km$. The choice of the route length was entirely for design purpose and it is intended to study the system behavior in meeting the objectives of this work. For transmission of electricity aluminum conductor is mostly preferred due to: (1) It is light in weight (2) It resistivity is high compare to copper.

ρ resistivity for aluminum conductor is $2.8254\times10^{-11}\Omega.km$

Cross sectional area a of the conductor used for this design is $100mm^2 = 100\times10^{-6}m^2$

Using equation (3.27) r_1 is calculated to be $r_1 = 1.41\,\Omega$.

More so, the inductance of the line can be calculated using **(Keyhani, 2011):**

$$L = 0.2 * line\,length\left(\ln\left(\frac{4 * line\,length}{d}\right) - 0.75\right)(nH) \tag{3.28}$$

Where:

L is the length of the line is in mm, d is the diameter of the conductor in mm

For a cable of $100mm^2 = 100\times10^{-6}m^2$,

The diameter d is calculated to be $0.01128\,m = 11.28\,mm$

Note $1000000mm = 1km$

Using equation (3.28), the inductance of the line $L_3 = 13.63mH$.

Load Power Requirement

PM dc Motor side

From equation (3.24) the voltage equation at steady state is

$$v_{bus} = i_a R_a + k_m \omega \tag{3.29}$$

where $\omega = \frac{2\pi N}{60}\ (r.p.s)$ (3.30)

where N is the motor speed in $r.p.m$

The input current for the machine based on known parameters of Table 3.3 at a speed of 3000 $r.p.m$ is calculated to be equal to 12 A.

From Table 3.3 the input power of the motor based on its ratings is $3hp = 3 \times 746 = 2238W$.

The losses on the dc grid line is found to be equal to

$$p_{grid\,loss} = 12^2 \times r_1 = 12^2 \times 1.41 = 203.43W \tag{3.31}$$

Total power at the output of the SEPIC is found to be equal to $2238 + 203.43 = 2441.43W$.

Under an assumed power management strategy 70% of the total load power is to be supplied by solar and 30% to be supplied by battery. Power from solar is calculated and found to be $1709W$ and that from battery is found to be equal to $732.43W$.

Battery side

The power of the battery can be found using:

$$P_{batt} = I_b v_b \tag{3.32}$$

Based on this equation (3.32), the current supplied by the battery can be calculated. Assuming the battery system voltage to be 48, i.e $v_b = 48V$, the current from the battery at steady state is calculated to be equal to equal to $I_b = 15.26A$.

The voltage input to the motor as given by the manufacturer is equal to $180V$ from Table 4.1.

At steady state the line drop on the dc grid line using the voltage equation (3.14). It is calculated to be equal to $12 \times 1.41 = 16.95V$. Equally, voltage at the output of the SEPIC at steady state is calculated and found to be equal to $v_{out} = 196.95V$.

Based on the above values obtained, the value of the duty ratio to guarantee CCM for the bi-directional converter can be found by using equation (3.17)

$$\frac{v_b - i_b r_2}{v_{out}} = (1 - D_4) \tag{3.33}$$

this value of the duty ratio for the Bi-directional converter is found to be $D_4 = 0.78$. In addition to this value of D_4 known, the current i_2 at steady state of the Bi-directional converter is found to be equal to $3.36A$, using equation (3.19).

Active Power Balance

The active power balance can be stated as:

$$\sum P_s + \sum P_{batt} + \sum P_L = 0 \tag{3.34}$$

Where:

P_s is the power supplied by the solar module.

P_{batt} is the power supplied by the battery.

P_L is the power delivered to the load

Note that equation (3.34) is key equation for the active power balance for the system under study. That is for any operating condition (with or without solar) at any instance of time, the algebraic sum of the active power from the solar and the active power of the load and the

power from the battery is equal to zero. Hence the battery can only be designed with a capacity to supply the balance of power between the supply and the load. The immediate consequence of this design criterion is that when there is loss of power supply from solar, the battery system might only be able to supply only a part of the load requirement. Hence the entire system has been designed so that the storage energy system (battery) only carters for a part of the load power requirements.

Power Allocation to Solar

The 70% power allocations of the solar found earlier is 1709 W. If the output voltage from solar is assumed to be $200V$, Current at the output of the solar is found using equation (3.3) to be $8.55A$.

Based on this current obtained and assumed output voltage of the solar, the number of cells in parallel and number of cells in series can be determined.

Assuming for a cell the voltage is $0.5V$/cell , the number of cells in series is found to be $n_s = \frac{200}{0.5} = 400 cells$. The most prevalent solar radiation from table 3.1 is found to be 850 w/m^2 obtained from NASA for Zaria. Using this value of solar radiation the number of cells in parallel can be calculated by using equation (3.1) and equation (3.2) together with solar parameter of Table 3.1. The number of parallel connected cells is found to be $n_p = 4$. With the current of 8.5 A obtain in this section.

SEPIC Inductor Filter Design

The schematic for the SEPIC is as shown in Figure 3.10. There are two operating regimes of the switches within the switching period T, which corresponds to the status of switch S_1 and switch S_2. Just as emphasized in section 2.2.1, for the first switching interval S_1 is on for a period defined by $t \epsilon [0, DT]$, while S_2 is off. During the next interval S_1 is off and S_2 is on for a period defined by the interval $t \epsilon [DT, T]$. In order to make the analysis here simpler it is assumed the converter is lossless, and that there is an internal control algorithm that adjusts the duty ratio of the converter to extract the maximum power from the panel. So for design

purposes, the input voltage and current to the SEPIC have been assumed maximum values from solar.

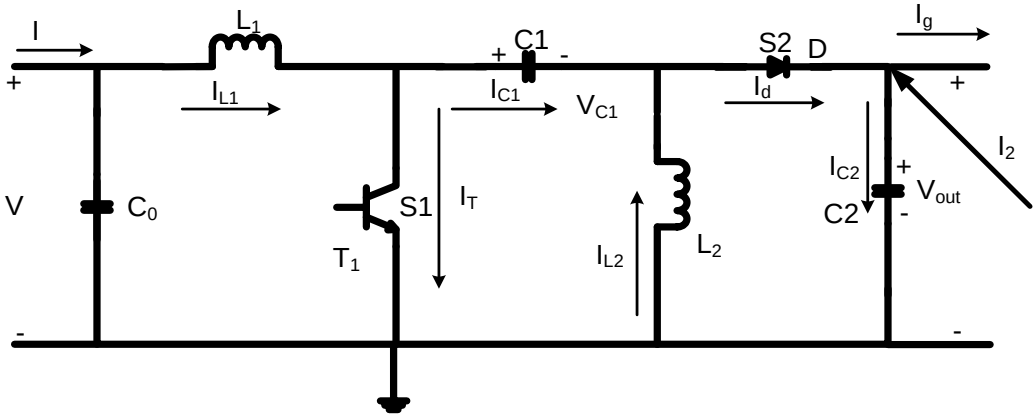


Figure 3.10 Schematic of SEPIC

The parameters of the SEPIC can be determined using the inductor current equations and capacitor voltage equation as given by **Rashid *et al*, 2003** considering the two modes of the operating regimes. To determine the values of inductor L_1 and L_2, moreso, capacitor values C_1 and C_2, the converter is assumed to operate in current conduction mode (CCM).

For Mode I:

The voltage across the inductor L_1 when switch S1 is on and switch S2 off is:

$$v = L_1 \frac{di_{L1}}{dt} \tag{3.35}$$

Applying small ripple approximation **(Ned, 2003)**, equation (3.35) can be written as

$$v = L_1 \frac{\Delta i_{L1}}{t_1} \tag{3.36}$$

Where : $t_1 = dT$,

Δi_{L1} is the peak to peak ripple current of inductor L_1.

d and T are duty ratio and switching period respectively.

$$\Delta i_{L1} = \frac{v \times t_1}{L_1} \tag{3.37}$$

For Mode II:

The voltage across the inductor L_1 when switch S1 is off and switch S2 on applying the same small ripple approximation is:

$$L_1 \frac{\Delta i_{L1}}{t_2} = -\left(v - v_{out} - v_{C1}\right) \tag{3.38}$$

$$\Delta i_{L1} = \frac{-(v - v_{out} - v_{C1}) \times t_2}{L_1} \tag{3.39}$$

Where $t_2 = (1-d)T$

$$t_2 = \frac{-\Delta i_{L1} \times L_1}{v - v_{out} - v_{C1}} \tag{3.40}$$

Applying voltage balance equation $\Delta i_{L1} = \Delta i_{L2}$, and with the respective value for t_1 and t_2 substituted, the expression for d is obtained,

$$d = \frac{v_{C1} + v_{out} - v}{v_{out} + v_{C1}} \tag{3.41}$$

And

$$1 - d = \frac{v}{v_{out} + v_{C1}} \tag{3.42}$$

From equation (3.42),

$$v_{C1} = \frac{v - (1-d)v_{out}}{(1-d)} \tag{3.43}$$

But note that $t_1 + t_2 = T$ (3.44)

Moreso, $T = \frac{1}{f}$

f = switching frequency

Substituting in equation (3.44) the values of t_1 and t_2, the following expression is obtained:

$$\Delta i_{L1} = \frac{v \times d}{L_1 f} \tag{3.45}$$

Similarly in finding Δi_{L2} for inductor L_2, applying similar approach used in obtaining equations (3.35)-(3.45). the expression for Δi_{L2} is calculated to be

$$\Delta i_{L2} = \frac{v_{out} \times (1-d)}{L_2 f} \tag{3.46}$$

Where:

Δi_{L2} is the peak to peak ripple current of inductor L_2

f = Switching frequency

v_{out} = Output voltage of the SEPIC

To calculate for values of inductor L_1 and equation L_2 equation (3.45) and (3.46) is used.

To calculate for C_1 and C_2:

Still from Figure 3.10. when switch S1 is off, Capacitor C_1 is charged through inductor L_1 for length of period the switch was off t_2. So

$$i_{L1} = C_1 \frac{dv_{C1}}{dt} \tag{3.47}$$

For Small ripple approximation, from equation (3.47)

$$\Delta v_{C1} = \frac{1}{C_1} \int_0^{t_2} i_{L1} dt \tag{3.48}$$

Where:,

But from equations (3.42) and equation (3.43)

$$\frac{v_{C1}d}{v_{out}} = (1-d) \tag{3.49}$$

Multiply both sides of equation (3.49) by T

$$\frac{v_{C1}dT}{v_{out}} = (1-d)T = t_2 \tag{3.50}$$

From equation (3.47),

$$\Delta v_{C1} = \frac{1}{C_1} \times i_{L1} \times t_2 \tag{3.51}$$

Substituting value for t_2 from equation (3.48), we have:

$$\frac{\Delta v_{C1}}{v_{C1}} = \frac{i_{L1} \times d}{fC_1 v_{out}} \tag{3.52}$$

Assume the load ripple current is small and almost negligible then;

$$\Delta i_{L2} = \Delta i_{C2} \tag{3.53}$$

$$i_{C2} = C_2 \frac{dv_{out}}{dt} \tag{3.54}$$

$$\Delta v_{out} = \frac{1}{C_2} \int_0^{\frac{T}{2}} i_{C2} dt \tag{3.55}$$

The average capacitor current is given by

$$\frac{1}{2} \times \Delta i_{L2} \times \frac{T}{2} = \frac{\Delta i_{L2}}{4} T \tag{3.56}$$

Subtitude for equation (3.55) into equation (3.54) and noting that $\Delta i_{L2} = \frac{v_{out} \times (1-d)}{L_2 f}$ from equation (3.45) then

$$\Delta v_{out} = \frac{v_{out}(1-d)}{8L_2 C_2 f^2} \tag{3.57}$$

Equations (3.45), (3.46), (3.47) and (3.57) are key equations for calculating L_1, L_2, C_1 and C_2 to guarantee CCM of the converter based on the specifications of Table 3.3. The values of L_1, L_2, C_1 and C_2 obtained using the equation are also tabulated in Table 3.3.

Based on the specified parameters for the SEPIC tabulated in Table 3.3, it can obtained using equation (3.45) and (3.46) the value of the inductance $L_1 = L_2$ to be equal to $3.21mH$ respectively. Similarly, using equation (3.52) and (3.57) the value of capacitor C_1 and C_2 is found to be equal to $40\mu F$ and $4\mu F$ respectively.

Bi-directional Converter Inductor Filter Design

Figure 3.11 shows the topology of the Bi-directional converter,

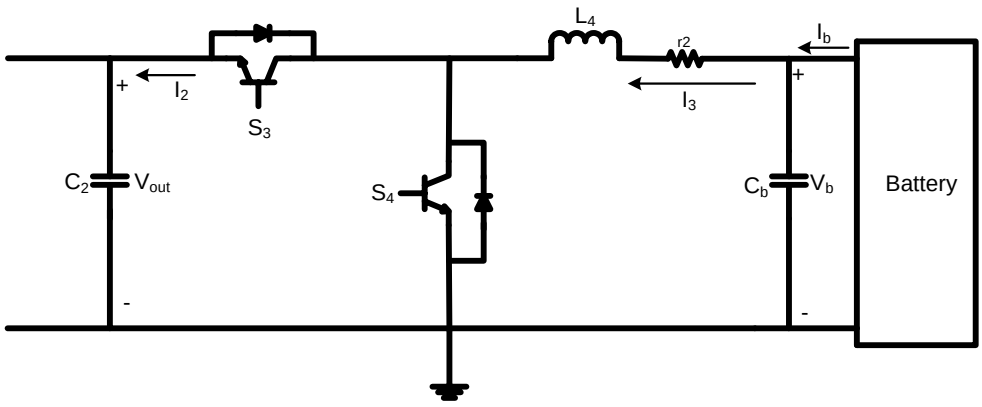


Figure 3.11 Schematic of Bi-Directional Converter

The parameters of the Bi-directional converter can be determined using the inductor current equations for the two modes of operations to determine the values of inductor L_4. Assuming the converter to operate in continuous current mode (CCM). **(Ned, 2003)**

For mode 1: $S_4 = 1$ and $S_3 = 0$

$$L_4 \frac{di_3}{dt} = v_b - i_3 r_2 \qquad (3.58)$$

For small ripple approximation and without loss of brevity,

$di_3 \approx \Delta i_3$; $dt = (t_1 - 0) = t_1$, Without loss of brevity

Then,

$$t_1 = \frac{L_4 \Delta i_3}{v_b - i_3 r_2} \tag{3.59}$$

Mode 2: $S_4 = 0$ and $S_3 = 1$

$$L_4 \frac{di_3}{dt} = v_b - v_{out} - i_3 r_2 \tag{3.60}$$

Applying small ripple approximation to equation (3.60),

$di_3 \approx \Delta i_3$, $dt = t_2$

$$t_2 = \frac{\Delta i_3 L_4}{v_{out} - v_b + i_3 r_2} \tag{3.61}$$

The switching period is define as:

$$t_1 + t_2 = T = \frac{1}{f} \tag{3.62}$$

Substituting for (3.59) and (3.61) into (3.62) we have:

$$L_4 = \frac{(v_b - i_3 r_2)(v_{out} - v_b + i_3 r_2)}{v_{out} f \Delta i_3} \tag{3.63}$$

Equation (3.63) is used to calculate the value of the inductor L_4 to guarantee CCM.

More so the value of the inductance L_4 for the Bi-directional converter to guarantee continuous conduction mode (CCM) is found to be equal to $1.1mH$.

Table 3.3. SYSTEM PARAMETERS

Motor Parameters	
Motor Type: MT40P4-61	
Rated Power P_m	$3\,Hp$
Rated Voltage v_{bus}	$180\ volts$
Rated Speed N	$3000\ r.p.m$
Moment of Inertial J	$0.0077\,kg/m^2$
Torque Constant $k_T = k_m$	$0.55\,N-m/A$
Voltage Constant $k_V = k_m$	$0.55\,N-m/A$
Armature Resistance R_a	$0.6\,\Omega$
Armature Inductance L_a	$3.0\,mH$
Solar Parameters	
Solar Type: TN-72-5M190 (Mahmud et al,2014)	
Peak Power $P_{\max}$	$190\,W$
Voltage v_{mp}	$37.1\,V$
Current i_{mp}	$5.11\,A$
Short-circuit current	$5.36\,A$
Open circuit voltage	$45.3\,V$
Cell temperature T	$-40/+85^0\,C$
SEPIC parameters	
Inductance L_1	$3.206\,mH$
Inductance L_2	$3.206\,mH$
Capacitance C_1	$40\,\mu F$
Capacitance C_2	$4\,\mu F$
Capacitance C_0	$100\,\mu F$
Switching Frequency f	$10kHz$
Output voltage ripple $\frac{\Delta v_{out}}{v_{out}}$	5%

Output Current ripple $\frac{\Delta i_{L2}}{i_{L2}}$	20%
Grid Parameters	
Grid resistance r_1	$1.41\,\Omega$
Grid Inductance L_3	$13.63\,mH$
Bi-Directional Converter Parameters	
Input Voltage v_b	$48\,V$
Resistance r_2	$0.32\,\Omega$
Inductance L_4	$1.1\,mH$
Capacitance C_b	$100\,\mu F$
Switching Frequency f	$10kHz$
Current i_3	$15.26\ A$
Ripple current Δi_3	$3.07\,A$
Duty cycle D_4	0.78
Battery Parameters (Karimi et al, 2011)	
Battery Voltage v_b	$48\,V$
Resistance R_{b1}, R_{b4}	$0.05\,\Omega$
Resistance R_{b2}	$0.001\,\Omega$
Resistance R_{b3}	$0.002\,\Omega$
Voltage v_{b1}	$50V$
Capacitance C_{b1}	$54000\,F$
Capacitance C_{b2}	$1\,F$

3.6 Simulation Equations

The equations for simulation have been obtained by manipulating equations (3.1) to (3.28) in Section 3.5.1.

For the PV:

$$i = n_p i_{ph} - n_p i_{rs}\left[\exp\left(\frac{qv}{k\theta A n_s}\right) - 1\right] \tag{3.64}$$

$$i_{ph} = \left[i_{src} + k_\theta\left(\theta - \theta_r\right)\right]\frac{S}{100} \tag{3.65}$$

For the SEPIC:

$$\left.\begin{aligned}
pv &= \frac{1}{C_0}[i - i_{L1}] \\
pi_{L1} &= \frac{1}{L_1}[v - (1 - S_1)(v_{C1} + v_{out})] \\
pi_{L2} &= \frac{1}{L_2}[S_1 v_{C1} - (1 - S_1) v_{out}] \\
pv_{C1} &= \frac{1}{C_1}[(1 - S_1) i_{L1} - S_1 i_{L2}] \\
pv_{out} &= \frac{1}{C_2}[i_{L1}(1 - S_1) + i_{L2}(1 - S_1) + (1 - S_4) i_3 - i_g]
\end{aligned}\right\} \tag{3.66}$$

For the grid:

$$\left.\begin{aligned}
pi_g &= \frac{1}{L_3}[v_{out} - v_{bus} - i_g r_1] \\
pv_{bus} &= \frac{1}{C_{bus}}[i_g - i_a]
\end{aligned}\right\} \tag{3.67}$$

For Motor

$$\left.\begin{aligned} pi_a &= \frac{1}{L_a}[v_{bus} - i_a R_a - k_m \omega_m] \\ p\omega_m &= \frac{1}{J}[k_m i_a - T_L - B\omega_m] \end{aligned}\right\} \tag{3.68}$$

For Bi-directional

$$\left.\begin{aligned} i_2 &= (1 - S_4) i_3 \\ pv_b &= \frac{1}{C_b}[i_b - i_3] \\ pi_3 &= \frac{1}{L_4}[v_b - (1 - S_4) v_{out} - i_3 r_2] \end{aligned}\right\} \tag{3.69}$$

For Battery

$$\left.\begin{aligned} pv_{Cb1} &= \frac{1}{R_{b1} C_{b1}}[i_b R_{b1} - v_{b1} - v_{Cb1}] \\ pv_{Cb2} &= \frac{1}{C_b R_{b2}}[i_b R_{b2} - v_{cb2}] \end{aligned}\right\} \tag{3.70}$$

3.7 Conclusion

The materials and method have been presented. Also the model derivation and some design considerations have been presented in this Chapter three. A compact model of the two converter systems by averaging the two operating regimes using switching functions approach was achieved. Each of the forms of the derived model will be used for various analyses in Chapter Four. Also in this Chapter, some design criteria were used and certain assumptions made to determine parameters of the system.

CHAPTER FOUR

RESULTS AND ANALYSIS

4.1 Introduction

The steady state analysis of the system under different operating conditions and the Open-Loop, Large-Signal Simulation study is carried out in this chapter. The harmonic balance technique has been deployed to the SEPIC steady state variables including the switches to determine and obtain plots of the ripple and steady state quantities. The developed model and system parameters have been employed in this Chapter. The simulation studies have been done using the full order model (involving the switching functions).

4.2 Steady State Analysis

Steady state is the state of the system in which all transient and disturbances have been cleared. At steady state, the differential equations become algebraic equations and easy to handle. The equations are then solved simultaneously rather than embarking on the cumbersome process of solving several differential equations.

4.2.1 Harmonic Balance Technique Applied to SEPIC System

The Harmonic Balance Technique is then applied to the Converter of Figure 3.4, in section 3.5.1. The state variable and switching function can therefore be defined as:

$$\left.\begin{aligned}
v_m &= v_m \\
i_{L1} &= i_{L10} + Re\left(i_{L11}e^{j\theta_s}\right) \\
i_{L2} &= i_{L20} + Re\left(i_{L21}e^{j\theta_s}\right) \\
v_{C1} &= v_{C10} + Re\left(v_{C11}e^{j\theta_s}\right) \\
v_{out} &= v_{C2} = v_{C20} + Re\left(v_{C21}e^{j\theta_s}\right) \\
i_T &= i_{T0} + Re\left(i_{T1}e^{j\theta_s}\right) \\
i_d &= i_{d0} + Re\left(i_{d1}e^{j\theta_s}\right) \\
v_T &= v_{T0} + Re\left(v_{T1}e^{j\theta_s}\right) \\
v_d &= V_{d0} + Re\left(v_{d1}e^{j\theta_s}\right) \\
S_i &= d_{i0} + Re\left(d_{i1}e^{j\theta_s}\right)
\end{aligned}\right\} \qquad (4.1)$$

The quantities $v_m, v_{C10}, v_{C20}, v_{T0}, v_{d0}, i_{L10}, i_{L20}, i_{d0}, i_{T0}, d_{i0}$ are the average (dc) values of supply voltage, capacitor voltage C_1, capacitor voltage C_2, transistor voltage T, diode voltage D, inductor current L_1, inductor current L_2, transistor current, diode current and switching function d. $v_{C11}, v_{C21}, v_{T1}, v_{d1}, i_{L11}, i_{L21}, i_{T1}, i_{d1}, d_{i1}$ are complex ripple harmonic peaks of capacitor voltage C_1, capacitor voltage C_2, inductor current L_1, inductor current L_2, transistor current, diode current and switching function d. Where $i = 1, 2, 3\ldots\ldots$, $\theta_s = \omega_s t$, where ω_s angular switching frequency in radians/seconds and t is time in seconds (See full detailed derivation at Appendix D).

Dynamic Equations For Average Quantities:

$$pi_{L10} = \frac{1}{L_1}\left(\begin{array}{l} v_m - v_{C20} - v_{C10} + d_{10}v_{C20} + d_{10}v_{C10} + \frac{1}{2}Re\left(d_{11}v_{C21}{}^*\right) \\ + \frac{1}{2}Re\left(d_{11}v_{C21}{}^*\right) + \frac{1}{2}Re\left(d_{11}v_{C11}{}^*\right) \end{array}\right) \tag{4.2}$$

$$pi_{L20} = \frac{1}{L_2}\left(d_{10}v_{C10} - v_{C20} + d_{10}v_{C20} + \frac{1}{2}Re\left(d_{11}v_{C11}{}^*\right) + \frac{1}{2}Re\left(d_{11}v_{C21}{}^*\right)\right) \tag{4.3}$$

$$pv_{C10} = \frac{1}{C_1}\left(-d_{10}i_{L20} + i_{L10} - d_{10}i_{L10} - \frac{1}{2}Re\left(d_{11}i_{L21}{}^*\right) - \frac{1}{2}Re\left(d_{11}i_{L11}{}^*\right)\right) \tag{4.4}$$

$$pv_{C20} = \frac{1}{C_2}\left(\begin{array}{l} i_{L10} + i_{L20} - d_{10}i_{L10} - d_{10}i_{L20} + i_2 - i_g - \frac{1}{2}Re\left(d_{11}i_{L11}{}^*\right) \\ - \frac{1}{2}Re\left(d_{11}i_{L21}{}^*\right) \end{array}\right) \tag{4.5}$$

Similarly, the other device currents and voltages are obtained and represented as follows:

$$i_{T0} = \left(d_{10}i_{L10} + d_{10}i_{L20} + \frac{1}{2}Re\left(d_{11}i_{L11}{}^*\right) + \frac{1}{2}Re\left(d_{11}i_{L21}{}^*\right)\right) \tag{4.6}$$

$$i_{T1} = d_{10}i_{L11} + d_{11}i_{L10} + d_{10}i_{L21} + d_{11}i_{L20} \tag{4.6a}$$

$$v_{T0} = \left(v_{C20} + v_{C10} - d_{10}v_{C20} - d_{10}v_{C10} - \frac{1}{2}Re\left(d_{11}v_{C21}{}^*\right) - \frac{1}{2}Re\left(d_{11}v_{C11}{}^*\right)\right) \tag{4.7}$$

$$v_{T1} = \left(v_{C21} + v_{C11} - d_{10}v_{C21} - d_{11}v_{C20} - d_{10}v_{C11} - d_{11}v_{C10}\right) \tag{4.8}$$

$$i_{d0} = \left(i_{L10} + i_{L20} - d_{10}i_{L10} - d_{10}i_{L20} - \frac{1}{2}Re\left(d_{11}{i_{L11}}^{*}\right) - \frac{1}{2}Re\left(d_{11}{i_{L21}}^{*}\right)\right) \tag{4.9}$$

$$i_{d1} = i_{L11} + i_{L21} - d_{10}i_{L11} - d_{11}i_{L10} - d_{10}i_{L21} - d_{11}i_{L20} \tag{4.10}$$

$$v_{d0} = -d_{10}v_{C20} - d_{10}v_{C10} - \frac{1}{2}Re\left(d_{11}{v_{C11}}^{*}\right) \tag{4.11}$$

$$v_{d1} = -d_{10}v_{C21} - d_{11}v_{C20} - d_{10}v_{C11} - d_{11}v_{C10} \tag{4.12}$$

Dynamic equations for ripple quantities:

$$pi_{L11} + j\omega_s i_{L11} = \frac{1}{L_1}\left(-v_{C21} - v_{C11} + d_{10}v_{C21} + d_{11}v_{C20} + d_{10}v_{C11} + d_{11}v_{C10}\right) \tag{4.13}$$

$$pi_{L21} + j\omega_s i_{L21} = \frac{1}{L_2}\left(d_{10}v_{C11} + d_{11}v_{C10} - v_{C21} + d_{10}v_{C21} + d_{11}v_{C20}\right) \tag{4.14}$$

$$pv_{C11} + j\omega_s v_{C11} = \frac{1}{C_1}\left(-d_{11}i_{L20} - d_{10}i_{L21} + i_{L11} - d_{10}i_{L11} - d_{11}i_{L10}\right) \tag{4.15}$$

$$pv_{C21} + j\omega_s v_{C21} = \frac{1}{C_2}\left(i_{L11} + i_{L21} - d_{10}i_{L11} - d_{11}i_{L10} - d_{10}i_{L21} - d_{11}i_{L20} + i_2 - i_g\right) \tag{4.16}$$

4.2.2 Steady State Calculations

Average Quantities:

At steady state, the derivatives of the peak values are zero, i.e. $px = 0$, therefore equations (4.2) through (4.5) for average quantities become:

$$0 = \left\{v_m - v_{C20} - v_{C10} + d_{10}v_{C20} + d_{10}v_{C10}\right\} \tag{4.17}$$

$$0 = \left\{d_{10}v_{C10} - v_{C20} + d_{10}v_{C20}\right\} \tag{4.18}$$

$$0 = -d_{10}i_{L20} + i_{L10} - d_{10}i_{L10} \tag{4.19}$$

$$0 = i_{L10} + i_{L20} - d_{10}i_{L10} - d_{10}i_{L20} + i_2 - i_g \tag{4.20}$$

From (4.19)

$$i_{L10} = \left(\frac{d_{10}}{1-d_{10}} \right) i_{L20} \tag{4.21}$$

Put (4.21) in (4.20)

$$i_{L20} = i_g - i_2 \tag{4.22}$$

From Equation (4.17) and (4.18)

$$v_{C10} = \left[\frac{(1-d_{10})}{d_{10}} \right] v_{C20} \tag{4.23}$$

$$v_{C20} = \frac{v_m d_{10}}{(1-d_{10})} \tag{4.24}$$

At steady state, $v_{C10} = v_m, v_{C20} = v_{0ut}$, $d_{10} = D$.

The above equation becomes:

$v_{out} = \frac{D}{1-D} v_m$, which agrees with that as obtained in literature **(Ned, 2003).**

Ripple Quantities

At steady state the derivatives of the peak values are zero, i.e. $px = 0$. Where x is a state variables. Therefore equations (4.13) through (4.16) for complex ripple quantities become: at $px = 0$

$$j\omega_s i_{L11} = \frac{1}{L_1}\left\{-v_{C21} - v_{C11} + d_{10}v_{C21} + d_{11}v_{C20} + d_{10}v_{C11} + d_{11}v_{C10}\right\} \tag{4.25}$$

$$j\omega_s i_{L21} = \frac{1}{L_2}\left\{d_{10}v_{C11} + d_{11}v_{C10} - v_{C21} + d_{10}v_{C21} + d_{11}v_{C20}\right\} \tag{4.26}$$

$$j\omega_s v_{C11} = \frac{1}{C_1}\left\{-d_{11}i_{L20} - d_{10}i_{L21} + i_{L11} - d_{10}i_{L11} - d_{11}i_{L10}\right\} \tag{4.27}$$

$$j\omega_s v_{C21} = \frac{1}{C_2}\left\{\begin{matrix} i_{L11} + i_{L21} - d_{10}i_{L11} - d_{11}i_{L10} - d_{10}i_{L21} - d_{11}i_{L20} \\ +i_2 - i_g \end{matrix}\right\} \tag{4.28}$$

$$\left\{j\omega_s L_1 i_{L11} + (1-d_{10})v_{C11} + (1-d_{10})v_{C21}\right\} = \left\{d_{11}v_{C20} + d_{11}v_{C10}\right\} \tag{4.29}$$

$$\left\{j\omega_s L_2 i_{L21} - d_{10}v_{C11} + (1-d_{10})v_{C21}\right\} = \left\{\beta d_{11}v_{C20} + d_{11}v_{C10}\right\} \tag{4.30}$$

$$j\omega_s C_1 v_{C11} - (1-d_{10})i_{L11} + d_{10}i_{L21} = -d_{11}i_{L20} \tag{4.31}$$

$$j\omega_s C_2 v_{C21} + i_2 - i_g - (1+d_{10})i_{L11} - (1+d_{10})i_{L21} = (d_{11}i_{L10} + d_{11}i_{L20}) \tag{4.32}$$

Representing the equation (4.25) to (4.28) in state space variable form:

$$x_i = \begin{bmatrix} i_{L11} \\ i_{L21} \\ v_{C11} \\ v_{C21} \end{bmatrix} \tag{4.33}$$

$$A_i = \begin{bmatrix} j\omega_s L_1 & 0 & (1-d_{10}) & (1-d_{10}) \\ 0 & j\omega_s L_2 & -d_{10} & (1-d_{10}) \\ -(1-d_{10}) & d_{10} & j\omega_s C_1 & 0 \\ -(1+d_{10}) & -(1+d_{10}) & 0 & j\omega_s C_2 \end{bmatrix} \tag{4.34}$$

$$b_i = \begin{bmatrix} d_{11}v_{C20} + d_{11}v_{C10} \\ d_{11}v_{C20} + d_{11}v_{C10} \\ -d_{11}i_{L20} - d_{11}i_{L10} \\ (d_{11}i_{L10} + d_{11}i_{L20}) + i_g - i_2 \end{bmatrix} \tag{4.35}$$

A MATLAB code is developed (see Appendix F) to calculate and plot the steady state values of the respective quantities. The result of the corresponding plots is shown in Figures (4.13) to (4.16). Moreso, Figure (4.1) shows the algorithm for obtaining the plots.

Figure 4.1 shows the algorithm for obtaining the ripple and steady state quantities.

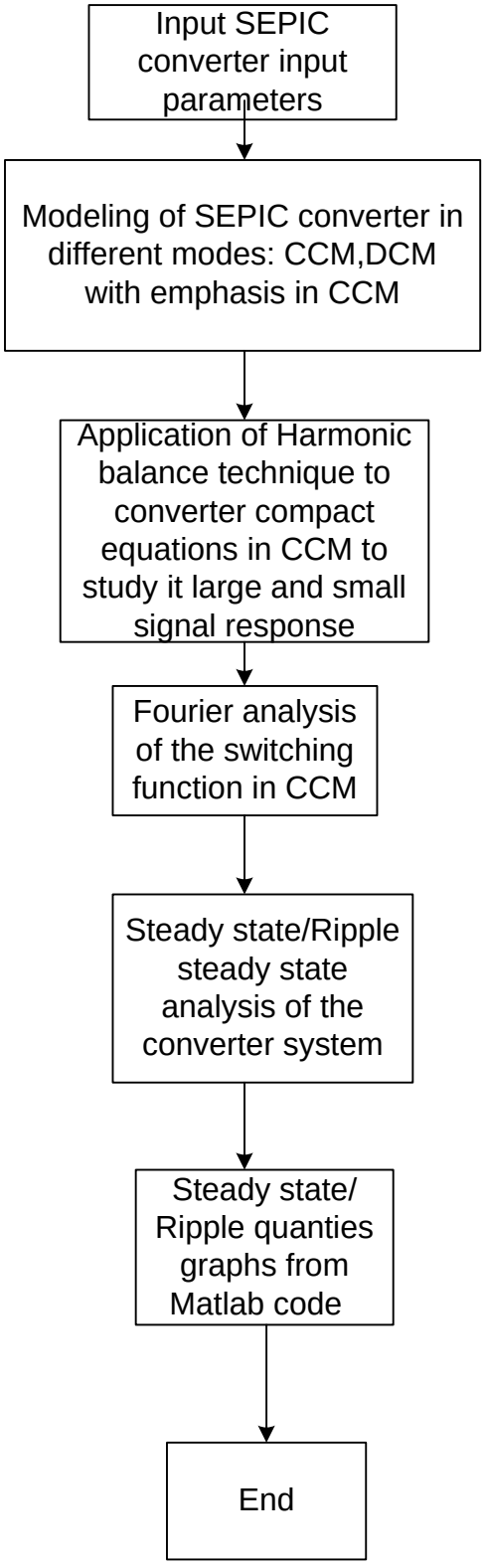


Fig. 4.1 Algorithm for Finding the Steady State and Ripple Quantities of SEPIC

4.3 RESULTS

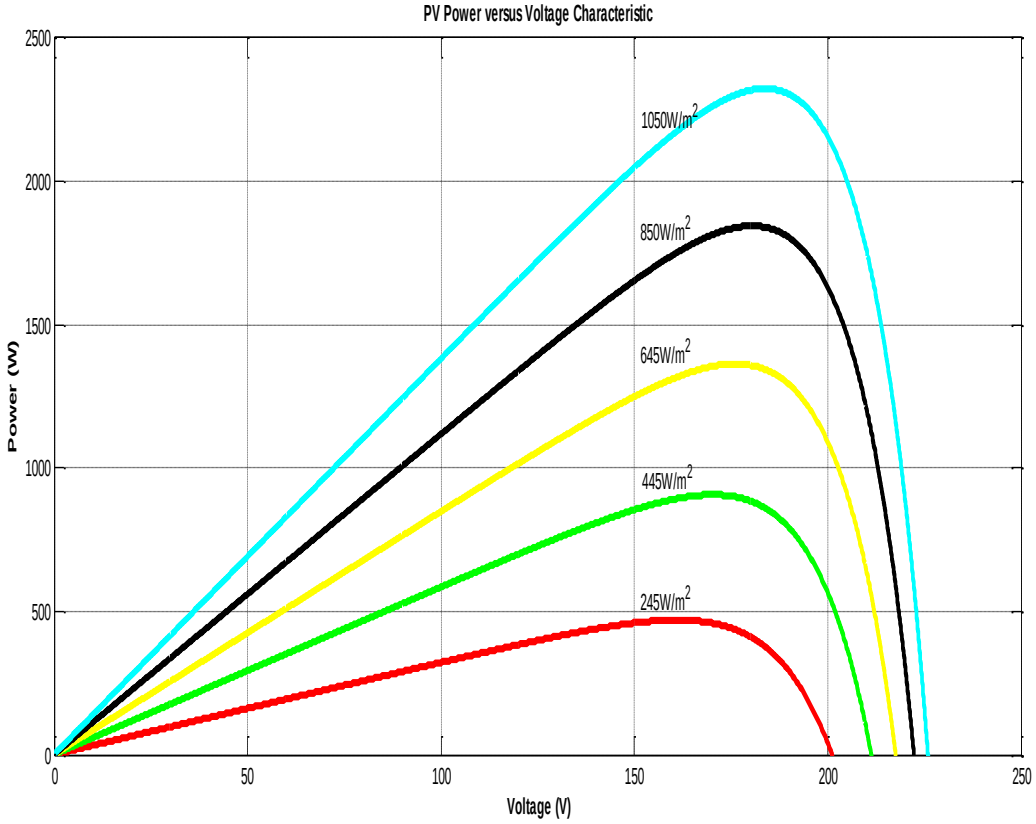


Figure 4.2 Power versus Voltage Curve of the Solar panel

Figure 4.2 shows the plot of PV module power against the voltage obtained for varying solar insolations as a parameter. The plot has been obtained using equations (3.9) to (3.10) and equation (3.3) together with solar insolation data of Table 3.1. In other to obtain maximum available power from the PV module, the PV module should be operated at the apex points of this maximum power curve. For a particular solar insolation as a parameter the power increases with increase in output voltage of the PV. This increase in power is further strengthen until a point on the curve where maximum power is extractable. Further increase in power beyond this point will cause the power available from the panel to reduce due to other factors which set in such as increase in temperature or the algorithm tracking mechanism of the converter unable to locate the maximum power point.

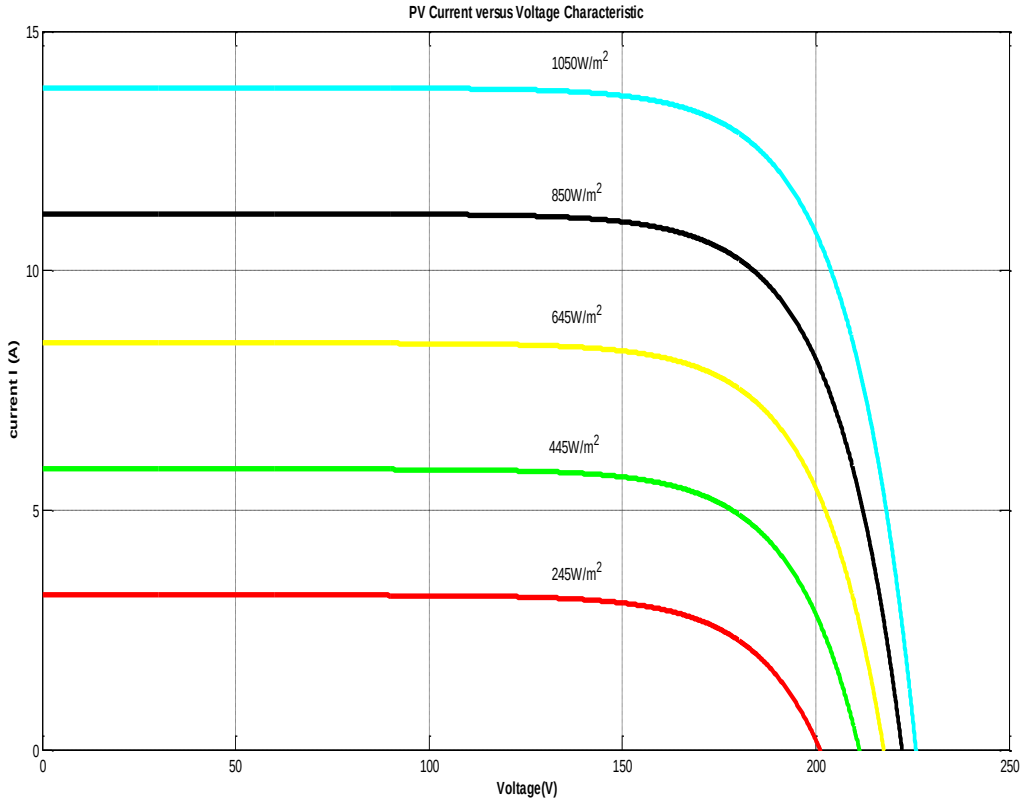


Figure 4.3 Current versus Voltage Curve of a Solar panel

Figure 4.3 shows a plot of the current versus voltage of the P-V module with varying solar insolation as a parameter. The plot have been obtained using equation (3.9) to (3.10) together with solar insolation data of Table 3.1. Maximum power from PV module is obtained by the area under the curve about the knee point for a particular solar insolation. it can be observed that the current remains appreciable constant as the voltage increases to some level, and falls back to zero in an attempt to increase the voltage further. This account the fact that the short cicuit current of a PV module can not sustain the current further beyond the voltage about the knee point.

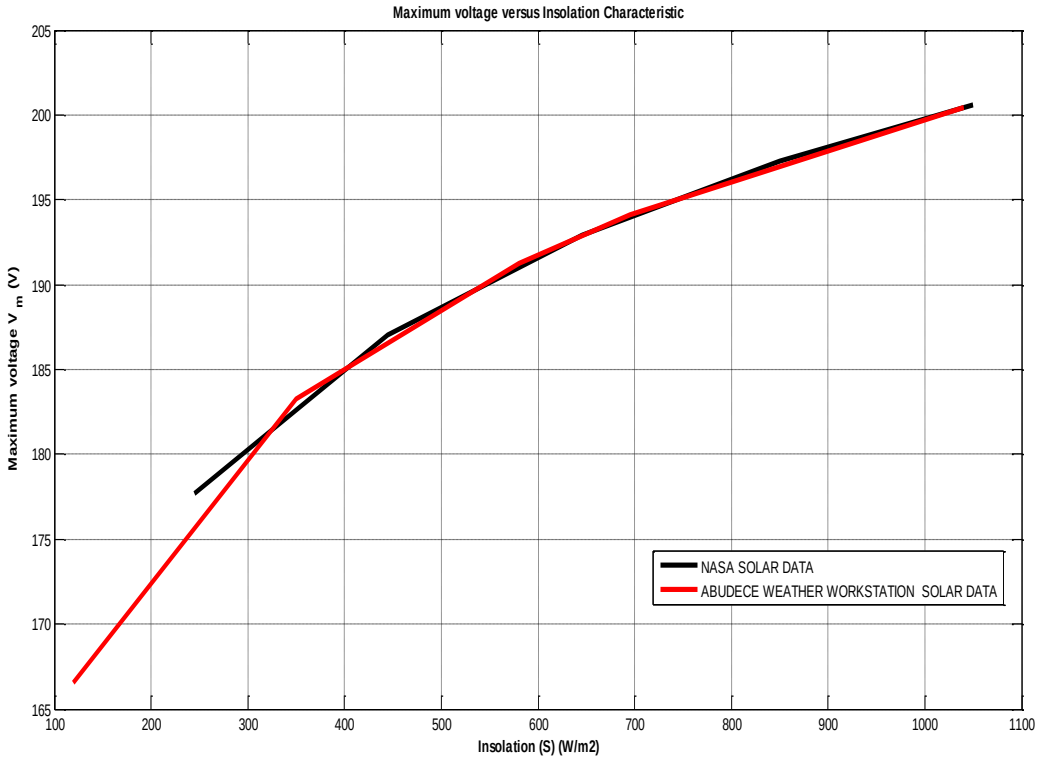


Figure 4.4 Voltage at Maximum Power versus Insolation

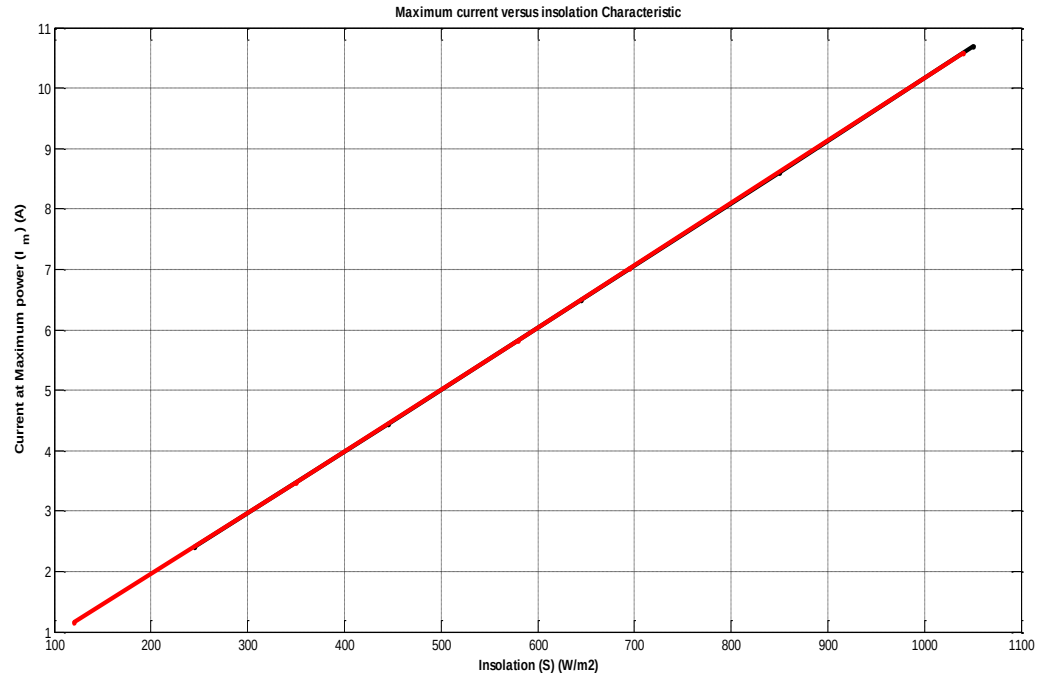


Figure 4.5 Output Current at Maximum Power versus Insolation

Figure 4.4 shows a comparison plot of voltage at maximum power against the varying insolation level for the two solar insolation data obtained from NASA and that obtained from the Weather Hawk IP (ABUDECE). It has been obtained using equation (3.9) and (3.10) and unique parameters of the solar panel alongside the solar insolation data in Table 3.1. The equation are key equations for obtaining the voltage at maximum power point analytically. The characteristics is plotted for optimum voltage versus change in insolation level. This graph is consequent to the fact that the optimum voltage available from the solar module changes with increase in insolation level. So, for maximum power to be extracted the SEPIC interfaced to the module should follow the curve as the insolation changes to extract maximum available power from the solar module. Figure 4.5 shows plot of current versus varying solar insolation levels. The plot was obtained based on the maximum voltage results of Figure 4.4 using equations (3.1)-(3.2) together with equations (3.9)-(3.10). The plot shows the variation of the current at maximum power point with varying solar insolations.

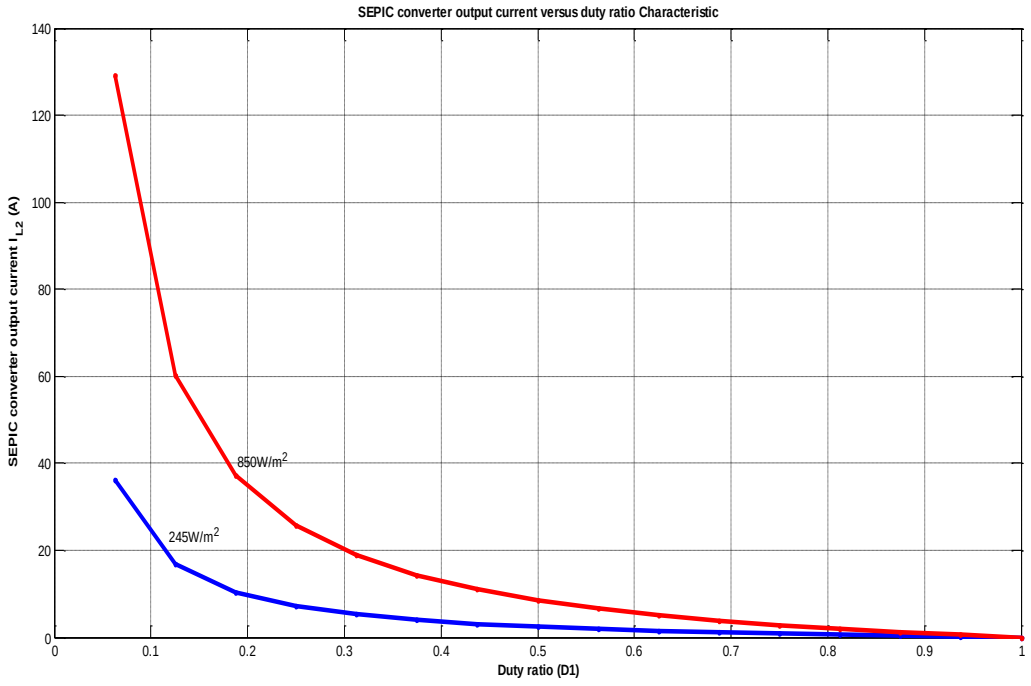


Figure 4.6 Output Current of the SEPIC versus Duty Ratio

Figure 4.6 shows the plot of the current from the SEPIC side provided for charging the battery and the dc motor connected via the dc grid, for varied duty ratio between zero(0) and one (1). The plot shows two solar insolation level for the study. Since the objective of the SEPIC based system is to supply load on the dc grid network; it is essential to have a measure

of the characteristics of output current from the SEPIC as the duty ratio is varied. Taking the lowest insolation level of $245W/m^2$ from Table 3.1, the nature of this graph have been obtained using equation (3.20), if the current balance was taking into consideration $i_{L2} = i_g - i_2$. In a case where the rated current of 12 A by the motor load is taken into account at duty ratio of 0.2, the current at the output of the SEPIC as shown by this plot will be insufficient. The deficit will have to be supplied by the the battery. However, if the insolation level were $850W/m^2$ as shown from the graph at duty ratio of 0.2 for the converter the current is 35 A. The current of 12 A will be sufficient for the motor and the remaining of the current will go into charging the battery. Nevertheless as the duty ratio is varied further, the current magnitude for both insolation levels falls slightly to zero signifying increase in duty ratio would not sustain full load current of the motor as oppose to operating the SEPIC at a duty ratio less than 0.2. Further more at very high insolation level of say $850W/m^2$ from the graph, operating the SEPIC at a duty ratio of less than 0.2 will lead to excessive current which will violate the philosophy of the research. As such the SEPIC conveter should be constrained to operate at duty ratio greater than 0.2 during period of high insolation and duty ratio of less than 0.2 for period of low solar insolation in order to meet full load requirement of the motor.

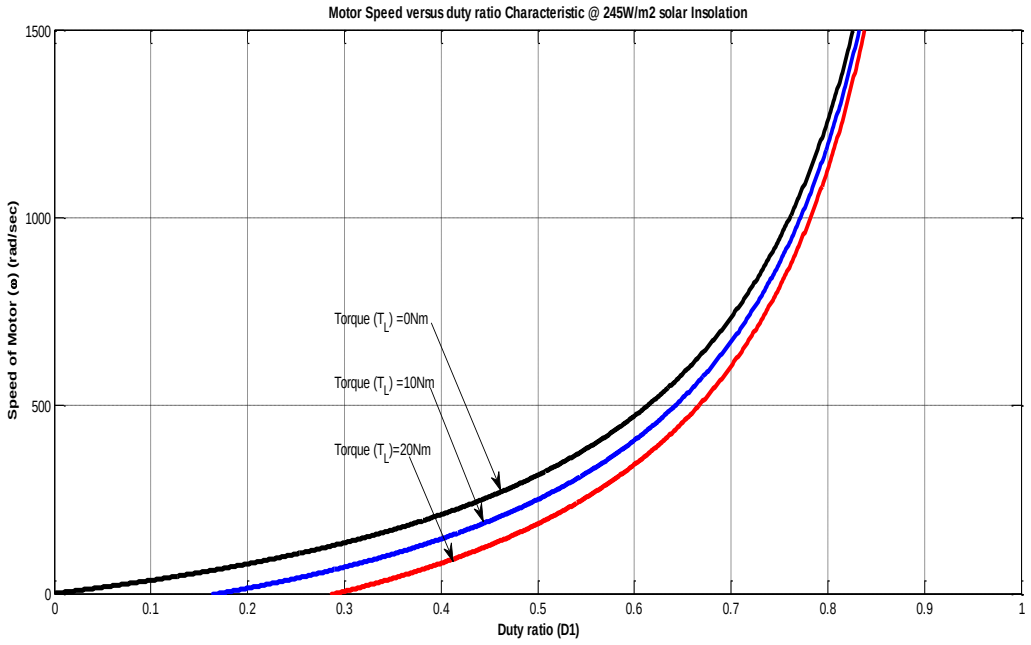


Figure 4.7 Motor Speed versus Duty Ratio with Load Torque as a Parameter at $245W/m^2$ Insolation Level

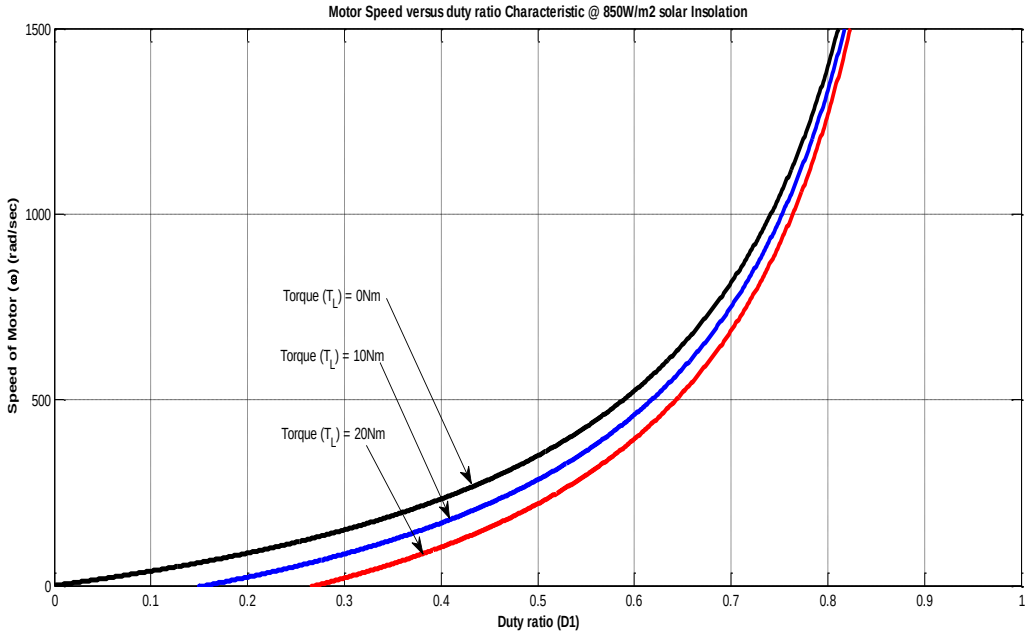
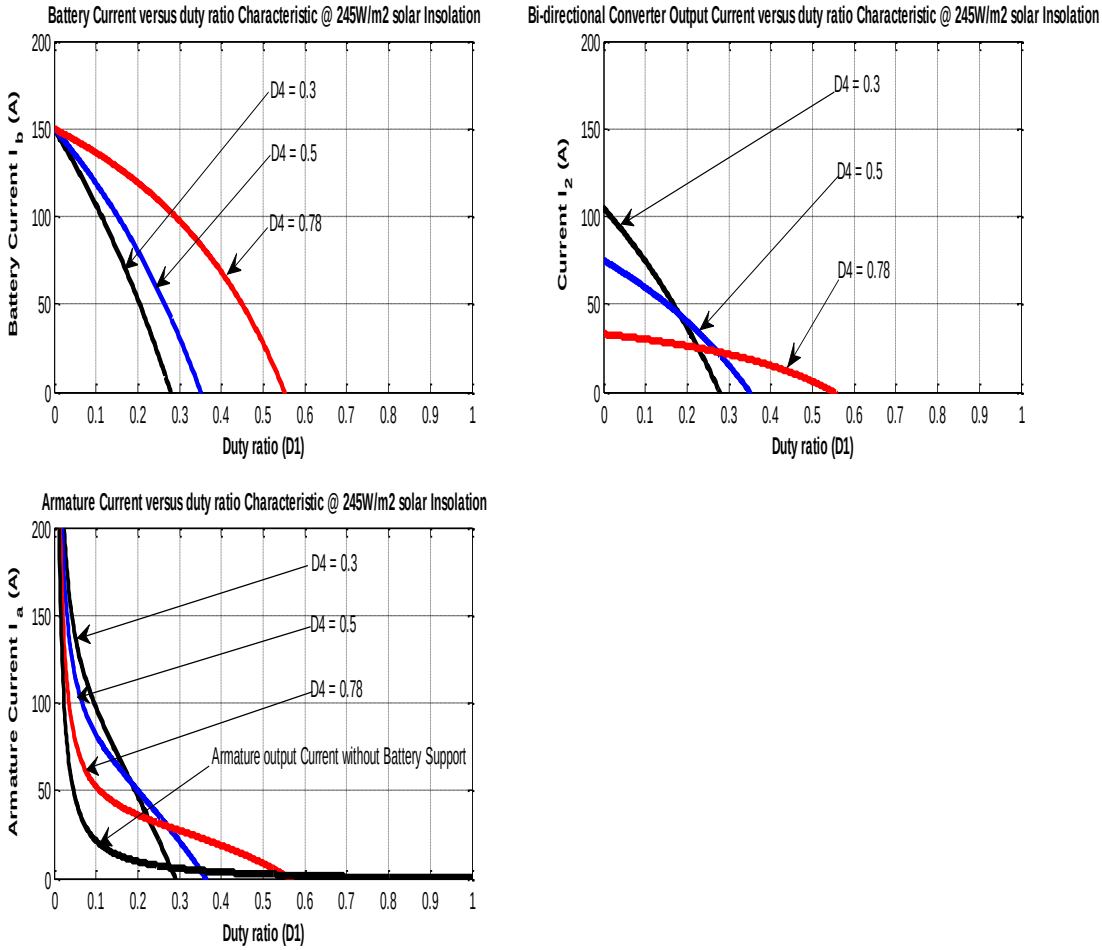


Figure 4.8 Motor Speed versus Duty Ratio with Load Torque as a Parameter at $850W/m^2$ Insolation Level

The characteristics of Figure 4.7 and Figure 4.8, is the speed versus duty ratio characteristics of SEPIC plotted for (i) solar insolation level of $245W/m^2$. (ii) solar insolation level of $850W/m^2$. The plots have been obtained using equation (3.26). The plots are consequent to the fact that the speed of the motor increases with inrease in duty ratio. Account from the two graphs shows that at no load ($T_L = 0\,Nm$), the motor finely increases and gain speed from zero with increase in duty ratio untill 0.5 and the relationship of this increase is almost linear. However, beyond the duty ratio of 0.5, the speed of the motor rises quickly as the duty ratio increases beyond this value. The consequent effect of this increase in speed is to decrease the current to the motor so as to keep the electromagnetic torque constant since the motor for this study is of fixed excitations. Drawing an inference from Figure 4.7, the plot shows that increase in load torque on the motor causes the speed to fall slightly from the no load speed to the new speed define by the speed curve with ($T_L = 10\,Nm$) as a parameter. This plot in Figure 4.7 shows that for $T_L = 10\,Nm$ and $T_L = 20\,Nm$ the converter will have to be operated at a duty ratios of approximately 0.2 and 0.3 respectively for the motor start from zero speed to any other speed as the duty ratio increases. Nevertheless as oppose to Figure 4.7, Figure 4.8 shows for load torque of $T_L = 10\,Nm$ and $T_L = 20\,Nm$ the motor will have to be operated

at a duty ratio of less than 0.2 and 0.3 for the motor to gain speed from zero speed to any other speed on the speed curve.



Figue 4.9 (a) Battery Current (b)Bi-Directional Output Current (c)Armature Current versus Duty Ratio of SEPIC

Figure 4.9 shows the plot of battery current, Bi-directional output current and armure current as a function of duty ratio with Bi-directional converter duty ratio as a parameter. The plots have been obtained using equations (3.18)-(3.19) and (3.21) for Bi-directional duty ratios of 0.3, 0.5, and 0.78 respectively. The choice of these duty ratios was to observe the system response to low solar insolation. At solar insolation level of $245W/m^2$, the battery discharges very rapidly as the duty ratio of the SEPIC is varied between zero(0) and one(1) with the Bi-directional converter duty ratio set at 0.3. This rapid discharge of the battery current account for the linearity of the graph. However, as the duty ratio is varied further with

the Bi-directional converter duty ratio set at another value of 0.5, the battery discharges. Further more as the duty ratio of the SEPIC is varied further with the Bi-directional converter duty ratio set at a value of 0.78, the battery discharge rate was not rapid compare to when the duty ratio of the Bi-directional converter was set at 0.3 and 0.5. This account to the fact that operating the duty ratio of the Bi-directional converter at 0.78 allows for the duty ratio of the SEPIC to be extended further beyond 0.2 to approximately 0.55. This is further made clear by the graph of Figure 4.9 (b) showing the current injected to the grid to support the armature current in a situation of low insolation. The graph of Figure 4.9 (b) shows the plot of the current injected to the dc grid for different Bi-directional duty ratios as the SEPIC duty ratio is varied. A closer observation of the Figure 4.9 (c) shows the plot of armature current without battery support plotted on the same graph with that with battery supports for different Bi-directional duty ratios as a parameter. This plot draws an inference that operating the Bi-directional converter at a duty ratio of 0.78, paid off than operating at any other duty ratio of 0.3 and 0.5. The contribution of the current from the battery was seen to mitigate the deficit from solar by operating the SEPIC duty ratio between 0.1 and 0.5.

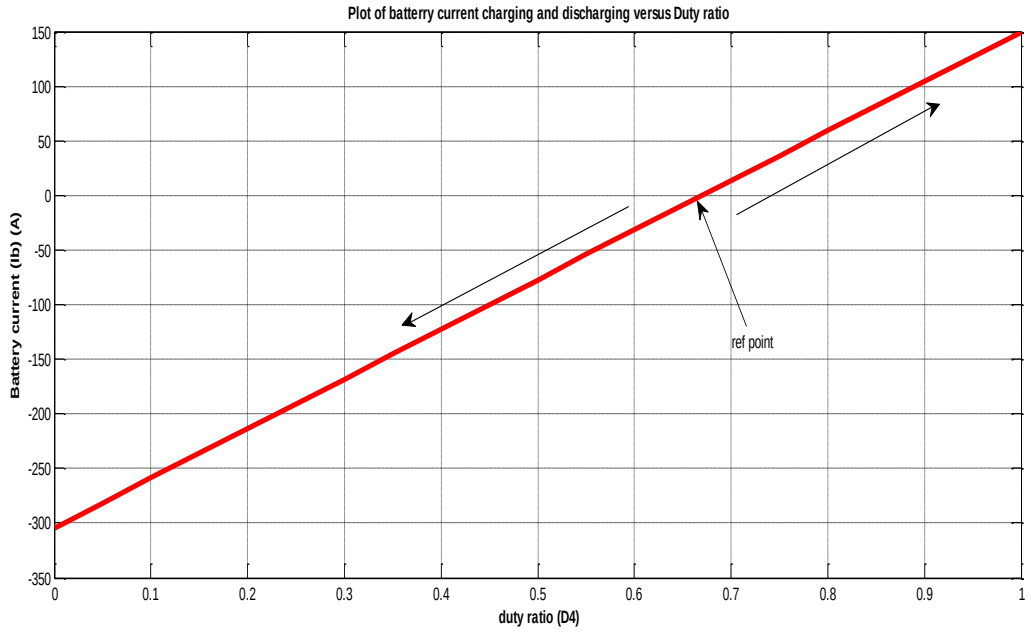


Figure 4.10 Battery Current versus Duty Ratio of Bi-Directional Converter

Figure 4.10 shows the plot of variation of the duty ratio of the Bi-directional converter with the battery current. The graph has been obtained using current equation (3.12). In this graph, a reference point has been highlighted denoting the battery is neither charging or discharging and this occur at a duty ratio of approximately 0.65. Here, negative current in this graph is termed the battery is charging, and positive current signifies the battery is delivering current to the grid through the Bi-directional converter.

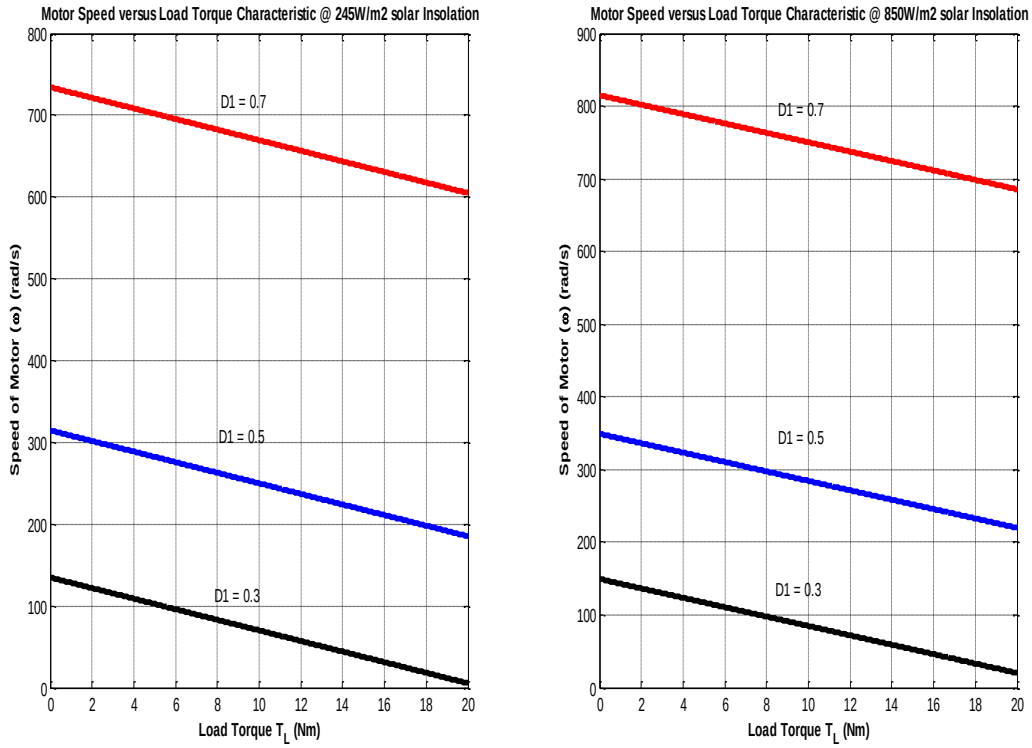


Fig. 4.11. Torque versus Speed Characteristics

The two plots of Figure 4.11 show the variation of load torque on the permanent magnet d.c motor with repect to change in speed at different Bi-directional converter duty ratios. The plots have been obtained using equation (3.26) for two solar insolation level of $245W/m^2$ and $850W/m^2$ respectively denoting the least and the most prevalent solar insolations . The nature of the graph is consequent to the fact that the speed of the motor drops under the influence of increase in load on the motor for different solar insolation and SEPIC duty ratios undertaken. However, if the desire is to increase the motor speed for a particular load torque, under a particular solar insolation level, the duty ratio would have to be increased to meet the increase in speed as quickly as possible. This is shown on the two plots of Figure 4.11.

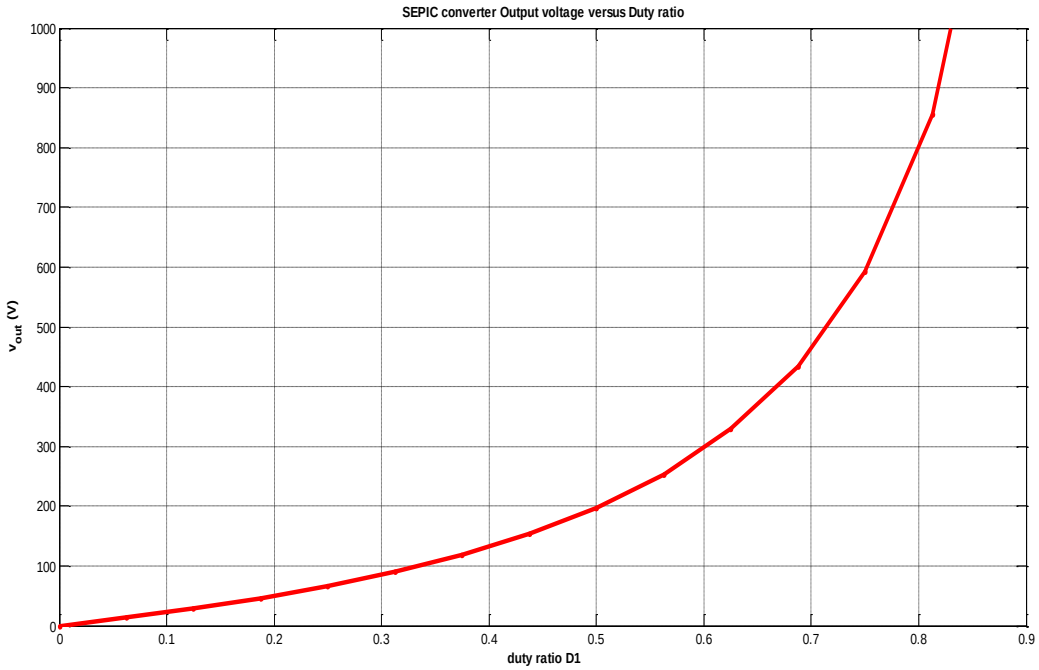


Fig. 4.12. SEPIC Output Voltage versus Duty Ratio

Figure 4.12 shows the output voltage of the SEPIC as the duty ratio is varied from zero(0) and 0.9. The plot has been obtained using equation (3.16). The plot is consequent to the fact that the output voltage of the SEPIC increases with increase in duty ratio. As the duty ratio is varied between 0 and 0.5, the plot is almost linear. But as the duty ratio is varied beyond 0.5, the voltage rises steeply denoting that for little increase in duty ratio beyond 0.5, more voltage magnitude can be gained as a result of little rise in duty ratio beyond value of 0.5.

Steady State Average and Ripple Quantity Plots Using Harmonic Balance Technique:

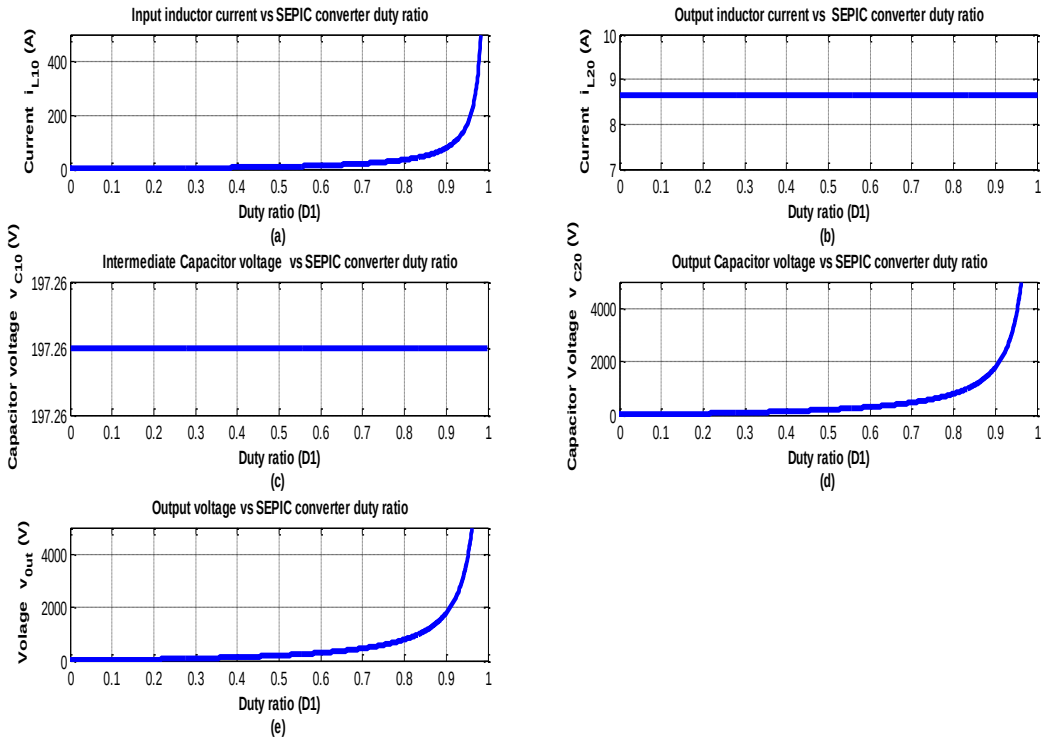


Figure 4.13: Steady State Average Quantities (State Variables), (a) i_{L10}, (b) i_{L20}, (c) v_{C10}, (d) v_{C20}, (e) v_{0ut},

Figure 4.13 shows steady state SEPIC state variables as the duty ratio is varied. The plots of (a) to (e) have been obtained using equations (4.21) to (4.24). A MATLAB code written to obtain this plot is shown in Appendix F. An algorithm for developing the MATLAB code is given in Figure 4.1. Plot of Figure 4.13(a), (d), (e) shows that the input inductor current, output capacitor voltage and output voltage increases with increase in duty ratio of the SEPIC. The plot of Figure 4.13(b), (c) shows that the current and voltages obtained are independent of the duty ratio of the converter. For this analysis, the intermediate capacitor voltage has been keep constant, it is assumed that the capacitor value is large enough to keep the voltage across it constant, this account for the constant voltage with respect to duty ratio variations.

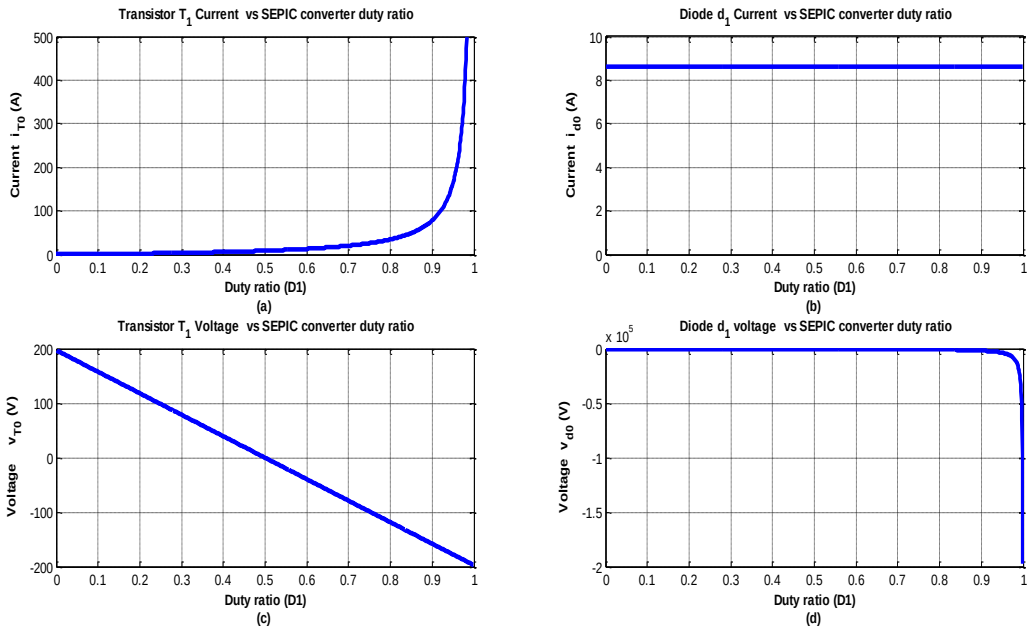


Figure 4.14: Steady State Average Quantities (Devices Current and Voltage), (a) i_{T0}, (b) v_{T0} (c) i_{d0}, (d) v_{d0}

Figures 4.14 (a) and (b) and Figure 4.14 (c) and (d) shows the respective steady state current and voltages for the switching devices for the SEPIC system. The plots have been obtained using equation (4.6). The plot of Figure 4.14(a) shows that the transistor current increases with increase in duty ratio from zero(0) and one(1) as oppose to the plot of the diode current shown in Figure 4.14(b), the plot shows that diode current is not affected by change in the duty ratio of the converter, this is consequent to the fact that the diode current depend on the inductor current i_{L20} at steady state, and i_{L20} does not depend on duty ratio from the analytical rigor from the harmonic balance technique used. Figure 4.14(c) depicts the variation of the transistor voltage with the converter duty ratio. The plot showed that the transistor voltage drops with increase in the converter duty ratio. Figure 4.14 (d) depicts the steady state diode voltage as the converter duty ratio is varied. The plots gives the diode voltage withstands capabilities as the duty ratio is varied between zero (0) and one (1).

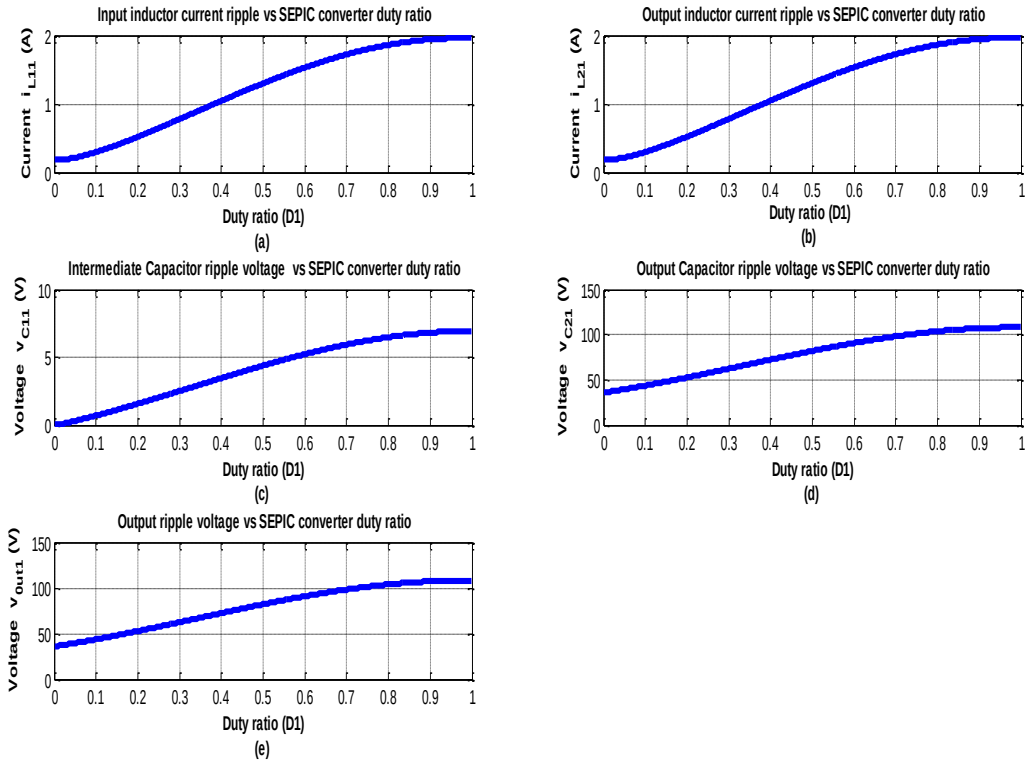


Figure 4.15: Steady State Average Ripple Quantities (State Variables),(a) i_{L11}, (b) i_{L21}, (c) v_{C11}, (d) v_{C21}, (e) v_{0ut1}

Figures 4.15 (a)-(e) depicts the plots of the inductor current and capacitor voltage ripples as the duty ratio is varied. The plots have been obtained using equations (4.33) to (4.35) altogether. The plots give an account of ripple quantities of the respective variables as the duty ratio is varied. For a particular operating duty ratio of the converter, the complex ripple quantities imposed on the current or voltages of the converter system can be determined. The plots shows that as the duty ratio is varied the complex ripple quantities of the respective variables shown on the plots increases. The ideology behind these plots was to select passive and filter components for the inductor and capacitor values with the less ripple for a particular duty ratio.

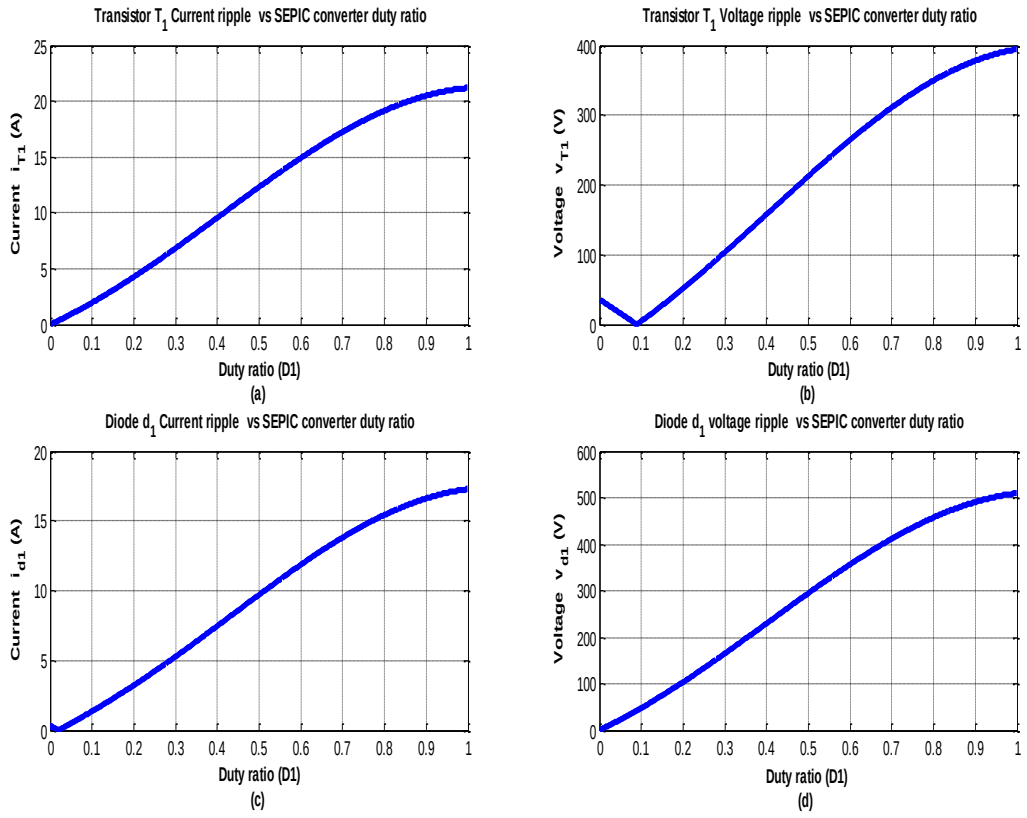


Figure 4.16: Steady State Ripple Quantities (Devices Current and Voltage), (a) i_{T1}, (b) v_{T1}, (c) i_{d1}, (d) v_{d1}

Figures 4.16 (a) to (d) depict the steady state average ripple quantities for the devices current and voltages used in the SEPIC system. The plots have been obtained using equation (4.6a), (4.8), (4.10), and (4.12). The plots are consequent to the fact that the ripples of the devices current and voltages increase with increase in duty ratio of the converter system. The plots are expected to grow of the form obtained as the duty ratio is increase, since the devices are switched at a very high frequency. Figure 4.16 (b) shows that when the duty ratio is varied from zero (0) and 0.1, the voltage ripple across the transistor collapses to zero (0). The reason for this was due to the fact that at start up, the voltage across the switching transistor drops to zero. But as the duty ratio is increase further beyond this value of 0.1 and 1, the voltage ripple increases.

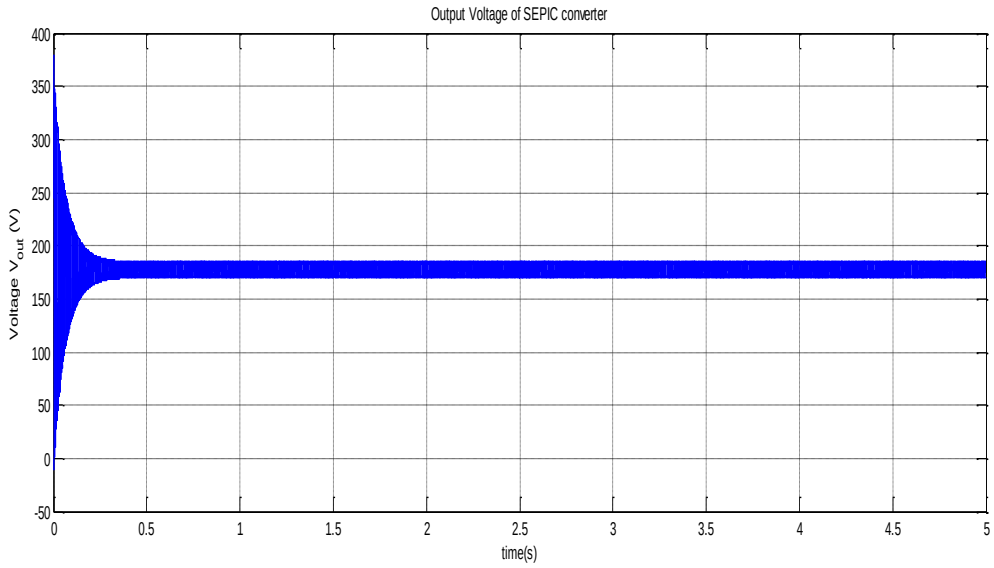


Figure 4.17 SEPIC Output Voltage versus time

Figure 4.17 shows the plot of the SEPIC voltage at run up. The plot has been obtained from the MATLAB/Simulink of the entire system shown in Appendix G. The plot shows that at start up the capacitor voltage rises during it transient period to approximately 350 V. The transient voltage gradually settles to steady state as the time progress. The essence of this sharp rise in voltage at run up is due to the fact that the initial condition of the capacitor was zero. The steady state is attained at $0.5\,s$ with the average capacitor voltage at approximately $190V$. This value of voltage when compared to steady state result obtained earlier from Figure 5.12 at duty ratio of 0.5 shows good agreement.

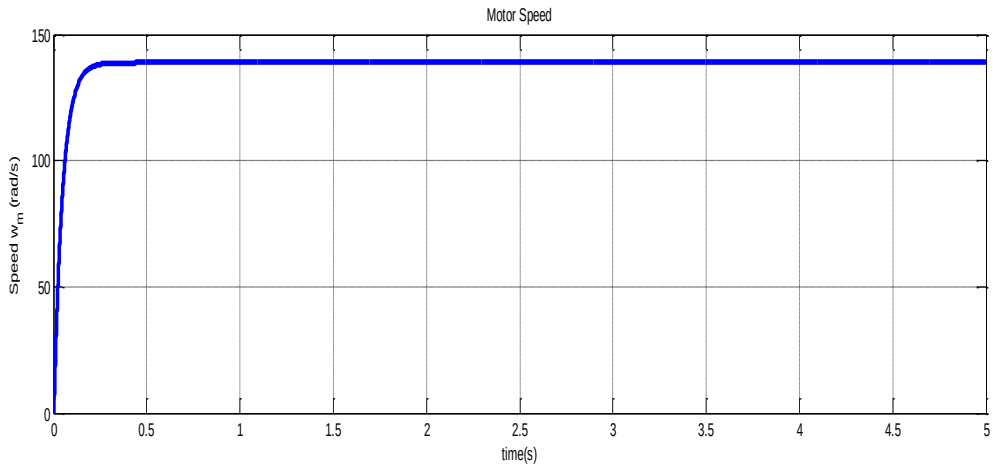


Figure 4.18 Motor Speed versus time

Figure 4.18 shows the plot of the permanent magnet dc motor speed at run up. The plot has been obtained from the MATLAB/Simulink of the entire system shown in Appendix G. The plot shows that at start up the motor build up speed from zero to a steady state of approximately 140 rad/s. This value of speed when compared to steady state result obtained earlier from Figure 5.11 at duty ratio of 0.3 shows good agreement.

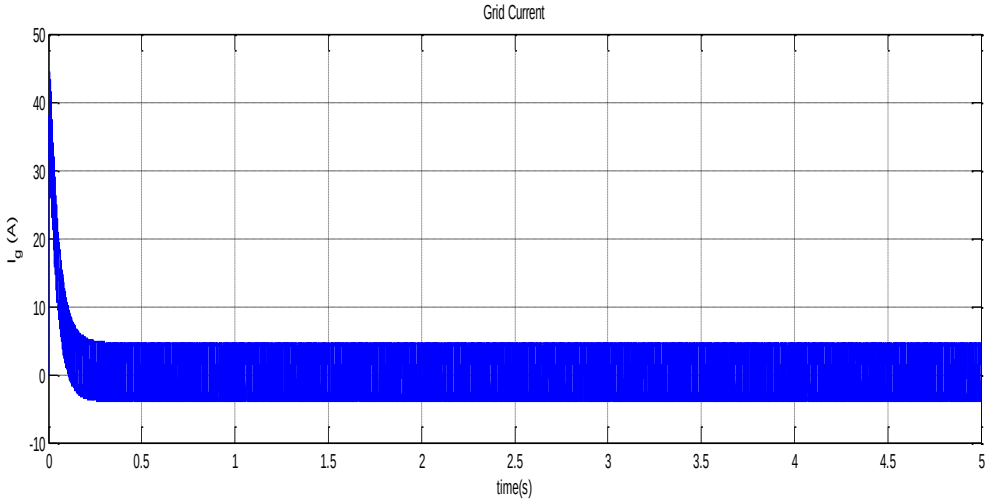


Figure 4.19 Grid Current versus time

Figure 4.19 shows the plot of the grid current at run up. The plot has been obtained from the MATLAB/Simulink of the entire system shown in Appendix G. The plot shows that at start up the grid current rises to approximately 40 A. The sharp rise in this current is due to the fact that at start up large amount of current is required by the motor to overcome it inertial and bring the motor up to speed. As the motor gain speed the current demand is less. This account for the current falling to steady state value as the time progresses as obtained in Figure 4.19.

4.4 Conclusion

The developed model of the system in Chapter Four has been solved in this chapter. A MATLAB script has been written to obtain the response of system under different operating conditions. The power flow within the system is shown including some simulation result of certain aspects of the system.

CHAPTER FIVE

CONCLUSION AND RECOMMENDATION

This chapter presents the conclusion of the work. A summary of the study is stated so also some recommendation for further work.

5.1 Summary

In this work, the Model, Analysis and Simulation of a SEPIC based Solar Electricity system has been studied for supplying current to dc load. This has been made possible by the inclusion of Energy Storage System (battery) in the DC-link of the grid. The battery is connected through a bi-directional DC-DC converter for efficient utilization.

An in-depth analytic study of the system has been done using the system model derived from first principle, MATLAB/Simulink and the solar data for Zaria obtained from NASA and solar data obtained from the ground weather work station at the ABUDECE power and machine Laboratory. This study has enabled the determination of the behavior of the system under various operating conditions. System shows capability to meet the load current requirement in a case of low solar insolation. Moreover, the variations of the duty ratio of the SEPIC with respect to complex ripple quantities and steady state quantities have been shown.

The operation of the system have been studied, the load current is supplied by the battery and the solar. The contribution of the battery current to the load is evident and depends on the converter duty ratio only to an extent.

5.2 Conclusion

This research has extended the functionality of dc grid SEPIC based electricity equipped with a battery to serve power to a permanent magnet dc motor. The system has been modeled to meet the current requirement of the load should the current from solar side falls below the dc motor demand.

i. A systematic step by step development of the system model has been carried out.
ii. The method of harmonic balance technique have been deployed to the SEPIC state variables to find the steady state average and steady state ripple quantities of the SEPIC for varied range of duty ratio.

iii. The terminal characteristics of the converter under steady state for continuous current mode at varied duty ratio have been studied. It has also been shown that, in a case of low solar insolation, the current supplied to the load for specific ranges of Bi-Directional converter duty ratio was improved upon.

iv. The dynamic analysis of the entire system has been carried out using MATLAB to study the system capabilities and collaboration in meeting system load power thereby ensuring efficient utilization of available alternative source of energy

5.3 Limitation of the Study

Whereas, solar data for the analysis was obtained from NASA and ABUDECE weather workstation, experimental validation was not completely possible since building the system itself is capital intensive.

5.4 Recommendation for Further Work

The following recommendations are made for the advancement of the current effort.

The solar data used from NASA and on ground measurement solar data obtained at the weather work station at the power and machine laboratory of the department of Electrical and Computer Engineering shows the behavior of load connected on the dc grid. However, it would be desirable to study how the behavior of solar data obtained from NIMET in comparison with on ground measure data at power and machine laboratory ABUDECE and that from NASA notably relate or fallout from one another. So it would be an improvement of the current effort if the data of these solar resources were tested on real system for ease of comparison so as to have strong judgment of the system behavior.

i. The battery can be sized depending on the maximum load it is to supply so that the exact behavior of the system can be observed at its extreme point.

ii. For determination of the exact current which the SEPIC can inject into the grid, there would be need to appropriately size the PV and battery. Factors such as ambient temperature, days of autonomy and so forth would then need to be considered. This is an area in which further work can be done.

iii. The system can be used as a Distributed Generation (DG) source such that other renewable energy source such as wind, bio fuel etcetera can be considered. In light

of this, an energy mix constituting the PV system, wind energy system and the energy storage will has to be properly sized.

v. Units of this solar based SEPIC based system can be built and integrated together in some form of radial network where the overall performance of the system can be investigated.

vi. This presentation in one volume of model development will serve as reference material for subsequent researchers.

REFERENCES

Badawy, M. O., Yilmaz, A. S., Sozer, Y., & Husain, I. (2014). Parallel Power Processing Topology for Solar PV Applications. IEEE Transactions on Industry Applications, 50(2), 1245 - 1255.

Caisheng Wang, & Nehrir, M. H. (2008). Power Management of a Stand-AloneWind/Photovoltaic/Fuel Cell Energy System. IEEE Transactions on Energy Conversion, 23(3), 957 - 967

Chang, Y.-C., & Liaw, C.-M. (2011). Establishment of a Switched-Reluctance Generator-Based Common DC Microgrid System. IEEE Transactions on Power Electronics, 26(9), 2512 - 2527

Chapra;, S. C., & Canale, R. P. (2010). Numerical methods for Engineers (sixth ed.). Singapore: Mc Graw Hill.

Chiang S.J, Hsin- Jang S, & Ming-Chieh C. (2009). Modeling and control of PV charger system with SEPIC. IEEE transactions on industrial electronics, 56(11), 4344-4353.

Chuang, Y.-C., Ke, Y.-L., Chuang, H.-S., & Chang, S.-Y. (2012). Battery Float Charge Technique Using Parallel-Loaded Resonant Converter for Discontinuous Conduction Operation. IEEE Transactions on Industry Applications 48(3), 1070 - 1078

Edwin, K. (2006). Advance Engineering Mathematics, 9th Edition. Wiley International edition.

Fanbo He, Zhengming Zhao, Ting Lu, & Liqiang Yuan. (2010). Predictive DC voltage control for three-phase grid-connected PV inverters based on energy balance modeling. 2nd IEEE International Symposium on Power Electronics for Distributed Generation Systems (PEDG) 516 - 519

Gonzalez-Llorente J.L, Eduardo I.O., & Andres D. (2009). A maximum power point tracker using positive feedforward control based on the dc motor dynamics and PVM mathematical model'. IEEE Electric Machines and Drives Conference (IEMDC), pp. 259-264.

Gujar M., Datta A., & P., M. (2013). Smart Mini Grid: An innovative distributed generationbased energy system. IEEE Innovative Smart Grid Technologies - Asia (ISGT Asia), 2013, 1 - 5.

Han B., Ledwich G., & Karaday G. (1999). Study of resonant Fly-back converter for dc distribution system. IEEE Transaction on Power delivery, 14(3), 1069-1074.

Karimi-Davijani, H., & Ojo, O. (2011). Modeling and steady-state analysis of a stand-alone, photo-voltaic-three phase inverter power system. Twenty-Sixth Annual IEEE Applied Power Electronics Conference and Exposition (APEC) 1259 - 1266

Keyhani, A. (2011). Design of Smart Power Grid Renewable Energy System (First ed.). NJ: John Wiley and Sons Inc., Hoboken, New Jersey.

Kuei-Hsiang Chao, Ching-Ju Li, & Ho, S.-H. (2008). Modeling and fault simulation of photovoltaic generation systems using circuit-based model. IEEE International Conference on Sustainable Energy Technologies, 2008. ICSET 2008. , 290 - 294

Lung-Sheng Yang, Tsorng-Juu Liang, & Chen, J.-F. (2009). Transformerless DC–DC Converters With High Step-Up Voltage Gain. IEEE Transactions on Industrial Electronics, 56(8), 3144 - 3152

Mahmud M.A, H.R Pota, M.J Hossain, & Roy, N. K. (2014). Robust partial feedback linearizing stabilization scheme for three phase grid connected photovoltaic systems. IEEE journal of photovoltaic, 4(1), 423-431.

Mapurunga Caracas, J. V., De Carvalho Farias, G., Moreira Teixeira, L. F., & de Souza Ribeiro, L. A. (2014). Implementation of a High-Efficiency, High-Lifetime, and Low-Cost Converter for an Autonomous Photovoltaic Water Pumping System. IEEE Transactions on Industry Applications, 50(1), 631 - 641.

National Aeronautical and Space Agency. (NASA, 2013).

Ned Mohan., Robbins W. P., & Underland;, T. M. (2003). Power Electronics Converters, Applications, and Design (Third ed.). NJ: John Wiley and Sons, INC.

Omran, W. A., Kazerani, M., & Salama, M. M. A. (2011). Investigation of Methods for Reduction of Power Fluctuations Generated From Large Grid-Connected Photovoltaic Systems. IEEE Transactions on Energy Conversion 26(1), 318 - 327

Rashid, M. H. (2005). Power Electronics Circuits, Devices, and Applications (Third ed.). New Delhi: Prentice-Hall of India Private Limited.

Roshan Y.M., & Moallem M. (2012). Maximum power point tracking using boost converter input resistance control by means of Lambert W-Function. 3rd IEEE International Symposium on Power Electronics for Distributed Generation Systems (PEDG), 2012 195 - 199.

Sangho Ko & Robert R. (2006). Identification for nonlinear feedback limit-cycle systems using harmonic balance methods. Proceeding of 45th IEEE Conference on decision and control. 2006, 2506-2511

Shihong Qin, Min Wang, Teng Chen, & Xiangling Yao. (2011). Comparative analysis of incremental conductance and perturb-and-observation methods to implement MPPT in photovoltaic system. International Conference on Electrical and Control Engineering (ICECE), 2011, 5792 - 5795

Thounthong, P. (2011). Model Based-Energy Control of a Solar Power Plant With a Supercapacitor for Grid-Independent Applications. IEEE Transactions on Energy Conversion, , 26(4), 1210 - 1218.

Veerachary, M. (2012). Two-Loop Controlled Buck–SEPIC for InputSource Power Management. IEEE Transactions on Industrial Electronics 59(11), 4075 - 4087

Wandhare, R. G., & Agarwal, V. (2012). Novel control scheme to reduce the effect of intermittent solar radiation on the grid connected PVsystem power output without losing MPPT. Twenty-Seventh Annual IEEE Applied Power Electronics Conference and Exposition (APEC) 79 – 85.

Xin Li, Bo Hu, Xisting Ling & Xuan Zeng (2002). A wavelet-Balance approach for Steadt state analysis of nonlinear circuit. IEEE transaction on circuit and systems-I,Fundamental theory and Application. 49(5), 689-694.

Yazdani, A., & Dash, P. P. (2009). A Control Methodology and Characterization of Dynamics for a Photovoltaic (PV) System InterfacedWith a Distribution Network. IEEE Transactions on Power Delivery, 24(3), 1538 - 1551

Zhao R., & Kwasinski A. (2009). Multiple input single ended primary inductance converter (SEPIC) converter distributed generation application. Energy conversion congress and exposition, 20(24), 1847-1185.

APPENDIX A

SEPIC SIDE

The SEPIC used for this research is shown in Figure A1. It consist of an input capacitor C_0, which serves as a voltage bank to the input of the SEPIC. Two inductors L_1 and L_2. Two capacitors C_1 and C_2. One active switch and a passive switch. For continuous conduction modes (CCM). There are two states of the switch within the switching period T, corresponding to the status of switch S_1 and switch S_2. S_1 could be a MOSFET, power bipolar junction transistor (BJT), Insulated gate bipolar transistor (IGBT), or any high power switching device. During the first switching interval S_1 is on for a period defined by $t \epsilon [0, DT]$, while S_2 is off. During the next interval S_1 is off and S_2 is on for a period within the interval $t \epsilon [DT, T]$. It is assumed the converter is lossless, and that there is an internal control algorithm that adjust the duty ratio of the converter to extract the maximum power from the panel

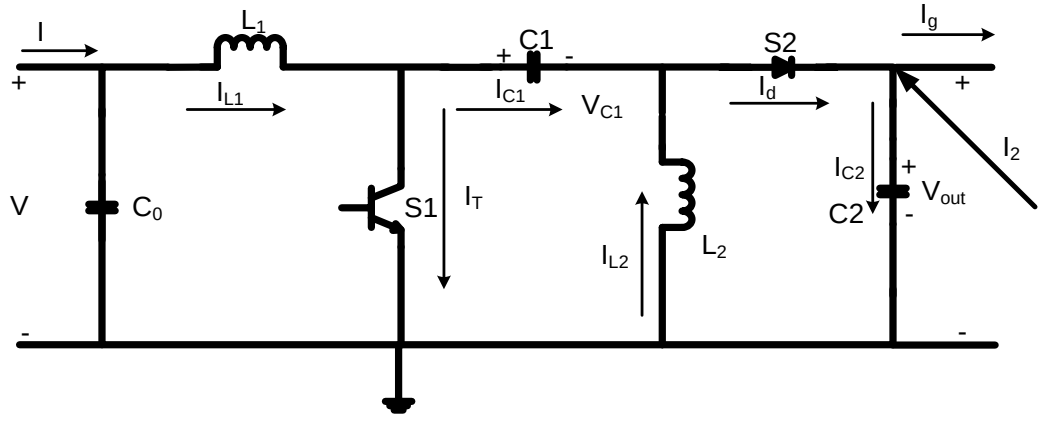


Figure A1. Schematic of SEPIC

MODE1.

S_1 is on and S_2 is off. The new topology of the circuit of Figure A1 is reduce to Figure A2

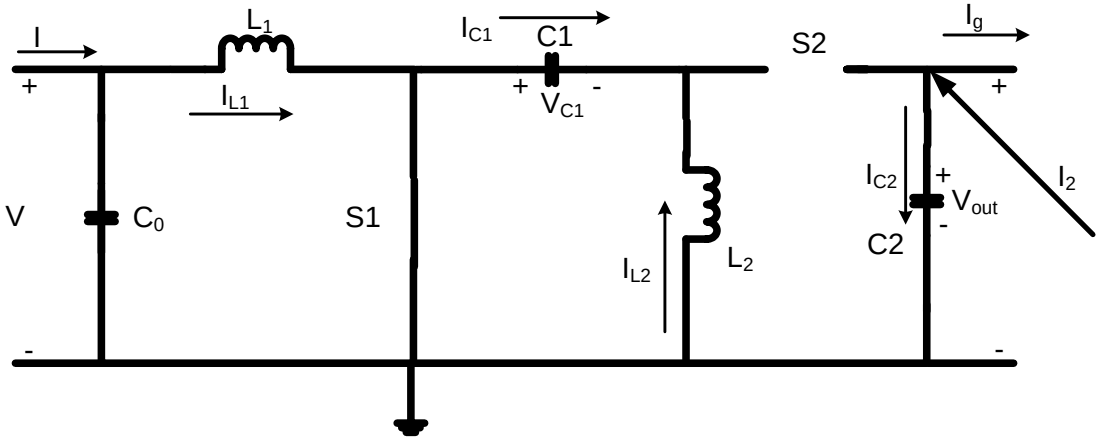


Figure A2 Mode 1 Circuit Topology

MODE 2.

S_1 is off and S_2 is on. The new topology of the circuit of Figure A1 is reduce to Figure A3

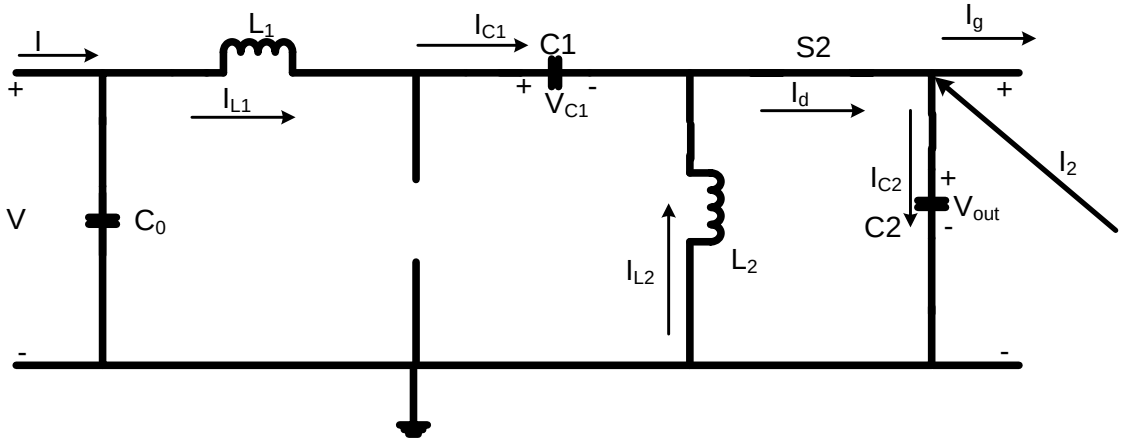


Figure A3 Mode 2 Circuit Topology

$$\left.\begin{aligned} C_0 pv &= i - i_{L1} \\ L_1 pi_{L1} &= v - (1-S_1)(v_{C1} + v_{out}) \\ L_2 pi_{L2} &= S_1 v_{C1} - (1-S_1) v_{out} \\ C_1 pv_{C1} &= (1-S_1) i_{L1} - S_1 i_{L2} \\ C_2 pv_{out} &= i_{L1}(1-S_1) + i_{L2}(1-S_1) + i_2 - i_g \end{aligned}\right\} \quad \text{(A.1)}$$

$$\left.\begin{aligned} i_T &= S_1 (i_{L1} + i_{L2}) \\ v_T &= (1-S_1)[v_{C1} + v_{out}] \\ i_d &= (1-S_1)[i_{L1} + i_{L2}] \\ v_d &= -S_1 v_{out} - S_1 v_{C1} \end{aligned}\right\} \quad \text{(A.2)}$$

Equation A.1 and A.2 respectively correspond to the combine equation of the two modes. To obtain mode 1 model equations S_1 is replace with the number 1. Similarly for mode 2, S_1 is replace with the number zero.

I. DESIGN OF SEPIC PARAMETERS:

The parameters of the SEPIC can be determined using the inductor current equations and capacitor voltage equation **(Rashid et al, 2003)** for the two modes of the operating regimes to determine the values of inductor L_1 and L_2. Also capacitor values C_1 and C_2. Assuming the converter to operate in continuous conduction mode (CCM).

For mode 1:

The voltage across the inductor L_1 when switch S1 is on and switch S2 off is:

$$v = L_1 \frac{di_{L1}}{dt} \quad \text{(A.3)}$$

Applying small ripple approximation, equation (A.3) can be written as

$$v = L_1 \frac{\Delta i_{L1}}{t_1} \quad \text{(A.4)}$$

Where $t_1 = dT$, d and T are duty ratio and switching period respectively.

$$\Delta i_{L1} = \frac{v \times t_1}{L_1} \quad \text{(A.5)}$$

For Mode 2:

The voltage across the inductor L_1 when switch S1 is off and switch S2 on applying the same small ripple approximation is:

$$L_1 \frac{\Delta i_{L1}}{t_2} = -\left(v - v_{out} - v_{C1}\right) \tag{A.6}$$

$$\Delta i_{L1} = \frac{-(v - v_{out} - v_{C1}) \times t_2}{L_1} \tag{A.7}$$

Where $t_2 = (1-d)T$

$$t_2 = \frac{-\Delta i_{L1} \times L_1}{v - v_{out} - v_{C1}} \tag{A.8}$$

Applying voltage balance equation $\Delta i_{L1} = \Delta i_{L2}$, and with the respective value for t_1 and t_2 substituted, we have,

$$d = \frac{v_{C1} + v_{out} - v}{v_{out} + v_{C1}} \tag{A.9}$$

And

$$1 - d = \frac{v}{v_{out} + v_{C1}} \tag{A.10}$$

From equation (A.10),

$$v_{C1} = \frac{v - (1-d)v_{out}}{(1-d)} \tag{A.11}$$

But note that $t_1 + t_2 = T$ (A.12)

Moreso, $T = \frac{1}{f}$

Substituting in equation (A.12) the value of t_1 and t_2, we have

$$\Delta i_{L1} = \frac{v \times d}{L_1 f} \tag{A.13}$$

Similarly in finding for Δi_{L2} inductor L_2, applying all the procedural steps followed above in deriving Δi_{L1}, we calculated Δi_{L2}

$$\Delta i_{L2} = \frac{v_{out} \times (1-d)}{L_2 f} \tag{A.14}$$

To calculate for values of inductor L_1 and equation L_2 equation (A.13) and (A.14) is used.

To calculate for C_1 and C_2:

Still from figure A.3 when switch S1 is off, Capacitor C_1 is charged through inductor L_1 for length of period the switch was off t_2. So

$$i_{L1} = C_1 \frac{dv_{C1}}{dt} \tag{A.15}$$

For Small ripple approximation, from (A.15)

$$\Delta v_{C1} = \frac{1}{C_1} \int_0^{t_2} i_{L1} dt \tag{A.16}$$

Where:,

But from equation (A.9) and (A.10)

$$\frac{v_{C1} d}{v_{out}} = (1-d) \tag{A.17}$$

Multiply both sides of (A.17) by T

$$\frac{v_{C1} dT}{v_{out}} = (1-d)T = t_2 \tag{A.18}$$

From (A.16),

$$\Delta v_{C1} = \frac{1}{C_1} \times i_{L1} \times t_2 \tag{A.19}$$

Substituting value for t_2 from (A.18), we obtain:

$$\frac{\Delta v_{C1}}{v_{C1}} = \frac{i_{L1} \times d}{f C_1 v_{out}} \quad \text{(A.20)}$$

Assume the load ripple current is small and almost negligible then;

$$\Delta i_{L2} = \Delta i_{C2} \quad \text{(A.21)}$$

$$i_{C2} = C_2 \frac{dv_{out}}{dt} \quad \text{(A.22)}$$

$$\Delta v_{out} = \frac{1}{C_2} \int_0^{\frac{T}{2}} i_{C2} dt \quad \text{(A.23)}$$

The average capacitor current under the idealize waveform = $\frac{1}{2} \times \Delta i_{L2} \times \frac{T}{2} = \frac{\Delta i_{L2}}{4} T$ (A.24)

Subtitude for (A.23) into (A.22) and noting that $\Delta i_{L2} = \frac{v_{out} \times (1-d)}{L_2 f}$ from equation (A.14) then

$$\Delta v_{out} = \frac{v_{out}(1-d)}{8 L_2 C_2 f^2} \quad \text{(A.25)}$$

Equation (A.13), (A.14), (A.20) and (A.25) are used together with the defined acceptable ripple values for capacitor voltage and inductor current and switching frequency for the converter specified in the parameter Table 3.3 for SEPIC. The values for L_1, L_2, C_1 and C_2 to guarantee CCM is calculated and tabulated in the tables of parameters for converters shown in appendix .

APPENDIX B

MAXIMUM POWER POINT DETERMINATION

The equations that describe the characteristics behavior of a P-V module is define by the equation (C.1). **(Karimi et al, 2011); (Yazdani et al, 2009)**

$$\begin{cases} i = n_p i_{ph} - n_p i_{rs}\left[\exp\left(\dfrac{qv}{kA\theta n_s}\right) - 1\right] \\ i_{ph} = \left[i_{src} + k_\theta\left(\theta - \theta_r\right)\right]\dfrac{S}{100} \end{cases} \tag{B.1}$$

At any instant the power measured at the output of the photovoltaic module is given by

$$P = iv \tag{B.2}$$

$$p = n_p i_{ph} v - n_p i_{rs} v[\exp(\frac{q}{k\theta A}\frac{v}{n_s}) - 1]$$

At maximum power point equation (C.3) holds!

$$\frac{dP}{dv} = 0 \tag{B.3}$$

$$\frac{dp}{dv} = n_p i_{ph} - n_p i_{rs}[\exp(\frac{qv}{k\theta A n_s}) - 1] - \frac{v n_p i_{rs} q}{k\theta A n_s}\exp(\frac{qv}{k\theta A n_s}) = 0 \tag{B.4}$$

Let v_m and i_m denote the voltage and current at maximum power point.

$$\frac{i_{ph}}{i_{rs}} + 1 - (1 + bv_m)\exp(bv_m) = 0 \tag{B.5}$$

But,

$$i_{ph} = [i_{src} + k_\theta(\theta - \theta_r)]\frac{S}{1000} \tag{B.6}$$

Putting (B.6) into (B.5) the equation obtained is further rearrange to obtain equation (B.7)

$$(1 + bv_m)\exp(bv_m) = a \tag{B.7}$$

Applying Lambert function to equation (B.7) **(Roshan et al, 2012),** the optimum voltage corresponding to maximum power point.

$$v_{\mathrm{m}} = \frac{W(ae^{1})}{b} \tag{B.8}$$

Where:

$$\begin{cases} a = \left[i_{src} + k_{\theta} \left(\theta - \theta_{r} \right) \right] \dfrac{S}{100 i_{rs}} \\ b = \dfrac{q}{k \theta A n_{s}} \end{cases}$$

$$i_{m} = n_{p} \left[i_{src} + k_{\theta} \left(\theta - \theta_{r} \right) \right] \frac{S}{100} - n_{p} i_{rs} \left[\exp\left(\frac{q v_{\mathrm{m}}}{k A \theta n_{s}} \right) - 1 \right] \tag{B.9}$$

$$P_{\max} = i_{\mathrm{m}} \times v_{\mathrm{m}} \tag{B.10}$$

So, with equation (B.10) the maximum power extractable for varying irradiation can be calculated.

APPENDIX C

BIDIRECTIONAL DC-DC CONVERTER MODEL

The bidirectional dc to dc converter is a sub circuit of the entire system included close to the output of the SEPIC to charge and discharge the battery respectively depending on the load conditions or variation of its duty ratio. In the absence of solar the battery discharges through the bi-directional boost converter and furnish the load with power. Where there is excess solar power, fractional part of this solar power service the load (permanent magnet dc motor) and remaining part of the power goes to charging the battery. From Figure C1, S_3 and S_4 are switching functions and are complimentary in their operations. Table C.1 show the truth table for this operation. The switching strategies are that, S_3 and S_4 are not to be switched on at the same, as their switching on at the same time will violate Kirchhoff current law (KCL) and Kirchhoff voltage law KVL. So, only one of the switches, have to be on one at time or otherwise. The asterisks (*) are the logic command that applies to the required switching strategies for the bi-directional dc to dc converter.

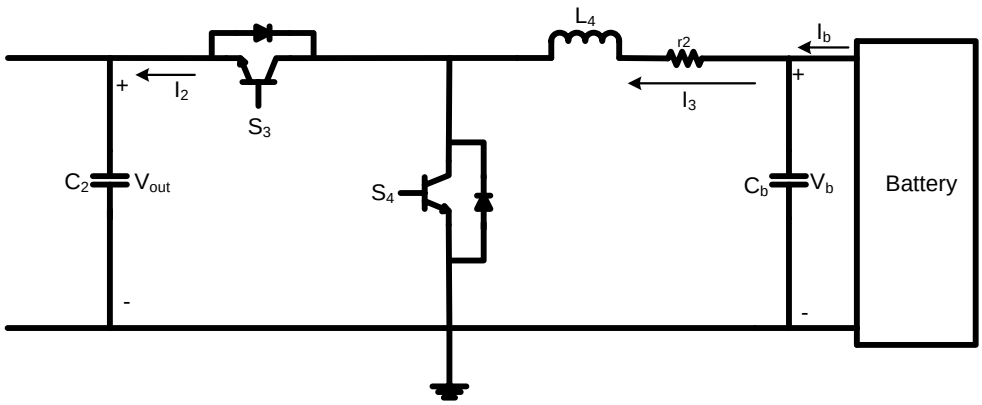


Figure C1. Bidirectional boost converter

Table C.1 Switching function truth table for bidirectional dc-dc converter

S_3	S_4	Output
0	0	0
0	1	1 *
1	0	1 *
1	1	1

The equation (C.1) is derived based on the two possible modes of operation of the converter dwell upon the switching constraint $S_3 + S_4 = 1$

$$\left.\begin{aligned} i_2 &= (1-S_4)\,i_3 \\ C_b p v_b &= i_b - i_3 \\ L_4 p i_3 &= v_b - (1-S_4)\,v_{out} - i_3 r_2 \end{aligned}\right\} \qquad \text{(C.1)}$$

So for mode 1 model equations, S_4 is replaced with 1 in equation C.1. For mode 2, S_4 is replaced with zero.

I. DESIGN OF BI-DIRECTIONAL CONVERTER PARAMETERS:

The parameters of the Bi-directional converter can be determined using the inductor current equations for the two modes of operations to determine the values of inductor L_4. Assuming the converter to operate in continuous conduction mode (CCM).

Using equation (C.1)

Mode 1: $S_4 = 1$ and $S_3 = 0$

$$L_4 \frac{di_3}{dt} = v_b - i_3 r_2 \qquad \text{(C.2)}$$

For small ripple approximation,

$$\frac{di_3}{dt} \approx \Delta i_3,\ dt = (t_1 - 0) = t_1$$

Then,

$$t_1 = \frac{L_4 \Delta i_3}{v_b - i_3 r_2} \tag{C.3}$$

Mode 2: $S_4 = 0$ and $S_3 = 1$

$$L_4 \frac{di_3}{dt} = v_b - v_{out} - i_3 r_2 \tag{C.4}$$

Applying small ripple approximation to equation (C.4),

$$\frac{di_3}{dt} \approx \Delta i_3, \; dt = t_2$$

$$t_2 = \frac{\Delta i_3 L_4}{v_{out} - v_b + i_3 r_2} \tag{C.5}$$

The switching period is define as:

$$t_1 + t_2 = T = \frac{1}{f} \tag{C.6}$$

Substituting for (C.3) and (C.5) into (C.6) we have:

$$L_4 = \frac{(v_b - i_3 r_2)(v_{out} - v_b + i_3 r_2)}{v_{out} f \Delta i_3} \tag{C.7}$$

Equation (C.7) is used to calculate the value of the inductor L_4 to guarantee CCM.

APPENDIX D

HARMONIC BALANCE TECHNIQUE ANAYSIS

SEPIC SYSTEM

$$\left.\begin{aligned} pi_{L1} &= \frac{1}{L_1}\left(v-(1-S_1)\left[+v_{C2}+v_{C1}\right]\right) \\ pi_{L2} &= \frac{1}{L_2}\left(S_1 v_{C1}-(1-S_1)v_{C2}\right) \\ pv_{C1} &= \frac{1}{C_1}\left(-i_{L2}S_1+(1-S_1)i_{L1}\right) \\ pv_{C2} &= \frac{1}{C_2}\left((1-S_1)(i_{L1}+i_{L2})-i_2+i_g\right) \\ v_{Out} &= v_{C2} \end{aligned}\right\} \qquad \text{(D.1)}$$

$$\left.\begin{aligned} i_T &= (S_1)(i_{L1}+i_{L2}) \\ v_T &= (1-S_1)\left[-v_{C2}+v_{C1}\right] \\ i_d &= (1-S_1)i_{L1}+i_{L2}(1-S_1) \\ v_d &= S_1\left[-v_{C2}-v_{C1}\right] \end{aligned}\right\} \qquad \text{(D.2)}$$

HARMONIC BALANCE TECHNIQUE

The state variable and switching function can therefore be defined as:

$$\left.\begin{aligned} v_m &= v_m \\ i_{L1} &= i_{L10}+Re\left(i_{L11}e^{j\theta_s}\right) \\ i_{L2} &= i_{L20}+Re\left(i_{L21}e^{j\theta_s}\right) \\ v_{C1} &= v_{C10}+Re\left(v_{C11}e^{j\theta_s}\right) \\ v_{C2} &= v_{C20}+Re\left(v_{C21}e^{j\theta_s}\right) \\ i_T &= i_{T0}+Re\left(i_{T1}e^{j\theta_s}\right) \\ i_d &= i_{d0}+Re\left(i_{d1}e^{j\theta_s}\right) \\ v_T &= v_{T0}+Re\left(v_{T1}e^{j\theta_s}\right) \\ v_d &= V_{d0}+Re\left(v_{d1}e^{j\theta_s}\right) \\ S_i &= d_{i0}+Re\left(d_{i1}e^{j\theta_s}\right) \end{aligned}\right\} \qquad \text{(D.3)}$$

The quantities $v_m, v_{C10}, v_{C20}, v_{T0}, v_{d0}, i_{L10}, i_{L20}, i_{d0}, i_{T0}, d_{i0}$ are the average (dc) values of supply voltage, capacitor voltage C_1, capacitor voltage C_2, transistor voltage T, diode voltage D, inductor current L_1, inductor current L_2, transistor current, diode current and switching function d. $v_{C11}, v_{C21,} v_{T1}, v_{d1}, i_{L11}, i_{L21}, i_{T1}, i_{d1}, d_{i1}$ are complex ripple harmonic peaks of capacitor voltage C_1, capacitor voltage C_2, inductor current L_1, inductor current L_2, transistor current, diode current and switching function d. Where $i = 1, 2, 3\ldots\ldots$, $\theta_s = \omega_s t$, where ω_s angular switching frequency in radians/seconds and t is time in seconds.

$$L_1 p i_{L1} = v_m - (1 - S_1)[v_{C2} + v_{C1}] \tag{D.4}$$

$$p\left(i_{L10} + Re\left(i_{L11} e^{j\theta_s}\right)\right) = \frac{1}{L_1}\begin{pmatrix} v_m - \left(1 - \left(d_{10} + Re\left(d_{11} e^{j\theta_s}\right)\right)\right) \times \\ \left(v_{C20} + Re\left(v_{C21} e^{j\theta_s}\right)\right) + \left(v_{C10} + Re\left(v_{C10} e^{j\theta_s}\right)\right) \end{pmatrix} \tag{D.5}$$

$$p\begin{pmatrix} i_{L10} + \\ Re\left(i_{L11} e^{j\theta_s}\right) \end{pmatrix} = \frac{1}{L_1}\begin{pmatrix} v_m - v_{C20} - Re\left(v_{C21} e^{j\theta_s}\right) - v_{C10} - Re\left(v_{C11} e^{j\theta_s}\right) \\ + d_{10} v_{C20} + d_{10} Re\left(v_{C21} e^{j\theta_s}\right) + v_{C20} Re\left(d_{11} e^{j\theta_s}\right) \\ + \frac{1}{2} Re\left(d_{11} {v_{C21}}^*\right) + \frac{1}{2} Re\left(d_{11} v_{C21} e^{j2\theta_s}\right) + d_{10} v_{C10} \\ + v_{C10} Re\left(d_{11} e^{j\theta_s}\right) + d_{10} Re\left(v_{C11} e^{j\theta_s}\right) \\ + \frac{1}{2} Re\left(d_{11} {v_{C11}}^*\right) + \frac{1}{2} Re\left(d_{11} v_{C11} e^{j2\theta_s}\right) \end{pmatrix} \tag{D.6}$$

$$p i_{L10} = \frac{1}{L_1}\begin{pmatrix} v_m - v_{C20} - v_{C10} + d_{10} v_{C20} + d_{10} v_{C10} + \frac{1}{2} Re\left(d_{11} {v_{C21}}^*\right) \\ + \frac{1}{2} Re\left(d_{11} {v_{C21}}^*\right) + \frac{1}{2} Re\left(d_{11} {v_{C11}}^*\right) \end{pmatrix} \tag{D.7}$$

$$p i_{L11} + j\omega_s i_{L11} = \frac{1}{L_1}\begin{pmatrix} -v_{C21} - v_{C11} + d_{10} v_{C21} \\ + d_{11} v_{C20} + d_{10} v_{C11} + d_{11} v_{C10} \end{pmatrix} \tag{D.8}$$

$$L_2 p i_{L2} = S_1 v_{C1} - (1 - S_1) v_{C2} \tag{D.9}$$

$$p\left(i_{L20} + Re\left(i_{L21} e^{j\theta_s}\right)\right) = \frac{1}{L_2}\begin{pmatrix} \left(d_{10} + Re\left(d_{11} e^{j\theta_s}\right)\right)\left(v_{C10} + Re\left(v_{C11} e^{j\theta_s}\right)\right) \\ -\left(1 - \left(d_{10} + Re\left(d_{11} e^{j\theta_s}\right)\right)\right)\left(v_{C20} + Re\left(v_{C21} e^{j\theta_s}\right)\right) \end{pmatrix} \tag{D.10}$$

$$p\begin{pmatrix} i_{L20} + \\ Re\left(i_{L21} e^{j\theta_s}\right) \end{pmatrix} = \frac{1}{L_2}\begin{pmatrix} d_{10} v_{C10} + d_{10} Re\left(v_{C11} e^{j\theta_s}\right) + v_{C10} Re\left(d_{11} e^{j\theta_s}\right) + \frac{1}{2} Re\left(d_{11} {v_{C11}}^*\right) \\ + \frac{1}{2} Re\left(d_{11} v_{C11} e^{j2\theta_s}\right) - v_{C20} - Re\left(v_{C21} e^{j\theta_s}\right) + \\ d_{10} v_{C20} + d_{10} Re\left(v_{C21} e^{j\theta_s}\right) + v_{C20} Re\left(d_{11} e^{j\theta_s}\right) + \frac{1}{2} Re\left(d_{11} {v_{C21}}^*\right) \\ + \frac{1}{2} Re\left(d_{11} v_{C21} e^{j2\theta_s}\right) \end{pmatrix} \tag{D.11}$$

$$p i_{L20} = \frac{1}{L_2}\left(d_{10} v_{C10} - v_{C20} + d_{10} v_{C20} + \frac{1}{2} Re\left(d_{11} {v_{C11}}^*\right) + \frac{1}{2} Re\left(d_{11} {v_{C21}}^*\right)\right) \tag{D.12}$$

$$p i_{L21} + j\omega_s i_{L21} = \frac{1}{L_2}\begin{pmatrix} d_{10} v_{C11} + d_{11} v_{C10} - v_{C21} \\ d_{10} v_{C21} + d_{11} v_{C20} \end{pmatrix} \tag{D.13}$$

$$p v_{C1} = \frac{1}{C_1}\left(-i_{L2} S_1 + (1 - S_1) i_{L1}\right) \tag{D.14}$$

$$\left(v_{C10} + Re\left(v_{C11} e^{j\theta_s}\right)\right) = \frac{1}{C_1}\begin{pmatrix} -\left(i_{L20} + Re\left(i_{L21} e^{j\theta_s}\right)\right)\left(d_{10} + Re\left(d_{11} e^{j\theta_s}\right)\right) + \\ \left(i_{L10} + Re\left(i_{L11} e^{j\theta_s}\right)\right) - \left(i_{L10} + Re\left(i_{L11} e^{j\theta_s}\right)\right) \times \\ \left(d_{10} + Re\left(d_{11} e^{j\theta_s}\right)\right) \end{pmatrix} \tag{D.15}$$

$$p\begin{pmatrix} v_{C10}+ \\ Re\left(v_{C11}e^{j\theta_s}\right) \end{pmatrix}=\frac{1}{C_1}\begin{pmatrix} -d_{10}i_{L20}-i_{L20}Re\left(d_{11}e^{j\theta_s}\right)-d_{10}Re\left(i_{L21}e^{j\theta_s}\right) \\ -\frac{1}{2}Re\left(d_{11}i_{L21}{}^{*}\right)-\frac{1}{2}Re\left(d_{11}i_{L21}e^{j2\theta_s}\right)+i_{L10} \\ +Re\left(i_{L11}e^{j\theta_s}\right)-d_{10}i_{L10}i_{L10}-Re\left(d_{11}e^{j\theta_s}\right) \\ -d_{10}Re\left(i_{L11}e^{j\theta_s}\right)-\frac{1}{2}Re\left(d_{11}i_{L11}{}^{*}\right)-\frac{1}{2}Re\left(d_{11}i_{L11}e^{j2\theta_s}\right) \end{pmatrix} \tag{D.16}$$

$$pv_{C10}=\frac{1}{C_1}\left(-d_{10}i_{L20}+i_{L10}-d_{10}i_{L10}-\frac{1}{2}Re\left(d_{11}i_{L21}{}^{*}\right)-\frac{1}{2}Re\left(d_{11}i_{L11}{}^{*}\right)\right) \tag{D.17}$$

$$pv_{C11}+j\omega_s v_{C11}=\frac{1}{C_1}\left(-d_{11}i_{L20}-d_{10}i_{L21}+i_{L11}-d_{10}i_{L11}-d_{11}i_{L10}\right) \tag{D.18}$$

$$C_2 pv_{C2}=\left(1-S_1\right)\left(i_{L1}+i_{L2}\right)-i_2+i_g \tag{D.19}$$

$$p\left(v_{C20}+Re\left(v_{C21}e^{j\theta_s}\right)\right)=\frac{1}{C_2}\begin{pmatrix} \left(1-\left(d_{10}+Re\left(d_{11}e^{j\theta_s}\right)\right)\right)\times\left[\left(i_{L10}+Re\left(i_{L11}e^{j\theta_s}\right)\right)+\right. \\ \left.\left(i_{L20}+Re\left(i_{L21}e^{j\theta_s}\right)\right)\right]-i_2+i_g \end{pmatrix} \tag{D.20}$$

$$p\left(v_{C20}+Re\left(v_{C21}e^{j\theta_s}\right)\right)=\frac{1}{C_2}\begin{pmatrix} i_{L10}+Re\left(i_{L11}e^{j\theta_s}\right)+i_{L20}+Re\left(i_{L21}e^{j\theta_s}\right)-d_{10}i_{L10} \\ -d_{10}Re\left(i_{L11}e^{j\theta_s}\right)-i_{L10}Re\left(d_{11}e^{j\theta_s}\right)—\frac{1}{2}Re\left(d_{11}i_{L11}{}^{*}\right) \\ -\frac{1}{2}Re\left(d_{11}i_{L11}e^{j2\theta_s}\right)-d_{10}i_{L20}-d_{10}Re\left(i_{L21}e^{j\theta_s}\right)- \\ i_{L20}Re\left(d_{11}e^{j\theta_s}\right)-\frac{1}{2}Re\left(d_{11}i_{L21}{}^{*}\right)-\frac{1}{2}Re\left(d_{11}i_{L21}e^{j2\theta_s}\right) \\ -i_2+i_g \end{pmatrix} \tag{D.21}$$

$$pv_{C20}=\frac{1}{C_2}\begin{pmatrix} i_{L10}+i_{L20}-d_{10}i_{L10}-d_{10}i_{L20}-i_2+i_g-\frac{1}{2}Re\left(d_{11}i_{L11}{}^{*}\right) \\ -\frac{1}{2}Re\left(d_{11}i_{L21}{}^{*}\right) \end{pmatrix} \tag{D.22}$$

$$pv_{C21}+j\omega_s v_{C21}=\frac{1}{C_2}\begin{pmatrix} i_{L11}+i_{L21}-d_{10}i_{L11}-d_{11}i_{L10}-d_{10}i_{L21}-d_{11}i_{L20} \\ -i_2+i_g \end{pmatrix} \tag{D.23}$$

Applying Harmonic balance Technique to devices (transistor and diode) currents and their voltages become:

$$i_T = S_1\left(i_{L1} + i_{L2}\right) \tag{D.24}$$

$$i_{T0} + Re\left(i_{T1}e^{j\theta_s}\right) = \left(d_{10} + Re\left(d_{11}e^{j\theta_s}\right)\right)\left[\left(i_{L10} + Re\left(i_{L11}e^{j\theta_s}\right)\right) + \left(i_{L20} + Re\left(i_{L21}e^{j\theta_s}\right)\right)\right] \tag{D.25}$$

$$i_{T0} + Re\left(i_{T1}e^{j\theta_s}\right) = \begin{pmatrix} d_{10}i_{L10} + d_{10}Re\left(i_{L11}e^{j\theta_s}\right) + i_{L10}Re\left(d_{11}e^{j\theta_s}\right) + \frac{1}{2}Re\left(d_{11}{i_{L11}}^*\right) \\ \frac{1}{2}Re\left(d_{11}i_{L11}e^{j2\theta_s}\right) + d_{10}i_{L20} + d_{10}Re\left(i_{L21}e^{j\theta_s}\right) + i_{L20}Re\left(d_{11}e^{j\theta_s}\right) + \\ \frac{1}{2}Re\left(d_{11}{i_{L21}}^*\right) + \frac{1}{2}Re\left(d_{11}i_{L21}e^{j2\theta_s}\right) \end{pmatrix} \tag{D.26}$$

$$i_{T0} = \left(d_{10}i_{L10} + d_{10}i_{L20} + \frac{1}{2}Re\left(d_{11}{i_{L11}}^*\right) + \frac{1}{2}Re\left(d_{11}{i_{L21}}^*\right)\right) \tag{D.27}$$

$$i_{T1} = d_{10}i_{L11} + d_{11}i_{L10} + d_{10}i_{L21} + d_{11}i_{L20} \tag{D.28}$$

$$v_T = \left(1 - S_1\right)\left[v_{C2} + v_{C1}\right] \tag{D.29}$$

$$v_{T0} + Re\left(v_{T1}e^{j\theta_s}\right) = \begin{pmatrix} \left(1 - \left(d_{10} + Re\left(d_{11}e^{j\theta_s}\right)\right)\right) + \left(v_{C20} + Re\left(v_{C21}e^{j\theta_s}\right)\right) + \\ \left(v_{C10} + Re\left(v_{C11}e^{j\theta_s}\right)\right)\end{pmatrix} \tag{D.30}$$

$$v_{T0}+Re\left(v_{T1}e^{j\theta_s}\right)=\begin{pmatrix} v_{C20}+Re\left(v_{C21}e^{j\theta_s}\right)+v_{C10}+Re\left(v_{C11}e^{j\theta_s}\right) \\ -d_{10}v_{C20}-d_{10}Re\left(v_{C21}e^{j\theta_s}\right)-v_{C20}Re\left(d_{11}e^{j\theta_s}\right) \\ -\frac{1}{2}Re\left(d_{11}{v_{C21}}^{*}\right)-\frac{1}{2}Re\left(d_{11}v_{C21}e^{j2\theta_s}\right)-d_{10}v_{C10}- \\ v_{C10}Re\left(d_{11}e^{j\theta_s}\right)-d_{10}Re\left(v_{C11}e^{j\theta_s}\right)-\frac{1}{2}Re\left(d_{11}{v_{C11}}^{*}\right) \\ -\frac{1}{2}Re\left(d_{11}v_{C11}e^{j2\theta_s}\right) \end{pmatrix} \tag{D.31}$$

$$v_{T0}=\begin{pmatrix} v_{C20}+v_{C10}-d_{10}v_{C20}-d_{10}v_{C10} \\ -\frac{1}{2}Re\left(d_{11}{v_{C21}}^{*}\right)-\frac{1}{2}Re\left(d_{11}{v_{C11}}^{*}\right) \end{pmatrix} \tag{D.32}$$

$$v_{T1}=\left(v_{C21}+v_{C11}-d_{10}v_{C21}-d_{11}v_{C20}-d_{10}v_{C11}-d_{11}v_{C10}\right) \tag{D.33}$$

$$i_d=\left(1-S_1\right)\left(i_{L1}+i_{L2}\right) \tag{D.34}$$

$$\left(i_{d0}+Re\left(i_{d1}e^{j\theta_s}\right)\right)=\left(1-\left(d_{10}+Re\left(d_{11}e^{j\theta_s}\right)\right)\right)\begin{bmatrix}\left(i_{L10}+Re\left(i_{L11}e^{j\theta_s}\right)\right) \\ +\left(i_{L20}+Re\left(i_{L21}e^{j\theta_s}\right)\right)\end{bmatrix} \tag{D.35}$$

$$\left(i_{d0}+Re\left(i_{d1}e^{j\theta_s}\right)\right)=\begin{pmatrix} i_{L10}+Re\left(i_{L11}e^{j\theta_s}\right)+i_{L20}+Re\left(i_{L21}e^{j\theta_s}\right) \\ -d_{10}i_{L10}-d_{10}Re\left(i_{L11}e^{j\theta_s}\right)-i_{L10}Re\left(d_{11}e^{j\theta_s}\right) \\ -\frac{1}{2}Re\left(d_{11}{i_{L11}}^{*}\right)-\frac{1}{2}Re\left(d_{11}i_{L11}e^{j2\theta_s}\right)-d_{10}i_{L20} \\ -d_{10}Re\left(i_{L21}e^{j\theta_s}\right)-i_{L20}Re\left(d_{11}e^{j\theta_s}\right)-\frac{1}{2}Re\left(d_{11}{i_{L21}}^{*}\right) \\ -\frac{1}{2}Re\left(d_{11}i_{L21}e^{j2\theta_s}\right) \end{pmatrix} \tag{D.36}$$

$$i_{d0}=\left(i_{L10}+i_{L20}-d_{10}i_{L10}-d_{10}i_{L20}-\frac{1}{2}Re\left(d_{11}{i_{L11}}^{*}\right)-\frac{1}{2}Re\left(d_{11}{i_{L21}}^{*}\right)\right) \tag{D.37}$$

$$i_{d1}=i_{L11}+i_{L21}-d_{10}i_{L11}-d_{11}i_{L10}-d_{10}i_{L21}-d_{11}i_{L20} \tag{D.38}$$

$$v_d = S_1\left[-v_{C2} - v_{C1}\right] \tag{D.39}$$

$$v_{d0} + Re\left(v_{d1}e^{j\theta_s}\right) = \begin{pmatrix} \left(d_{10} + Re\left(d_{11}e^{j\theta_s}\right)\right) \times \left[-\left(v_{C20} + Re\left(v_{C21}e^{j\theta_s}\right)\right)\right. \\ \left.-\left(v_{C10} + Re\left(v_{C11}e^{j\theta_s}\right)\right)\right] \end{pmatrix} \tag{D.40}$$

$$v_{d0} + Re\left(v_{d1}e^{j\theta_s}\right) = \begin{pmatrix} -d_{10}v_{C20} - d_{10}Re\left(v_{C21}e^{j\theta_s}\right) - v_{C20}Re\left(d_{11}e^{j\theta_s}\right) \\ -\frac{1}{2}Re\left(d_{11}{v_{C21}}^*\right) - \frac{1}{2}Re\left(d_{11}v_{C21}e^{j2\theta_s}\right) \\ -d_{10}v_{C10} - d_{10}Re\left(v_{C11}e^{j\theta_s}\right) - v_{C10}Re\left(d_{11}e^{j\theta_s}\right) \\ -\frac{1}{2}Re\left(d_{11}{v_{C11}}^*\right) - \frac{1}{2}Re\left(d_{11}v_{C11}e^{j2\theta_s}\right) \end{pmatrix} \tag{D.41}$$

$$v_{d0} = d_{10}i_{L20}r_{C1} - \beta d_{10}v_{C20} - d_{10}v_{C10} + \frac{1}{2}r_{C1}Re\left(d_{11}{i_{L21}}^*\right) - \frac{1}{2}Re\left(d_{11}{v_{C11}}^*\right) \tag{D.42}$$

$$v_{d1} = d_{10}i_{L21}r_{C1} + d_{11}i_{L20}r_{C1} - \beta d_{10}v_{C21} - \beta d_{11}v_{C20} - d_{10}v_{C11} - d_{11}v_{C10} \tag{D.43}$$

APPENDIX E

Table E.1. SYSTEM PARAMETERS

Motor Parameters	
Motor Type: MT40P4-61	
Rated Power P_m	$3\ Hp$
Rated Voltage v_{bus}	$180\ volts$
Rated Speed N	$3000\ r.p.m$
Moment of Inertial J	$0.0077\ kg/m^2$
Torque Constant $k_T = k_m$	$0.55\ N-m/A$
Voltage Constant $k_V = k_m$	$0.55\ N-m/A$
Armature Resistance R_a	$0.6\ \Omega$
Armature Inductance L_a	$3.0\ mH$
Solar Parameters	
Solar Type: TN-72-5M190 (Mahmud et al,2014)	
Peak Power $P_{\max}$	$190\ W$
Voltage v_{mp}	$37.1\ V$
Current i_{mp}	$5.11\ A$
Short-circuit current	$5.36\ A$
Open circuit voltage	$45.3\ V$
Cell temperature T	$-40/+85^0\ C$
SEPIC parameters	
Inductance L_1	$3.206\ mH$
Inductance L_2	$3.206\ mH$
Capacitance C_1	$40\ \mu F$
Capacitance C_2	$4\ \mu F$
Capacitance C_0	$100\ \mu F$
Switching Frequency f	$10kHz$
Output voltage ripple	5%

Output Current ripple	20%
Grid Parameters	
Grid resistance r_1	$1.41\,\Omega$
Grid Inductance L_3	$13.63\,mH$
Bi-Directional Converter Parameters	
Input Voltage v_b	$48\,V$
Resistance r_2	$0.32\,\Omega$
Inductance L_4	$1.1\,mH$
Capacitance C_b	$100\,\mu F$
Switching Frequency f	$10kHz$
Current i_3	$15.26\ A$
Ripple current Δi_3	$3.07\,A$
Duty cycle D_4	0.78
Battery Parameters (Karimi et al, 2011)	
Battery Voltage v_b	$48\,V$
Resistance R_{b1}, R_{b4}	$0.05\,\Omega$
Resistance R_{b2}	$0.001\,\Omega$
Resistance R_{b3}	$0.002\,\Omega$
Voltage v_{b1}	$50V$
Capacitance C_{b1}	$54000\,F$
Capacitance C_{b2}	$1\,F$

APPENDIX F

PROGRAM LISTING

F.1 MATLAB CODE FOR ENTIRE SYSTEM

```
clc;
clear;
%%%%%%Program listing for M.sc thesis titled ''Modeling, simulation and
steady %%%%%%%%%
%%%%state analysis of a solar based SEPIC based electicity for dc
loads''%%%%%
%%%%%%%%%%%%%%%%%%%%%%%%%written by Ajayi Samuel Taiwo
%%%%%%%%%%%%%%%%%%%%%%%%%%%%%%%%

%%%%%% Defining all the parameters %%%%%%%%%%%%%%

S = [245 445 645 850 1050];      % solar Insolation data from NASA
SS = [120 350 580 695 1040];     % solar Insolation data from on ground
measurement weather work station ABUDECE
I_rr = 2.0793e-6;                % Reverse saturation current at reference
temperature
T = 309;                         %T  =  400;  Surface  temperature  of  PV  in
Kelvin
Tr = 298;                        %Tr = 301.18;
q = 1.602e-19;                   %Electronic charge
A = 1.6;                         %Ideality constant
k_i = 1.7e-3;                    %Short circuit temperature coefficient
Iss = 3.27;                      %PV short circuit current
k = 1.38e-23;                    %Boltzman constant
E_gap = 1.1;                     %Energy of the band gap for silicon
ns = 400;                        %413;%550, Number of cells in series
np = 4;                          %13;%433, Number of cells in parallel
Ra = 0.6;                        %Armature resistance
La = 3e-3;                       %Armature inductance
r1 = 1.41;                       %Grid resistance
L3 = 13.63e-3;                   %Grid inductance
v_bus = 180;                     %Input voltage to motor
N = 3000;                        %speed of motor in r.p.m
J =0.0077;                       %Moment of inertial of the permanent Magnet
dc motor
km = 0.55;                       %Torque constant for motor
L1 = 3.21e-3;                    %Inductance of SEPIC
L2 = 3.21e-3;                    %Inductance of SEPIC
C1 = 40e-6;                      %Capacitance of the SEPIC
C2 = 4e-6;                       %Capacitance of SEPIC
C0 = 100e-6;                     %Input capacitance of SEPIC
fs = 10e3;                       %Converter switching frequency
vb = 48;                         %Battery voltage
r2 = 0.32;                       %Bi-directional converter parasitic
resistance
L4 = 1.1e-3;                     %Inductance of SEPIC
Cb = 100e-6;                     %Input capacitance of Bi-directional
converter
Ts = 1/fs;                       %switching period
B = 0.004;                       %Viscous torque constant
Ib = 16.90;                      %15.26;% Battery current at steady state
for D4 = 0.78
b = q/(k*T*A*ns);                %Thermal voltage of the module
```

```
% calculating speed in (revolution per seconds)r.p.s;
Ns = 2*pi*N/60;

% calculating the saturation current;

I_sat = I_rr*((T/Tr)^3)*(exp(((q*E_gap)/(k*A))*((1/Tr)-(1/T))));


%%%%%%%%%%%%%% F1 Solar Insolation and Battery studies%%%%%%%%%%%%
%%%%%%%%%%%%%%%%%%%%%%%%%%%%%%%%%%%%%%%%%%%%%%%%%%%%%%%%%%%%%%%%%


%%%%calculating the photonic current in terms of Insolation S;%%%%%
%%%%%%%%%%%%%%%%Using Solar data from NASA%%%%%%%%%%%%%%%%%%%%%%%%

I_ph_1 = (Iss+k_i*(T-Tr))*(S(1)/1000);
I_ph_2 = (Iss+k_i*(T-Tr))*(S(2)/1000);
I_ph_3 = (Iss+k_i*(T-Tr))*(S(3)/1000);
I_ph_4 = (Iss+k_i*(T-Tr))*(S(4)/1000);
I_ph_5 = (Iss+k_i*(T-Tr))*(S(5)/1000);

%%%%calculating the photonic current in terms of Insolation S;%%%%%
%%%%%%%%%%%%%%%%Using Solar data from ABUDECE%%%%%%%%%%%%%%%%%%%%%%%%

I_pph_1 = (Iss+k_i*(T-Tr))*(SS(1)/1000);
I_pph_2 = (Iss+k_i*(T-Tr))*(SS(2)/1000);
I_pph_3 = (Iss+k_i*(T-Tr))*(SS(3)/1000);
I_pph_4 = (Iss+k_i*(T-Tr))*(SS(4)/1000);
I_pph_5 = (Iss+k_i*(T-Tr))*(SS(5)/1000);


%%%%%%%calculating output current based on individual fixed insolations;%%%
%%%%%%%%%%%%%%%% NASA results%%%%%%%%%%%%%%%%%%%%%%%%%%%%%%%%%%%%%%%%%%%
v=0:0.01:230;
I_pv_1 = np*I_ph_1-np*I_sat*(exp((q.*v)./(A*k*T*ns))-1);
I_pv_2 = np*I_ph_2-np*I_sat*(exp((q.*v)./(A*k*T*ns))-1);
I_pv_3 = np*I_ph_3-np*I_sat*(exp((q.*v)./(A*k*T*ns))-1);
I_pv_4 = np*I_ph_4-np*I_sat*(exp((q.*v)./(A*k*T*ns))-1);
I_pv_5 = np*I_ph_5-np*I_sat*(exp((q.*v)./(A*k*T*ns))-1);

%%%%%%%calculating output current based on individual fixed insolations;%%%
%%%%%%%%%%%%%%%% ABUDECE
results%%%%%%%%%%%%%%%%%%%%%%%%%%%%%%%%%%%%%%%%%%%%%%%%%%%%%%%%%%%%%%%
v=0:0.01:230;
I_ppv_1 = np*I_pph_1-np*I_sat*(exp((q.*v)./(A*k*T*ns))-1);
I_ppv_2 = np*I_pph_2-np*I_sat*(exp((q.*v)./(A*k*T*ns))-1);
I_ppv_3 = np*I_pph_3-np*I_sat*(exp((q.*v)./(A*k*T*ns))-1);
I_ppv_4 = np*I_pph_4-np*I_sat*(exp((q.*v)./(A*k*T*ns))-1);
I_ppv_5 = np*I_pph_5-np*I_sat*(exp((q.*v)./(A*k*T*ns))-1);

%%%%%%Calculating PV-power ;%%%%%%%%%
%%%%%%%%%%% NASA%%%%%%%%%%%%%%%

P_1 = I_pv_1.*v;
P_2 = I_pv_2.*v;
P_3 = I_pv_3.*v;
P_4 = I_pv_4.*v;
```

```
P_5 = I_pv_5.*v;


% Calculating PV-power ;%%%%%%%%%
%%%%%%%%%% ABUDECE%%%%%%%%%%%%%%

PP_1 = I_ppv_1.*v;
PP_2 = I_ppv_2.*v;
PP_3 = I_ppv_3.*v;
PP_4 = I_ppv_4.*v;
PP_5 = I_ppv_5.*v;

figure (1)
plot(v,P_1,'r-',v,P_2,'g-',v,P_3,'y-',v,P_4,'k-',v,P_5,'c-
','lineWidth',3.0); grid on;axis([0 250 0 2500]);
xlabel('\bf Voltage (V)'),ylabel('\bf Power
(W)');gtext('245W/m^2');gtext('445W/m^2');gtext('645W/m^2');gtext('850W/m^2
');gtext('1050W/m^2');grid on
title ('\bf PV Power versus Voltage Characteristic'); grid on;

figure (2)
plot(v,I_pv_1,'r-',v,I_pv_2,'g-',v,I_pv_3,'y-',v,I_pv_4,'k-',v,I_pv_5,'c-
','lineWidth',3.0);axis([0 250 0 15]);
xlabel('\bf Voltage(V)'),ylabel('\bf current I
(A)');gtext('245W/m^2');gtext('445W/m^2');gtext('645W/m^2');gtext('850W/m^2
');gtext('1050W/m^2');grid on
title ('\bf PV Current versus Voltage Characteristic'); grid on;

% Calculating the voltage at maximum power point using Lambert function;
%%%%%%%%%%%%%%%%%%%%%%%%%%%% NASA %%%%%%%%%%%%%%%%%%%%%%%%%%%%%%%%%%%%%%%%%%%%

a_1(1) = (I_ph_1/I_rr)+1;
a_2(2) = (I_ph_2/I_rr)+1;
a_3(3) = (I_ph_3/I_rr)+1;
a_4(4) = (I_ph_4/I_rr)+1;
a_5(5) = (I_ph_5/I_rr)+1;

% Calculating the voltage at maximum power point using Lambert function as
a function of irradiance;
%%%%%%%%%%%%%%%% ABUDECE%%%%%%%%%%%%%%%%%%%%%%%%%%%%%%%%%%%%%%%%%%%%%%%%%%%%

aa_1(1) = (I_ph_1/I_rr)+1;
aa_2(2) = (I_ph_2/I_rr)+1;
aa_3(3) = (I_ph_3/I_rr)+1;
aa_4(4) = (I_ph_4/I_rr)+1;
aa_5(5) = (I_ph_5/I_rr)+1;

%%%%%%%%%%Voltage at maximum power point using NASA Solar
data%%%%%%%%%%%%%%%%%

V_max_1 = (lambertw(a_1(1)*exp(1))-1)/b;
V_max_2 = (lambertw(a_2(2)*exp(1))-1)/b;
V_max_3 = (lambertw(a_3(3)*exp(1))-1)/b;
V_max_4 = (lambertw(a_4(4)*exp(1))-1)/b;
V_max_5 = (lambertw(a_5(5)*exp(1))-1)/b;

%%%%%%%%% Voltage at maximum power point using ABUDECE Solar
data%%%%%%%%%%
```

```
VV_max_1 = (lambertw(aa_1(1)*exp(1))-1)/b;
VV_max_2 = (lambertw(aa_2(2)*exp(1))-1)/b;
VV_max_3 = (lambertw(aa_3(3)*exp(1))-1)/b;
VV_max_4 = (lambertw(aa_4(4)*exp(1))-1)/b;
VV_max_5 = (lambertw(aa_5(5)*exp(1))-1)/b;


for j=1:5;
    S = [245 445 645 850 1050];
    Iph(:,j) = (Iss+k_i*(T-Tr)).*(S./1000);
    a_11(:,j) = (Iph(:,j)./I_rr)+1;
    Vmax = (lambertw(a_11(:,j).*exp(1))-1)/b;
    Imax = np.*Iph(:,j)-np*I_sat*(exp((q.*Vmax)./(A*k*T*ns))-1);
end


for j=1:5;
    SS = [120 350 580 695 1040];
    Ipph(:,j) = (Iss+k_i*(T-Tr)).*(SS./1000);
    aa_11(:,j) = (Ipph(:,j)./I_rr)+1;
    VVmax = (lambertw(aa_11(:,j).*exp(1))-1)/b;
    IImax = np.*Ipph(:,j)-np*I_sat*(exp((q.*VVmax)./(A*k*T*ns))-1);
end

%%%%Plot showing Comparison of voltage at maximum power point using NASA
Solar data with%%%%
%%%%%%% Voltage at maximum power point using ABUDCE Solar data%%%%%%%%%%%%

figure (3)
plot (S,Vmax,'k-','LineWidth',3.0);hold on;plot (SS,VVmax,'r-
','LineWidth',3.0);
xlabel('\bf Insolation (S) (W/m2)'),ylabel('\bf Maximum voltage V_{m}
(V)');grid on
title ('\bf Maximum voltage versus Insolation Characteristic'); grid on;

figure (4)
plot (S,Imax,'k.-','LineWidth',3.0);hold on;plot (SS,IImax,'r.-
','LineWidth',3.0);
xlabel('\bf Insolation (S) (W/m2)'),ylabel('\bf Current at Maximum power
(I_{m}) (A)');grid on
title ('\bf Maximum current versus insolation Characteristic'); grid on;

%%% Calculating the Output current of the SEPIC for varying duty
%%%%%%%%%% ratio @ Solar Insolation level of 245W/m2 %%%%%%%%%%%%%%%%%%%%%%

for p=1:17;
    D1 = 0:1/16:1;
    D3 = D1';
    IL2 = Imax (1).*((1-D3)./D3);
end

%%% Calculating the Output current of the SEPIC for varying duty%%
%%%%%%%%%% ratio @ Solar Insolation level of 850W/m2 %%%%%%%%%%%%%%%%%%%%%%

for p=1:17;
    D1 = 0:1/16:1;
    D3 = D1';
    ILL2 = Imax (4).*((1-D3)./D3);
end
```

```
figure (5)
plot (D1,IL2,'b.-','LineWidth',3.0);hold on; plot (D1,ILL2,'r.-
','LineWidth',3.0);
xlabel('\bf Duty ratio (D1)','LineWidth',2.0);
ylabel('\bf SEPIC output current I_L_2
(A)','LineWidth',2.0);gtext('245W/m^2');gtext('850W/m^2');grid on;
title ('\bf SEPIC output current versus duty ratio Characteristic'); grid
on;

%%%%%%%%% Variation of motor speed with SEPIC duty ratio studies%%%%%%%
%%%%%%%% for two cases of insolation level @ 245W/m2 and @ 850W/m2
%%%%%%%%%


% @ 245W/m2 insolation voltage at maximum power point is Vm = 177.7V
%%% Three cases of load Torque will be considered: TL = 0 Nm, TL = 10 Nm,
TL = 20 Nm.

d = []; % creat a vector matrice for storing duty ratio data
W1 = [];% creat a vector matrice for storing speed data @ load torque TL =
0 Nm
W2 = [];% creat a vector matrice for storing speed data @ load torque TL =
10 Nm
W3 = [];% creat a vector matrice for storing speed data @ load torque TL =
20 Nm

for D = 0:0.001:1;  % Varying SEPIC duty ratio
    TL = [0 10 20]; % Load Torque
    Vm = 177.7;     % Voltage at maximum power point for @ 245W/m2
insolation level
    Ra = 0.6;
    r1 = 1.41;
    km = 0.55;
    B = 0.004;
    w1 = ((Vm*km*D/(1-D))-((Ra+r1)*TL(1)))/(B*(Ra+r1)+km^2); % speed @ load
Torque of 0 Nm
    w2 = ((Vm*km*D/(1-D))-((Ra+r1)*TL(2)))/(B*(Ra+r1)+km^2);% speed @ load
Torque of 10 Nm
    w3 = ((Vm*km*D/(1-D))-((Ra+r1)*TL(3)))/(B*(Ra+r1)+km^2); % speed @ load
Torque of 20 Nm
    d = [d D];
    W1 = [W1 w1];
    W2 = [W2 w2];
    W3 = [W3 w3];
end


% @ 850W/m2 insolation level voltage at maximum power point is Vm = 197.26V
%%% Three cases of load Torque will be considered: TL = 0 Nm, TL = 10 Nm,
TL = 20 Nm.

d = [];   % creat a vector matrice for storing duty ratio data
W11 = []; % creat a vector matrice for storing speed data @ load torque TL
= 0 Nm
W22 = []; % creat a vector matrice for storing speed data @ load torque TL
= 10 Nm
W33 = []; % creat a vector matrice for storing speed data @ load torque TL
= 20 Nm
```

```
for D = 0:0.001:1;      % Varying SEPIC duty ratio
    TL = [0 10 20];     % Load Torque
    Vm = 197.26;    % Voltage at maximum power point for @ 850W/m2
insolation level
    Ra = 0.6;
    r1 = 1.41;
    km = 0.55;
    B = 0.004;
    w11 = ((Vm*km*D/(1-D))-((Ra+r1)*TL(1)))/(B*(Ra+r1)+km^2); % speed @
load Torque of 0 Nm
    w22 = ((Vm*km*D/(1-D))-((Ra+r1)*TL(2)))/(B*(Ra+r1)+km^2); % speed @
load Torque of 10 Nm
    w33 = ((Vm*km*D/(1-D))-((Ra+r1)*TL(3)))/(B*(Ra+r1)+km^2); % speed @
load Torque of 20 Nm
    d = [d D];
    W11 = [W11 w11];
    W22 = [W22 w22];
    W33 = [W33 w33];
end

figure (6)

%subplot(1,2,1)
plot(d,W1,'k-','LineWidth',3.0);hold on;plot (d,W2,'b-
','LineWidth',3.0);hold on;...
plot(d,W3,'r-','LineWidth',3.0);axis([0 1 0 1500]);
xlabel('\bf Duty ratio (D1)','LineWidth',2.0);
ylabel('\bf Speed of Motor (\omega)
(rev/min)','LineWidth',3.0);gtext('TL=0Nm');gtext('TL=10Nm');gtext('TL=20Nm
');grid on
title ('\bf Motor Speed versus duty ratio Characteristic @ 245W/m2 solar
Insolation'); grid on;

%subplot(1,2,2)

plot (d,W11,'k-','LineWidth',3.0);hold on;plot (d,W22,'b-
','LineWidth',3.0);hold on;...
plot (d,W33,'r-','LineWidth',3.0);axis([0 1 0 1500])
xlabel('\bf Duty ratio (D1)','LineWidth',2.0);
ylabel('\bf Speed of Motor (\omega)
(rev/min)','LineWidth',3.0);gtext('TL=0Nm');gtext('TL=10Nm');gtext('TL=20Nm
');grid on
title ('\bf Motor Speed versus duty ratio Characteristic @ 850W/m2 solar
Insolation'); grid on;


%%%%%%%%% ploting the torque speed characteristics%%%%%%%%%%%%%%%%

% @ 245W/m2 insolation voltage at maximum power point is Vm = 177.7V
%%% Three cases of duty ratios will be considered: D = 0.3, D = 0.5, D =
0.7.

Tl = []; % creat a vector matrice for storing Load torque data
W1 = []; % creat a vector matrice for storing speed data @ duty  D = 0.3
W2 = []; % creat a vector matrice for storing speed data @ duty  D = 0.5
W3 = []; % creat a vector matrice for storing speed data @ duty  D = 0.7

for TL = 0:0.01:20;  % Varying Load torque in Nm
```

```
    D = [0.3 0.5 0.7];% duty ratio
    Vm = 177.7; % Voltage at maximum power point for @ 245W/m2 insolation
level
    Ra = 0.6;
    r1 = 1.41;
    km = 0.55;
    B = 0.004;
    w1 = ((Vm*km*D(1)/(1-D(1)))-((Ra+r1)*TL))/(B*(Ra+r1)+km^2); % speed @
duty ratio of 0.3
    w2 = ((Vm*km*D(2)/(1-D(2)))-((Ra+r1)*TL))/(B*(Ra+r1)+km^2); % speed @
duty ratio of 0.5
    w3 = ((Vm*km*D(3)/(1-D(3)))-((Ra+r1)*TL))/(B*(Ra+r1)+km^2); % speed @
duty ratio of 0.7
    Tl = [Tl TL];
    W1 = [W1 w1];
    W2 = [W2 w2];
    W3 = [W3 w3];
end


% @ 850W/m2 insolation level voltage at maximum power point is Vm = 197.26V
%%% Three cases of duty ratios will be considered: D = 0.3, D = 0.5, D =
0.7.

Tl = [];  % creat a vector matrice for storing Load torque data
W11 = []; % creat a vector matrice for storing speed data @ duty  D = 0.3
W22 = []; % creat a vector matrice for storing speed data @ duty  D = 0.5
W33 = []; % creat a vector matrice for storing speed data @ duty  D = 0.7

for TL = 0:0.01:20; % Varying Load torque in Nm
    D = [0.3 0.5 0.7];  % duty ratio
    Vm = 197.26; % Voltage at maximum power point for @ 850W/m2 insolation
level
    Ra = 0.6;
    r1 = 1.41;
    km = 0.55;
    B = 0.004;
    w11 = ((Vm*km*D(1)/(1-D(1)))-((Ra+r1)*TL))/(B*(Ra+r1)+km^2); % speed @
duty ratio of 0.3
    w22 = ((Vm*km*D(2)/(1-D(2)))-((Ra+r1)*TL))/(B*(Ra+r1)+km^2); % speed @
duty ratio of 0.5
    w33 = ((Vm*km*D(3)/(1-D(3)))-((Ra+r1)*TL))/(B*(Ra+r1)+km^2); % speed @
duty ratio of 0.7
    Tl = [Tl TL];
    W11 = [W11 w11];
    W22 = [W22 w22];
    W33 = [W33 w33];
end

figure (7)

subplot(1,2,1)
plot(Tl,W1,'k-','LineWidth',3.0);hold on;plot (Tl,W2,'b-
','LineWidth',3.0);hold on;...
plot(Tl,W3,'r-','LineWidth',3.0);
xlabel('\bf Load Torque','LineWidth',3.0);
ylabel('\bf Speed of Motor (\omega) (rev/min)','LineWidth',3.0); gtext('D1
= 0.3');gtext('D1 = 0.5');gtext('D1 = 0.7');grid on;
title ('\bf Motor Speed versus Load Torque Characteristic @ 245W/m2 solar
Insolation'); grid on;
```

```
subplot(1,2,2)

plot (Tl,W11,'k-','LineWidth',3.0);hold on;plot (Tl,W22,'b-
','LineWidth',3.0);hold on;...
plot (Tl,W33,'r-','LineWidth',3.0);
xlabel('\bf Load Torque','LineWidth',3.0);
ylabel('\bf Speed of Motor (\omega) (rev/min)','LineWidth',3.0);gtext('D1 =
0.3');gtext('D1 = 0.5');gtext('D1 = 0.7');grid on;
title ('\bf Motor Speed versus Load Torque Characteristic @ 850W/m2 solar
Insolation'); grid on;

%%%%%%%%%%%%%%%%%%%%%%%%%%%%%%%%%%%%%%%%%%%%%%%%%%%%%%%%%%%%%%%%%%%%%%%%%%%%%%%%
%%%%%%%%%%%%%%%%%%%%%%%%
%%%%%%% Battery Current Studies for supplying Load current system
%%%%%%%%%%%


d = [];   % creat a vector matrice for storing duty ratio data
Ib1 = []; % creat a vector matrice for storing battery current data
Ib2 = []; % creat a vector matrice for storing battery current data
Ib3 = []; % creat a vector matrice for storing battery current data
I21 = []; % creat a vector matrice for storing grid current data
I22 = []; % creat a vector matrice for storing grid current data
I23 = []; % creat a vector matrice for storing grid current data
Ia1 = []; % creat a vector matrice for storing armature current data
Ia2 = []; % creat a vector matrice for storing armature current data
Ia3 = []; % creat a vector matrice for storing armature current data
IL2 = []; %creat a vector matrice for storing armature current data
for D = 0:0.001:1; % Varying SEPIC duty ratio
    D4 = [0.3 0.5 0.78];% Bi-directional Converter duty ratio
    Vm = 177.7;% Voltage at maximum power point for @ 245W/m2 insolation
level
    r2 = 0.32; % On resistance of Bi-directionnal Converter
    im = 2.5;  %Current at maximum Power point
    vb = 48;   %Voltage of the battery
    iL2 = Imax(1)*((1-D)/D); %Output Current from SEPIC for varying duty
ratio between zero and one
    ib1 = ((vb*(1-D))-(Vm*(1-D4(1))*D))/(r2*(1-D));% Battery Current for
Varying duty ration at D4 = 0.3
    ib2 = ((vb*(1-D))-(Vm*(1-D4(2))*D))/(r2*(1-D));% Battery Current for
Varying duty ration at D4 = 0.5
    ib3 = ((vb*(1-D))-(Vm*(1-D4(3))*D))/(r2*(1-D));% Battery Current for
Varying duty ration at D4 = 0.78
    i21 = ib1*(1-D4(1));  %Current injected to grid through Bi-directional
converter for Varying duty ration at D4 = 0.3
    i22 = ib2*(1-D4(2));  %Current injected to grid through Bi-directional
converter for Varying duty ration at D4 = 0.5
    i23 = ib3*(1-D4(3));  %Current injected to grid through Bi-directional
converter for Varying duty ration at D4 = 0.78
    ia1 = (im*(1-D)/D)+i21; %Armature Current for Varying duty ration at D4
= 0.3
    ia2 = (im*(1-D)/D)+i22; %Armature Current for Varying duty ration at D4
= 0.5
    ia3 = (im*(1-D)/D)+i23; %Armature Current for Varying duty ration at D4
= 0.78

    d = [d D];
    Ib1 = [Ib1 ib1];
    Ib2 = [Ib2 ib2];
```

```
    Ib3 = [Ib3 ib3];
    I21 = [I21 i21];
    I22 = [I22 i22];
    I23 = [I23 i23];
    Ia1 = [Ia1 ia1];
    Ia2 = [Ia2 ia2];
    Ia3 = [Ia3 ia3];
    IL2 = [IL2 iL2];
end


figure (8)

subplot(2,2,1)
plot(d,Ib1,'k-','LineWidth',3.0);hold on;plot (d,Ib2,'b-
','LineWidth',3.0);hold on;...
plot(d,Ib3,'r-','LineWidth',3.0);axis([0 1 0 200])
xlabel('\bf Duty ratio (D1)','LineWidth',3.0);
ylabel('\bf Battery Current I_b (A)','LineWidth',3.0);gtext('D4 =
0.3');gtext('D4 = 0.5');gtext('D4 = 0.78');grid on
title ('\bf Battery Current versus duty ratio Characteristic @ 245W/m2
solar Insolation'); grid on;

subplot(2,2,2)

plot (d,I21,'k-','LineWidth',3.0);hold on;plot (d,I22,'b-
','LineWidth',3.0);hold on;...
plot (d,I23,'r-','LineWidth',3.0);axis([0 1 0 200]);
xlabel('\bf Duty ratio (D1)','LineWidth',3.0);
ylabel('\bf Current I_2 (A)','LineWidth',3.0);gtext('D4 = 0.3');gtext('D4 =
0.5');gtext('D4 = 0.78');grid on
title ('\bf Bi-directional Converter Output Current versus duty ratio
Characteristic @ 245W/m2 solar Insolation'); grid on;


subplot(2,2,3)

plot (d,Ia1,'k-','LineWidth',3.0);hold on;plot (d,Ia2,'b-
','LineWidth',3.0);hold on;...
plot (d,Ia3,'r-','LineWidth',3.0);hold on;plot(d,IL2,'y-
','LineWidth',3.0);axis([0 1 0 200]);
xlabel('\bf Duty ratio (D1)','LineWidth',3.0);
ylabel('\bf Armature Current I_a (A)','LineWidth',2.0);gtext('D4 =
0.3');gtext('D4 = 0.5');gtext('D4 = 0.78');
gtext('Armature output Current without Battery Support');grid on
title ('\bf Armature Current versus duty ratio Characteristic @ 245W/m2
solar Insolation'); grid on;



Vb = 48;
D = 0:1/16:1;
%D(1) = 0.001;
%D(17) = 0.98;
v_out = Vmax(4).*(D./(1-D));

for i = 1:17;
    D4 = 0.78;
    D1 = 0:1/16:1;
```

```
    D3 = D1';
    ib = ((Vb.*(1-D3))-(Vmax(1)*(1-D4).*D3))./(r2*(1-D3));
    i2 = (1-D4).*ib;
    Ia = (Imax(1).*(1-D3)./D3)+i2;% Armature current= grid current
    IL2 = Imax(1).*((1-D3)./D3);
end

figure (9)

plot (D,v_out,'r.-','LineWidth',3.0);
xlabel('\bf duty ratio D1','LineWidth',3.0),ylabel('\bf v_o_u_t
(V)','LineWidth',3.0);axis([0 0.9 0 1000]);
title('\bf SEPIC Output voltage versus Duty ratio'); grid on;

figure (10)

%plot (D3,ib,'k-.','LineWidth',2.0);hold on;
plot (D3,i2,'b.-','LineWidth',3.0);hold on;plot
(D3,Ia,'r','LineWidth',3.0);hold on;plot(D3,IL2,'k.-','LineWidth',3.0);
xlabel('\bf duty ratio D1','LineWidth',3.0),ylabel('\bf Currents   (I_a),
(I_2),  (I_b) (A)','LineWidth',3.0);axis([0 1 0 80]);
gtext('Bi-directional Output current');gtext('Armature
Current');gtext('Sepic Output current');grid on
title('\bf SEPIC, Injected current and Armature current versus Duty
ratio'); grid on;

%%%%%% plot of battery current during charging and discharging;

for i=1:21;
    D4 = 0:0.05:1;
    D1 = 0.45;
Ib11(:,i) = ((vb.*(1-D1)-(V_max_1.*(1-D4).*D1))./(r2.*(1-D1)));
Ib21(:,i) = ((vb.*(1-D1)-(V_max_2.*(1-D4).*D1))./(r2.*(1-D1)));
Ib31(:,i) = ((vb.*(1-D1)-(V_max_3.*(1-D4).*D1))./(r2.*(1-D1)));
Ib41(:,i) = ((vb.*(1-D1)-(V_max_4.*(1-D4).*D1))./(r2.*(1-D1)));
Ib51(:,i) = ((vb.*(1-D1)-(V_max_5.*(1-D4).*D1))./(r2.*(1-D1)));
end

figure (11)
plot (D4,Ib11(:,i),'r','LineWidth',3.0);xlabel('\bf duty ratio
(D4)','LineWidth',3.0),ylabel('\bf Battery current (Ib)
(A)','LineWidth',3.0);grid on;
title('\bf Plot of batterry current charging and discharging versus Duty
ratio');gtext('ref point'); grid on;

figure (12)

plot (d,W11,'k-','LineWidth',3.0);hold on;plot (d,W22,'b-
','LineWidth',3.0);hold on;...
plot (d,W33,'r-','LineWidth',3.0);axis([0 1 0 1500])
xlabel('\bf Duty ratio (D1)','LineWidth',2.0);
ylabel('\bf Speed of Motor (\omega)
(rev/min)','LineWidth',3.0);gtext('TL=0Nm');gtext('TL=10Nm');gtext('TL=20Nm
');grid on
title ('\bf Motor Speed versus duty ratio Characteristic @ 850W/m2 solar
Insolation'); grid on;
```

F.2 MATLAB CODE FOR HARMONIC BALANCE TECHNIQUE

```
clc;
clear all;

T = 100e-6;
fs = 1/T;
ws = 2*pi*fs;

%%%%%%%%%%%%%%%%%%%%%%%%%%%%%%%%%%%%%%%%%%%%%%%%%%%%%%%%%%%%%%%%%%%%%%%%%%%%%%%
%%%%%%%%%%%%% create a vector matrices for state variable
data%%%%%%%%%%%%%%

% D = 0.8
 d = []; VC10 =[]; IL10 = []; VC20 = []; V00 = [];
IT0 = []; VT0 = [];  Id0 = [];  Vd0 = []; IL20 = [];

IL11 = []; IL21 = []; VC11 = []; IT1 = [];
Id1 = [];  Vd1 = []; VC21=[]; V01 = [];VT1 = [];


%%%%%%%%%%%%%%%%%%%%%%%%%%%%%%%%%%%%%%%%%%%%%%%%%%%%%%%%%%%%%%%%%%%%%%%%%%%%%%%
%%%%%%%%%%%%%%%%%%%%%%%%%%%%%%%%%%%%%%%%%%%%%%%%%%%%%%%%%%%%%%%%%%%%%%%%%%%%%%%
%%Determination of Steady state and Ripple quantities for SEPICconverter%%%
%%%%%%%%%%%%%%%%%% Harmonic Balance Technique %%%%%%%%%%%%%%%%%%%%%%%%%%%%%%%%


for D = 0:0.001:1 % Vary the duty ratio between 0 and 1

    v = 197.26;
    L1 = 3.206e-3;
    L2 = 3.206e-3;
    C1 = 40e-6;
    C2 = 4e-6;
    ig = 12;
    i2 = 3.36;
    d10 = D;
    d11 = 1/pi*sqrt(2-2*cos(2*pi*D));

    % Output capacitor voltage;
    vC20 = v*(d10/(1-d10));

    %Tranfer capacitor voltage;
    vC10 = vC20*((1-d10)/d10);

    %Output inductor current;
    iL20 = ig-i2;

    %Input current;
    iL10 = iL20*(d10/(1-d10));

    % Output voltage;
    v00 = vC20;

    %Transistor and diode currents;
    iT0 = d10*(iL10+iL20);
    id0 = iL10*(1-d10)+iL20*(1-d10);
```

```
    %Transistor and diode voltages;
     vT0 = vC10*(1-d10)-vC20*(1-d10);
     vd0 = d10*(-vC20-vC10);


     %%%%%%%%%%%%%%%%%%%%%%%%%%%%%%%%%%%%%%%%%%%%%%%%%%%%%%%%%%%%%%%%%%%%%%
    %Ripple quantities calculation:
    %%%%%%%%%%%%%%%%%%%%%%%%%%%%%%%%%%%%%%%%%%%%%%%%%%%%%%%%%%%%%%%%%%%%%%


   A1 = [j*ws*L1 0 (1-d10) (1-d10);
       0 j*ws*L2 -d10 (1-d10);
       -(1-d10) d10 j*ws*C1 0;
       -(1+d10) -(1+d10) 0 j*ws*C2];


   b1 = [d11*vC20+d11*vC10;
            d11*vC20+d11*vC10;
            -d11*iL20-d11*iL10;(d11*iL10+d11*iL20)+iL20];

    %%%%%%%%%%%%%%%%%%%%%%%%%%%%%%%%%%%%%%%%%%%%%%%%%%%%%%%%%%%%%%%%%%%%%%

        x1 = A1\b1;

        iL11 = abs(x1(1));
        iL21 = abs(x1(2));
        vC11 = abs(x1(3));
        vC21 = abs(x1(4));

     %%%%%%%% Output DC ripple Voltage%%%%%%%%%%%%%%%%%%%%%%%%%%%%%%%%%%
     v01 = vC21;

     %%%%%%%%%%%%%%%%%%%%%%%%%%%%%%%%%%%%%%%%%%%%%%%%%%%%%%%%%%%%%%%%%%%%%%
        i_T1 = d10*(iL11+iL21)+d11*(iL10+iL20);
        i_d1 = iL11*(1-d10)+iL21*(1-d10)-d11*(iL10+iL20);
        v_T1 = -vC21*(1-d10)+vC11*(1-d10)+d11*vC20+d11*vC10;

        v_d1 = -d10*vC21-d11*vC20-d10*vC11-d11*vC10;

        iT1 = abs(i_T1);
        id1 = abs(i_d1);
        vT1 = abs(v_T1);
        vd1 = abs(v_d1);
    %%%%%%%%%%%%%%%%%%%%%%%%%%%%%%%%%%%%%%%%%%%%%%%%%%%%%%%%%%%%%%%%%%%%%%

    d = [d D]; VC10 = [VC10 vC10]; V00 = [V00 v00];
    IL10 = [IL10 iL10]; IL20 = [IL20 iL20]; VC20 = [VC20 vC20]; IT0 = [IT0
iT0];
    Id0 = [Id0 id0];  VT0 = [VT0 vT0];  Vd0 = [Vd0 vd0];

    IL11 = [IL11 iL11]; IL21 = [IL21 iL21]; VC21 = [VC21 vC21];
    IT1 = [IT1 iT1];  VT1 = [VT1 vT1];  Id1 = [Id1 id1];
    Vd1 = [Vd1 vd1];  VC11 =[VC11 vC11]; V01 = [V01 v01];


end
```

```
%%%%%%%%%%%%%%%%%%%%%%% Steady state values %%%%%%%%%%%%%%%%%%%%%%%%%%%%%%%%

figure(12);

subplot(3,2,1)
    plot(d,IL10,'lineWidth',3.0); grid on;axis([0 1 0 500]);grid on;
    title('\bf Input inductor current vs SEPIC duty
ratio','LineWidth',3.0);
    ylabel('\bf Current  i_L_1_0 (A)','LineWidth',3.0);
    xlabel('\bf Duty ratio (D1)','LineWidth',3.0);


    subplot(3,2,2)
    plot(d,IL20,'lineWidth',3.0); grid on;
    title('\bf Output inductor current vs  SEPIC duty
ratio','LineWidth',3.0');
    ylabel('\bf Current  i_L_2_0 (A)','LineWidth',3.0);
    xlabel('\bf Duty ratio (D1)','LineWidth',3.0');

    subplot(3,2,3)
    plot(d,VC10,'lineWidth',3.0); grid on;
    title('\bf Intermediate Capacitor voltage  vs SEPIC duty
ratio','LineWidth',3.0');
    ylabel('\bf Capacitor voltage  v_C_1_0 (V)','LineWidth',3.0');
    xlabel('\bf Duty ratio (D1)','LineWidth',3.0');

    subplot(3,2,4)
    plot(d,VC20,'lineWidth',3.0);axis([0 1 0 5000]); grid on;
    title('\bf Output Capacitor voltage vs SEPIC duty
ratio','LineWidth',3.0');
    ylabel('\bf Capacitor Voltage  v_C_2_0 (V)','LineWidth',3.0');
    xlabel('\bf Duty ratio (D1)','LineWidth',3.0');

    subplot(3,2,5)
    plot(d,V00,'lineWidth',3.0);axis([0 1 0 5000]); grid on;
    title('\bf Output voltage vs SEPIC duty ratio');
    ylabel('\bf Volage  v_0_u_t (V)','LineWidth',3.0');
    xlabel('\bf Duty ratio (D1)','LineWidth',3.0');


    figure(13);

    subplot(2,2,1)
    plot(d,IT0,'lineWidth',3.0);axis([0 1 0 500]); grid on;
    title('\bf Transistor T_1 Current  vs SEPIC duty
ratio','LineWidth',3.0');
    ylabel('\bf Current  i_T_0 (A)','LineWidth',3.0');
    xlabel('\bf Duty ratio (D1)','LineWidth',3.0');

    subplot(2,2,2)
    plot(d,Id0,'lineWidth',3.0); axis([0 1 0 10]);grid on;
    title('\bf Diode d_1 Current  vs SEPIC duty ratio','LineWidth',3.0');
    ylabel('\bf Current  i_d_0 (A)','LineWidth',3.0');
    xlabel('\bf Duty ratio (D1)','LineWidth',3.0');

    subplot(2,2,3)
    plot(d,VT0,'lineWidth',3.0); grid on;
```

```
    title('\bf Transistor T_1 Voltage  vs SEPIC duty
ratio','LineWidth',3.0');
    ylabel('\bf Voltage    v_T_0 (V)','LineWidth',3.0');
    xlabel('\bf Duty ratio (D1)','LineWidth',3.0');

    subplot(2,2,4)
    plot(d,Vd0,'lineWidth',3.0); grid on;
    title('\bf Diode d_1 voltage  vs SEPIC duty ratio','LineWidth',3.0');
    ylabel('\bf Voltage  v_d_0 (V)','LineWidth',3.0');
    xlabel('\bf Duty ratio (D1)','LineWidth',3.0');

    %Ripple values
    figure(14);

subplot(3,2,1)
    plot(d,IL11,'lineWidth',3.0); grid on;
    title('\bf Input inductor current ripple vs SEPIC duty
ratio','LineWidth',3.0');
    ylabel('\bf Current  i_L_1_1 (A)','LineWidth',3.0');
    xlabel('\bf Duty ratio (D1)','LineWidth',3.0');

    subplot(3,2,2)
    plot(d,IL21,'lineWidth',3.0); grid on;
    title('\bf Output inductor current ripple vs SEPIC duty
ratio','LineWidth',3.0');
    ylabel('\bf Current  i_L_2_1 (A)','LineWidth',3.0');
    xlabel('\bf Duty ratio (D1)','LineWidth',3.0');

    subplot(3,2,3)
    plot(d,VC11,'lineWidth',3.0); grid on;
    title('\bf Intermediate Capacitor ripple voltage  vs SEPIC duty
ratio','LineWidth',3.0');
    ylabel('\bf Voltage  v_C_1_1 (V)','LineWidth',3.0');
    xlabel('\bf Duty ratio (D1)','LineWidth',3.0');

    subplot(3,2,4)
    plot(d,VC21,'lineWidth',3.0); grid on;
    title('\bf Output Capacitor ripple voltage vs SEPIC duty
ratio','LineWidth',3.0');
    ylabel('\bf Voltage  v_C_2_1 (V)','LineWidth',3.0');
    xlabel('\bf Duty ratio (D1)','LineWidth',3.0');

    subplot(3,2,5)
    plot(d,V01,'lineWidth',3.0); grid on;
    title('\bf Output ripple voltage vs SEPIC duty
ratio','LineWidth',3.0');
    ylabel('\bf Voltage  v_0_u_t_1 (V)','LineWidth',3.0');
    xlabel('\bf Duty ratio (D1)','LineWidth',3.0');

    figure(15);

    subplot(2,2,1)
    plot(d,IT1,'lineWidth',3.0); grid on;
    title('\bf Transistor T_1 Current ripple  vs SEPIC duty
ratio','LineWidth',3.0');
    ylabel('\bf Current  i_T_1 (A)','LineWidth',3.0');
    xlabel('\bf Duty ratio (D1)','LineWidth',3.0');

    subplot(2,2,2)
```

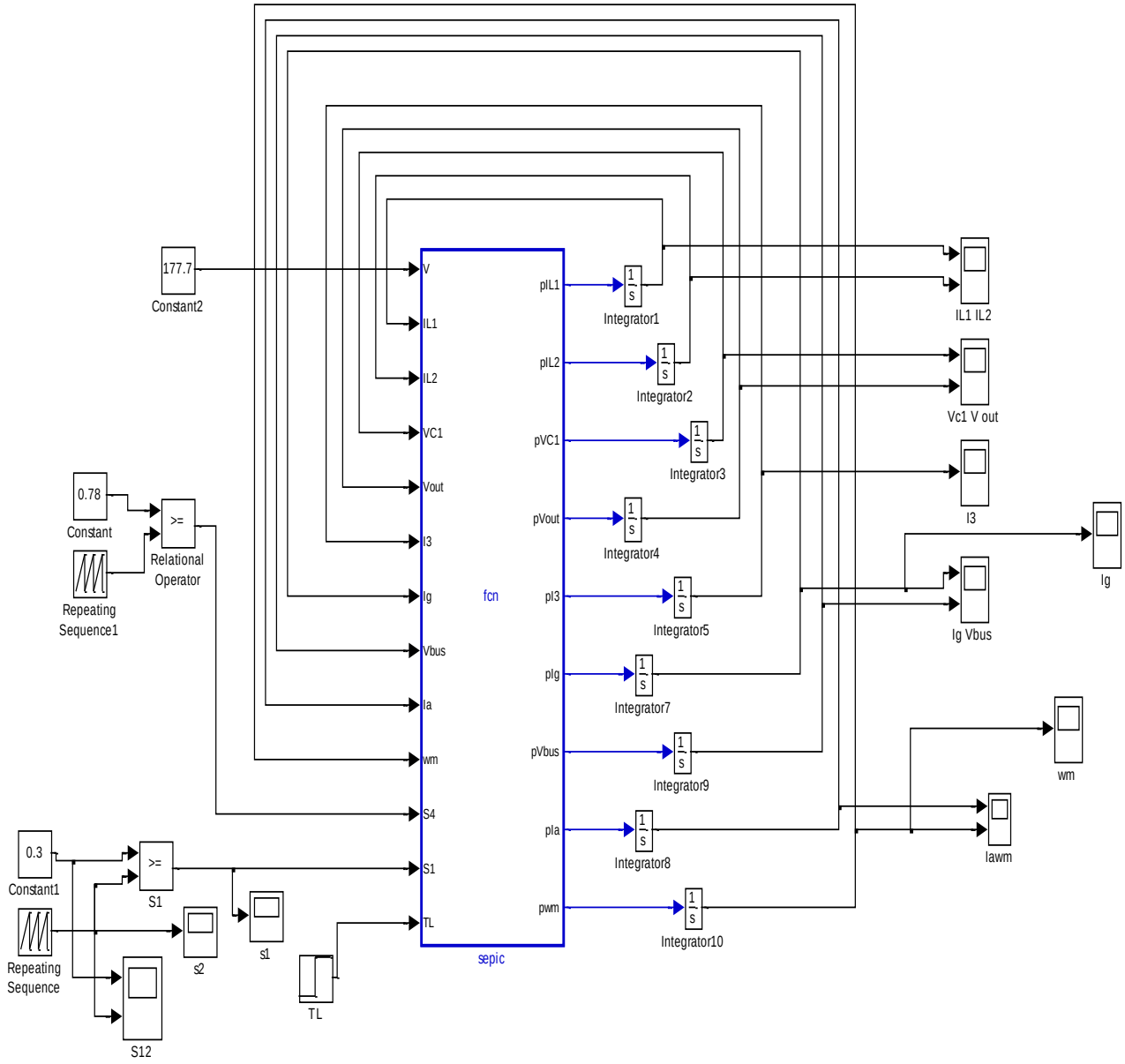
```
    plot(d,VT1,'lineWidth',3.0); grid on;
    title('\bf Transistor T_1 Voltage ripple  vs SEPIC duty
ratio','LineWidth',3.0');
    ylabel('\bf Voltage  v_T_1 (V)','LineWidth',3.0');
    xlabel('\bf Duty ratio (D1)','LineWidth',3.0');

    subplot(2,2,3)
    plot(d,Id1,'lineWidth',3.0); grid on;
    title('\bf Diode d_1 Current ripple  vs SEPIC duty
ratio','LineWidth',3.0');
    ylabel('\bf Current  i_d_1 (A)','LineWidth',3.0');
    xlabel('\bf Duty ratio (D1)','LineWidth',3.0');

    subplot(2,2,4)
    plot(d,Vd1,'lineWidth',3.0); grid on;
    title('\bf Diode d_1 voltage ripple  vs SEPIC duty
ratio','LineWidth',3.0');
    ylabel('\bf Voltage  v_d_1 (V)','LineWidth',3.0');
    xlabel('\bf Duty ratio (D1)','LineWidth',3.0');
```

APPENDIX G

SIMULINK MODEL FOR SIMULATION STUDIES



APPENDIX H

HOURLY SOLAR INSOLATION IN ZARIA

NASA Surface meteorology and Solar Energy - Available Tables

Latitude 11.067^{0}N / Longitude 7.7^{0}E was chosen.

Geometry Information

Elevation: **559** meters
taken from the
NASA GEOS-4
model elevation

Northern boundary
12

Western boundary
7

Center
Latitude **11.5**
Longitude **7.5**

Eastern boundary
8

Southern boundary
11

Parameters for Sizing and Pointing of Solar Panels and for Solar Thermal Applications:

Monthly Averaged Insolation Incident On A Horizontal Surface At Indicated GMT Times (kW/m^2) for year 2013

Lat 11.067 Lon 7.7	Jan	Feb	Mar	Apr	May	Jun	Jul	Aug	Sep	Oct	Nov	Dec
Average@00	n/a	n/a	n/a	n/a	n/a	n/a	n/a	n/a	n/a	n/a	n/a	n/a
Average@03	n/a	n/a	n/a	n/a	n/a	n/a	n/a	n/a	n/a	n/a	n/a	n/a
Average@06	0.04	0.05	0.06	0.09	0.10	0.09	0.07	0.06	0.08	0.08	0.08	0.06

Average@09	0.52	0.56	0.63	0.65	0.63	0.56	0.50	0.47	0.56	0.62	0.62	0.55
Average@12	0.79	0.88	0.90	0.89	0.86	0.79	0.71	0.67	0.75	0.80	0.79	0.76
Average@15	0.41	0.48	0.49	0.47	0.42	0.43	0.41	0.37	0.36	0.35	0.36	0.36
Average@18	0.01	0.02	0.02	0.02	0.02	0.02	0.02	0.02	0.01	0.00	0.00	0.00
Average@21	n/a	n/a	n/a	n/a	n/a	n/a	n/a	n/a	n/a	n/a	n/a	n/a

A frequency table was constructed from the above data as follows:

Table H.1 Frequency Table for Solar Insolation in Zaria (NASA)

Solar insolation W/m^2	Frequency	Class Mark W/m^2
-95-140	24	
150-340	0	245
350-540	15	445
550-740	12	645
750-940	9	845
950-1140	0	1045

Table H.2 Frequency Table for Solar Insolation in Zaria obtained from the solarimeter at the power and machine lab, ABU Zaria.

Solar insolation W/m^2	Frequency	Class Mark W/m^2
10-230	190	120
240-460	203	350
470-690	142	580
700-920	198	695
930-1150	63	1040